NOTICE

The quality of this microform is heavily dependent upon the quality of the original thesis submitted for microfilming. Every effort has been made to ensure the highest quality of reproduction possible.

If pages are missing, contact the university which granted the degree.

Some pages may have indistinct print especially if the original pages were typed with a poor typewriter ribbon or if the university sent us an inferior photocopy.

Reproduction in full or in part of this microform is governed by the Canadian Copyright Act, R.S.C. 1970, c. C-30, and subsequent amendments.

AVIS

La qualité de cette microforme dépend grandement de la qualité de la thèse soumise au microfilmage. Nous avons tout fait pour assurer une qualité supérieure de reproduction.

S'il manque des pages, veuillez communiquer avec l'université qui a conféré le grade.

La qualité d'impression de certaines pages peut laisser à désirer, surtout si les pages originales ont été dactylographiées à l'aide d'un ruban usé ou si l'université nous a fait parvenir une photocopie de qualité inférieure.

La reproduction, même partielle, de cette microforme est soumise à la Loi canadienne sur le droit d'auteur, SRC 1970, c. C-30, et ses amendements subséquents.

THE UNIVERSITY OF ALBERTA

OPTICAL DOSIMETRY AND PHOTODYNAMIC THERAPY OF EXPERIMENTAL PROSTATE TUMORS

BY

MARK ROBERT ARNFIELD

A THESIS

SUBMITTED TO THE FACULTY OF GRADUATE STUDIES AND RESEARCH IN PARTIAL FULFILMENT OF THE REQUIREMENTS FOR THE DEGREE OF DOCTOR OF PHILOSOPHY

DEPARTMENT OF ELECTRICAL ENGINEERING

EDMONTON, ALBERTA

SPRING 1989

ISBN 0-315-52941-5

THE UNIVERSITY OF ALBERTA

RELEASE FORM

NAME OF AUTHOR: MARK ROBERT ARNFIELD

TITLE OF THESIS: OPTICAL DOSIMETRY AND PHOTODYNAMIC THERAPY OF EXPERIMENTAL PROSTATE TUMORS

DEGREE: DOCTOR OF PHILOSOPHY

YEAR THIS DEGREE GRANTED: 1989

Mark Arnfield

3509 - 43 Avenue

Edmonton, Alberta

T6L 4J5

April 1, 1989

THE UNIVERSITY OF ALBERTA

FACULTY OF GRADUATE STUDIES AND RESEARCH

The undersigned certify that they have read, and recommend to the Faculty of Graduate Studies and Research for acceptance, a thesis entitled OPTICAL DOSIMETRY AND PHOTODYNAMIC THERAPY OF EXPERIMENTAL PROSTATE TUMORS

submitted by MARK ROBERT ARNFIELD

in partial fulfilment of the requirements for the degree of DOCTOR OF PHILOSOPHY.

.....
Supervisor

.....

.....

.....

.....

Date: March 7, 1989

To

Sherry

and

My Parents

ABSTRACT

Hypoxia in solid tumors may represent a limitation to curability by photodynamic therapy (PDT), which requires oxygen for a therapeutic effect. PDT of R3327-AT rat prostate tumors, which have a 20-30% hypoxic fraction, produced growth delays but no cures. The co-administration of the hypoxic cell cytotoxic agent misonidazole (MISO) with PDT, produced cures in this anaplastic tumor in 17/35 animals. Combined PDT plus MISO therapy of the R3327-H rat prostate tumor also significantly enhanced the therapeutic effect, producing cures in 8/12 animals. The R3327-H tumor has no hypoxic fraction, which suggests that MISO cytotoxicity was directed against cells made hypoxic by PDT. These results suggest that the addition of MISO may be effective in treating PDT-resistant cells in human tumors and in enhancing the killing of cells rendered hypoxic after PDT.

Knowledge of tissue optical properties is essential to accurate dosimetry in PDT. Measurements in R3327-AT tumors revealed strongly forward peaked scattering, and absorption and scattering coefficients of 0.49 cm^{-1} and 270 cm^{-1} respectively. The use of multiple, implanted fiber optic light sources is an effective means of overcoming limited light penetration in tissue. Anisotropic light

distributions, emitted from an optical fiber implanted in excised solid tumors, were described by an analytic model of light propagation. This model was used to calculate light distributions in tumors and a lipid phantom, which were produced by arrays of interstitial cylindrical sources in translucent plastic needles. These calculations consisted of interpolations from measurements that were taken by placing a miniature light probe in a plastic needle, while illuminating a source in a nearby needle. Typical values of derived absorption coefficients in excised and *in vivo* tumors were 0.50 cm^{-1} and 0.8 cm^{-1} respectively; corresponding penetration depths were 2.6 mm and 1.9 mm. Light penetration within *in vivo* tumors progressively decreased during dosimetry experiments, probably due to leakage of blood from damaged vasculature. The calculation of dose distributions by interpolating light measurements from interstitial needles, may provide a clinically feasible dosimetry technique which could be undertaken prior to PDT, in which the light sources are placed within the same needles.

ACKNOWLEDGEMENT

I would like to express my appreciation to Dr. John Tulip and Dr. Malcolm McPhee for their enthusiastic support and helpful ideas and suggestions in the course of this work.

Finn Mortensen, Erich Schartner, Lorenz Stenger and Don Burdeniuk of the Cross Cancer Institute Medical Physics Department provided many valuable contributions to the fabrication of the experimental equipment.

Finally, I would like to acknowledge the expert assistance of Joyce Spicer, Frank LoCicero and Richard Besse of the Cross Cancer Institute Audio Visual Department.

TABLE OF CONTENTS

LIST OF TABLES

LIST OF FIGURES

Number Page

Number Page

LIST OF PLATES

Chapter I: INTRODUCTION

Photodynamic therapy (PDT) is a relatively new method of cancer treatment that has been shown to be capable of destroying superficial tumors in various sites, including esophagus, head, neck and skin, lung and bladder[1]. PDT is based on the fact that certain chemicals can function as photosensitizing agents. When a photosensitizer is present within tissue, the application of light of an appropriate wavelength initiates photodynamic action and consequent cytoxicity. The drug in current clinical use is Photofrin II, a proprietary derivative of hematoporphyrin which is activated by red light at 630 nm. Initial encouraging results from various centers have led to multi-center stage III clinical trials of PDT for esophageal, bladder and lung cancer which are currently underway in the United States and Canada. Individual investigators have treated various other sites with PDT, which include cancers of the brain[2] and eye[3], and gynecological tumors[4].

In 1982 a research program was initiated at the Cross Cancer Institute, with the eventual aim of applying PDT to human prostate cancer and other solid tumors. The incidence of prostate cancer is second only to lung cancer among North American men. The majority of patients present with either locally extensive or metastatic disease, for which there is no completely satisfactory therapy. Unfortunately, the two

currently accepted methods of treatment for localized prostate cancer, radical prostatectomy and radiotherapy, may be associated with serious complications including incontinence, impotence and in the case of radiotherapy, cystitis and proctitis. For these reasons, an effective alternate treatment method with potentially fewer and less harmful side effects would be highly desirable.

A particular technique for treating larger tumors with PDT, involves the implantation of multiple fiber optic light sources directly within the tumor. The fibers are illuminated by a dye laser beam, which is passed through a beamsplitting device and focused separately onto the ends of the optical fibers. The other ends of the fibers are implanted in the tumor. Interstitial PDT has shown promise in treating both animal and human solid tumors[5,6].

Although some encouraging results have been obtained with solid tumors, most successful PDT treatments have involved superficial and non-invasive cancers. The main problem in treating large tumors is due to the limited penetration of red light in tissue. Thus, optical dosimetry is of critical importance in defining the limits of this form of therapy. Most of this thesis is concerned with various aspects of optical dosimetry in tissue as applied to interstitial photodynamic therapy.

Another aspect of the application of PDT examined in this thesis is the problem of hypoxic regions in solid tumors. It has been suggested that the successful treatment of solid tumors with PDT may be limited by regions of hypoxia within tumors[7,8]. Photodynamic cytotoxity is caused by highly reactive singlet oxygen $^1O_2$, which is produced via an energy transfer process after the absorption of light by the photosensitizer. Studies both *in vitro* and *in vivo* have demonstrated that by reducing the amount of available oxygen, the photodynamic effect can be inhibited[9,10]. We have investigated the efficacy of PDT on a tumor model with a known hypoxic fraction, the Dunning R3327-AT rat prostate tumor. These results are summarized in Chapter II.

Outline of Contents

Chapter II

The responses of Dunning R3327-AT and R3327-H experimental rat prostate tumors to various interstitial PDT treatment protocols are assessed. The best responses in both tumor models are seen when PDT is used in combination with the hypoxic cell cytotoxic drug misonidazole, under conditions of mild or moderate hyperthermia.

Chapter III

This chapter describes basic studies of the optical characteristics of excised R3327-AT tumors. This knowledge is central to the development in later chapters of techniques for interstitial light dosimetry. Direct measurements are made of absorption, scattering and attenuation coefficients and a simple model is described, which gives the space irradiance in tissue in terms of these parameters. The theoretical model is shown to be consistent with direct measurements of optical intensities within these experimental tumors.

Chapter IV

The model of light propagation described in chapter III is developed as a basis for optical dosimetry in solid tumors, using interstitial light sources. Predictions of light dosimetry using the model are interpolated in individual tumors from sample measurements of optical intensity, taken with a miniature light detector placed in plastic needles within the tumor. Calculations of space irradiance from four interstitial cylindrical irradiators are compared to direct measurements, made using fiber optic probes.

Chapter V

The technique described in Chapter IV for interpolating light distributions from interstitial sources is extended to a larger array of cylindrical irradiators. Tests are

described in both *in vivo* as well as *postmortem* tumors and a tissue-equivalent phantom. The calculation of light dose *in vivo* is found to be complicated by significant variations in local attenuation within individual tumors. Also, light absorption and attenuation appear to increase with time during dosimetry experiments.

Chapter VI

The final chapter presents a discussion of some of the current problems and considerations involved in developing light dosimetry for clinical interstitial PDT.

LITERATURE CITED

1. T. J. Dougherty, "Photosensitization of malignant tumors," Sem. Surg. Oncol. 2:24-37, 1986.

2. E.R. Laws, D.A. Cortese, J.H. Kinsey, et al., "Photoradiation therapy in the treatment of malignant brain tumors. A phase 1 (feasibility) study," Neurosurg. 9:672-678, 1981.

3. R.A. Bruce, Jr.,"Photoradiation of choroidal malignant melanoma." In: Porphyrin Localization and Treatment of Tumors, D.R. Doiron and C.J. Gomer (eds.). New York: Alan R. Liss, 1984, pp.777-784.

4. M.A. Rettenmaier, M.L. Berman, P.J. Disaia, R.G. Burns, G.D. Weinstein, J.L. McCullough and M.W. Berns,"Gynecologic uses of photoradiation therapy," IBID, pp.767-775.

5. R.A. Gatenby, W.H. Hartz, P.F. Engstrom, et al., "CT-guided laser therapy in resistant human tumors; phase 1 clinical trials," Therap. Radiol. 163:172-175, 1987.

6. T.J. Dougherty, R.E. Thoma, D.G. Boyle and K.R. Weishaupt, " Interstitial photoradiation therapy for primary solid tumors in pet cats and dogs," Cancer Res. 41: 401, 1981.

7. I. Freitas, "Hypoxia in tumors suggests improvements of photoradiation therapy clinical protocols." In: Primary Photo Processes in Biology and Medicine, R.V. Benasson, G. Jori, E.J. Land and T.G. Truscott (eds.). Plenum Press, 1985, pp.417-419.

8. J. B. Mitchell, S. McPherson, W. DeGraff, J. Gamson, A. Zabell and A. Russo, "Oxygen dependence of hematoporphyrin derivative-induced photoinactivation of Chinese hamster cells," Cancer Res. 45: 2008-2011, 1985.

9. J. Moan and S. Sommer, "Oxygen dependence of the photosensitizing effect of hematoporphyrin derivative in NHIK 3025 cells," Cancer Res. 45:1608-1610, 1985.

10. B.W. Henderson and V.H. Fingar, "Relationship of tumor hypoxia and response to photodynamic treatment in an experimental mouse tumor," Cancer Res. 47:3110-3114, 1987.

CHAPTER II: TREATMENT OF DUNNING R3327-AT AND R3327-H RAT PROSTATE TUMORS WITH INTERSTITIAL PHOTODYNAMIC THERAPY IN COMBINATION WITH MISONIDAZOLE*

I. INTRODUCTION

Prostate cancer is a leading cause of death in men over the age of 55. The disease is characterized on presentation by a great diversity among patients with respect to pathology, degree of differentiation, rate of tumor growth and responsiveness to various therapeutic modalities.

The availability of animal models of human malignant disease can greatly aid in the development of improved therapies. The inherent diversity of prostate cancer suggests that multiple animal models may be needed to mimic the various forms of the disease. However, despite the importance of this disease relatively few animal models exist[1]. The Dunning rat prostate adenocarcinomas have been found to be particularly useful. At least four distinct transplantable sublines of this tumor have described, all of which

* Two versions of this chapter have been published. S. Gonzales, M.R. Arnfield, B.E. Meeker, J. Tulip, W.H. Lakey, J.D. Chapman and M.S. McPhee,"Treatment of Dunning R3327-AT rat prostate tumors with photodynamic therapy in combination with misonidazole," Cancer Research 46:2858-2862, 1986. B.D. Hirsch, N.C. Walz, B.E. Meeker, M.R. Arnfield, J. Tulip, M.S. McPhee and J.D. Chapman, "Photodynamic therapy-induced hypoxia in rat tumors and normal tissues," Photochemistry and Photobiology 46:847-852, 1987.

originated from the same tumor that arose spontaneously in the prostate of an aged Copenhagen rat[2,3].

Two of the Dunning sublines that exhibit greatly different growth kinetic and histologic characteristics are the R3327-H and R3327-AT tumors. These two tumors can be considered to represent two extremes of malignant potential within the spectrum of human prostate cancer. The R3327-H tumor is hormonally sensitive, slow growing, well differentiated, well vascularized and relatively sensitive to radiotherapy. The R3327-AT tumor is an anaplastic variant of the R3327-H tumor that is hormonally insensitive, rapidly growing, poorly differentiated, poorly vascularized and extremely resistant to radiotherapy.

A series of studies have been conducted at the Cross Cancer Institute on the response of these two tumor models to radiotherapy and various chemotherapeutic agents[4,5]. In 1982, a program was initiated aimed at evaluating the effects of photodynamic therapy (PDT) as an alternative treatment method. Since that time, a series of studies have been conducted to investigate different parameters which affect the response to PDT.

II. MATERIALS AND METHODS

A. Animal and Tumor Procedures

First generation (F1) males from matings of Fisher (female) and Copenhagen (male) rats were used as hosts for both tumor lines. The R3327-AT tumor material was originally obtained from Dr. D. Coffey at Johns Hopkins University, Baltimore, MD and the R3327-H tumor was obtained from the Papanicolaou Institute, Miami, Fl. Tumors selected as donors for transplantation had doubling times of three days or less in the case of R3327-AT tumors and twelve days or greater in the case of R3327-H tumors. Cubes of approximately 2-3 mm were cut into sterile saline and subsequently implanted in the flanks of animals at least 6 weeks of age, after which the flank was sutured. Both tumor lines were examined histologically at least twice yearly in order to check tumor cell drift. Tumors that exhibited drift by either growth kinetic or histological criteria were not used as donor material.

The R3327-H tumor typically showed a latency period of 3 to 4 months before becoming palpable, whereas the R3327-AT tumor became palpable at 1 to 2 weeks following implantation. After becoming palpable, tumors were measured with calipers in three mutually orthogonal directions at least once a week while the animals were under light halothane anesthesia. Tumor volumes were calculated as an

elliptical mass, according to the formula

$$V = \frac{\pi}{6} \times D_1 \times D_2 \times D_3$$

Each dimension D_i was obtained by subtracting 1.3 mm from the respective caliper measurement, to account for the thickness of a double layer of skin. Animals were randomized into specific treatment protocols when the tumors reached volumes of 0.5-0.8 cm^3. The day of treatment was in all cases designated as day 0. Data from treatment protocols was graphed in either of two ways: in one case, as the average tumor volume among the treatment group vs time post treatment and in the other, as the percentage of the treatment group which regrew to 10x treatment volume vs time post treatment.

B. Hematoporphyrin Derivative

Two types of hematoporphyrin derivative (HPD), Photofrin I and II, were obtained from Photofrin Medical Inc., Cheektowaga, N.Y. Photofrin I was used only in the experiment designated Protocol I; Photofrin II was used in all other experiments. The drugs were administered i.p. four hours prior to laser phototherapy, at doses of 20 mg/kg and 15 mg/kg for Photofrin I and II respectively.

C. Misonidazole

Pure drug MISO (1-(2- hydroxy-3- methoxypropyl)-2 nitroimidazole) was supplied by Hoffman-La Roche Ltd., Etobicoke, Ontario. MISO was prepared at a concentration of 10 mM in sterile physiological saline immediately before each animal experiment and administered i.p. at a dose of 0.5 mg/g. Animals that were treated by PDT alone received a comparable volume of sterile physiological saline i.p.

D. Laser Phototherapy

The experimental set-up for laser phototherapy is shown in Fig.II-1. A beam splitting device was used to divide the beam from a Coherent CR-599 argon-driven dye laser into four separate beams, which were focussed onto the proximal ends of four 600 micron core diameter optical fibers. The wavelength of the laser was maintained at 630 ± 0.1 nm and was checked regularly with a monochromator. The fiber distal ends were prepared by attaching 1.0 cm long cylindrical diffusing tips (see Appendix I). These tips have been previousley described in detail[6]. The four tips were inserted interstitially to 1.0 cm depth in tumors in a 0.7 x 0.7 cm square grid pattern. The power output per fiber, which ranged between 75 and 300 mW depending on the particular experiment, was measured by means of an integrating sphere, attached to a radiometer (Model 161 optometer and model 2525 integrating sphere, United Detector

Technology, Culver City, CA). Total treatment time ranged from 30-55 min.

E. Tumor Temperature

Tumor core and peripheral temperatures were monitored in most experiments, since previous studies had shown that hyperthermia can enhance tumor response to PDT [7]. The temperature probes consisted of thermocouples mounted within 30 gauge needles, which were attached to a monitor device capable of recording data from up to 10 probes simultaneously (OM-202 temperature logger, Omega Engineering, Stamford, CT). Temperatures were maintained within predetermined ranges in order to separate the effects of hyperthermia from the photodynamic response. Two different methods were used for controlling tumor temperature. In the first method, tumors were surface cooled by an external water flow so that intratumor temperatures were maintained in either of two ranges, 40-41°C or 44-45°C. In the second method, an electronic shutter device (designed by the Medical Physics Department of the Cross Cancer Institute) was used to automatically maintain the intratumor temperature in one of the two ranges, by intermittently turning the laser light on or off. For example, to maintain the temperature in the range 40-41°C, if the temperature rose to greater than 41°C, the shutter would automatically block the beam and it would

remain blocked until the temperature dropped to below 40°C, at which point the shutter would re-open.

III. RESULTS

A. Protocol I: Effect of Light Dose in PDT of the R3327-AT Tumor

Photofrin I (20 mg/kg) was administered i.p. four hours prior to laser phototherapy to animals bearing R3327-AT tumors of volume approximately 0.5 cm^3. Laser light was applied to tumors interstitially by four fibers at a dose rate of 300 mW per fiber for either 17 min or 33 min, resulting in a total light dose of 1224 J or 2376 J in the two groups. In both groups tumor core temperatures were maintained in the range 44-45°C. Figure II-2 shows average tumor regrowth as a function of time for the two treatment groups and a control group. The growth delays for the 1224 and 2376 J groups were significantly different ($p<.01$), at 3.1 days and 8.1 days respectively (see Table II-1).

B. Protocol II: Effect of Hyperthermia in PDT of the R3327-AT Tumor

Photofrin II (15 mg/kg) was administered i.p. four hours prior to laser phototherapy, which was applied at a dose rate of 300 mw per fiber for 30 min, resulting in a total light dose of 2160 J. In two separate groups external water cooling was used to maintain tumor temperature at 40-41°C or 44-45°C. Table II-1 gives the average growth delays, which

were 8.8 days for the lower temperature group and 13.3 days for the higher temperature group. Figure II-3 shows average tumor regrowth vs time post treatment, together with an untreated control group and a fourth group which was treated with laser light alone (2160 J) and maintained at 44-45°C. This latter group was included to separate the effects of hyperthermia alone from the effects of PDT plus hyperthermia. However, little or no growth delay is evident when compared to the untreated controls. No cures of the R3327-AT tumors were observed after PDT treatments in either temperature range.

The 13.3 day growth delay produced by Photofrin II and 2160 J of light at 44-45°C was significantly greater than the 8.1 days observed for Photofrin I and 2376 J in the previous protocol ($p<0.01$), despite the lower dose of drug (15 mg/kg vs 20 mg/kg) and the slightly lower light dose. This difference was attributed to greater photodynamic activity, since Photofrin II is a more purified form of HpD than Photofrin I.

C. Protocol III: Effect of Combined PDT and MISO Therapy on the R3327-AT Tumor

A third protocol was devised to investigate the combined effects of PDT and MISO on the response of the R3327-AT tumor. Table II-1 shows the results of administering MISO (0.5 mg/g) i.p. either 30 min before or immediately after

laser phototherapy at 40-41°C. With the addition of MISO, growth delays were increased from 8.8 to 15.2 days when added prior to phototherapy and to 16.3 days when added after. The responses of individual tumors to PDT plus MISO therapy was extremely variable, with some cures observed. For this reason, instead of displaying the data as an average tumor regrowth curve, it was plotted in Fig.II-4 as the number of tumors that regrew to 10x their initial treatment volume vs time post-treatment. This graphical method was preferred to the previous method for this case since locally controlled or cured tumors were immediately evident from the graph. The MISO before or after PDT groups are combined in Fig.II-4 into a single (N=20) group of which 9 tumors were cured (defined as no regrowth by 36 days). No cures were observed in the PDT only group.

The response to combined PDT and MISO therapy is the best response of the radiation resistant R3327-AT tumor to any treatment method to date. The above experiment was repeated a year after it was first performed to confirm these findings. Results of a similar experiment are shown in Fig.II-5. The untreated control group regrew to 10x their treatment volume by 12-16 days post laser therapy. The PDT only group (2160 J) exhibited significant tumor regression after treatment, but subsequently regrew to 10x treatment volume by 20-40 days after therapy. Of the combined therapy group, 7/15 animals received MISO before laser therapy of

which 4 local cures were observed. The remaining 8 animals received MISO after laser therapy, with 4 of these resulting in local cures. These results confirm the results of the first experiment, where 7/20 animals had complete responses to combined PDT plus MISO therapy. The 8/15 animals in the second experiment that were complete responders showed no regrowth by day 44. Seven of these died of lung metastases between 73-128 days post treatment, with no evidence of local tumor recurrence upon autopsy. The remaining animal showed no recurrence at 270 days post treatment.

D. Protocol IV: Effect of Hyperthermia in MISO Cytotoxicity in the R3327-AT Tumor

Previous studies have reported enhancement of MISO cytotoxicity at hyperthermic temperatures[8,9]. A group of animals given MISO (0.5 mg/g) without laser treatment was compared with groups given MISO followed by laser light (2160 J), which were maintained at 40-41°C and 44-45°C. Observed tumor growth delays for the MISO alone, 40-41°C and 44-45°C groups were 0.2, 2.2 and 4.4 days respectively (see Table II-1). The effect of MISO alone at 37°C was not statistically significant vs a control group. However the difference in response between the two elevated temperature groups was statistically significant, as was the response of these groups with respect to the MISO alone group ($p<0.01$).

E. Protocol V: Effect of Combined PDT Plus MISO Therapy on the R3327-H Tumor

Animals were randomized into five treatment groups to study the effects of two different light doses and MISO on the response of the slow growing R3327-H tumor. The percentage of tumors that regrew to 10x their treatment volume is shown in Fig.II-6. All tumors had regrown to 10x treatment size by 13.9, 14.9 and 13.8 weeks for the control, laser only and MISO only groups respectively. The MISO only group is not shown in Fig.II-6 for the sake of clarity, since it is partially overlapped by the other two curves. Significant growth delays were observed in a group treated with PDT at 1000 J, which was maintained at 40-41°C by external water flow. Slightly greater growth delays were observed in a similar group that was maintained at 40-41°C by intermittent application of laser light, however all tumors in both of these groups ultimately regrew. Photodynamic therapy at 2000 J (water cooled) produced a better response, with 3/8 tumors responding partially and 5/8 completely. However of the 5 tumors that responded completely, 4 regrew after a latency period of between 15 and 43 weeks. A single animal remained free of local recurrence at 47 weeks.

PDT combined with MISO before (N=6) or after (N=6) resulted in 11 complete responses and 1 partial response. Three of the complete responders regrew, after latency periods of approximately 20 weeks. The other 8 animals remained free

of local recurrence and were presumed cured after follow up periods of 40-56 weeks. Table II-2 gives a comparison of these R3327-H tumor results from PDT and MISO treatments with results from equivalent experiments with R3327-AT tumors. Both PDT and PDT plus MISO were more effective when applied to the R3327-H tumor than to the R3327-AT tumor.

IV. DISCUSSION

Significant growth delays in both the R3327-AT and R3327-H tumor models were elicited by the application of PDT. Five out of eight R3327-H tumors had a complete response to PDT, with one long term cure. The response of the R3327-AT tumor was dose dependent, with a greater growth delay observed for 2376 J than for 1224 J. However out of 18 animals treated with 2000/2160 J at 40-41°C, only 4 complete responses and no cures were observed. These results demonstrate the inadequacy of PDT alone in producing long term local control in these tumor models.

Hyperthermia at 44-45°C by itself had little or no effect on the growth of R3327-AT tumors. However, mild to moderate hyperthermia appears to have been beneficial in conjunction with PDT. PDT at 44-45°C gave a significantly greater growth delay than at 40-41°C. This is consistent with other reports of hyperthermic enhancement of PDT [7,10]. The tumor response to PDT was better when 1000 J of laser light was applied intermittently, than when the tumors were cooled by

an external water drip. The response to PDT with external cooling may have been inhibited since the tumor periphery was kept well below the core temperature of 40-41°C. A temperature of 39.5°C has been shown to improve tumor oxygenation by stimulating blood flow[11], which may enhance photodynamic effects.

The R3327-AT tumor is known to contain a large fraction of hypoxic cells whereas the R3327-H tumor has a well developed vasculature and is presumably well oxygenated[4]. It is likely that the better oxygenation status of the R3327-H tumor was a factor rendering it more susceptible to PDT than the R3327-AT tumor model. Photodynamic action required the presence of oxygen for the production of the main cytotoxic agent, singlet oxygen $^1O_2$. It has been shown <u>in vitro</u> that photodynamic destruction of cells can be completely suppressed under anoxic conditions but that such effects increase with increasing oxygen tension[12]. The R3327-AT studies presented here support the contention that hypoxic cells in solid tumors may be a limiting factor in the PDT of some tumors.

The administration of MISO in combination with PDT resulted in striking improvements to growth delays and cure rates in protocols involving both tumor lines. MISO is known to be cytotoxic to hypoxic cells upon prolonged incubation[13]. The significant improvement in tumor response was approximately

the same, whether MISO was given 30 min prior to or immediately after phototherapy. This suggests that MISO was not directly potentiating the effects of PDT, but rather had a direct cytotoxic action against hypoxic cells in the tumor. MISO binding studies in this laboratory have shown that MISO can diffuse into R3327-H and R3327-AT tumors in significant concentrations if administered immediately after PDT. Graschew and Shopova[14] also observed significantly improved therapeutic responses in both rat K173 colon carcinomas and mouse 180 sarcomas when MISO was administered one hour prior to phototherapy with Photofrin II.

These results are consistent with reports that ischemia and hypoxia resulting from PDT-induced vascular damage is a primary cause of tumor necrosis[15,16]. The therapeutic response is enhanced by the addition of MISO which is selectively lethal to hypoxic cells. The presence of a hypoxic fraction prior to treatment is apparently not necessary for MISO adjunct therapy to be effective as witnessed by the excellent result with the well oxygenated R3327-H tumor. The combination of PDT and MISO has produced the best therapeutic response of the R3327-AT tumor to date. Studies with other hypoxic cell cytotoxic agents together with PDT are currently in progress in our laboratory to explore further this promising treatment modality.

TABLE II-1
Growth Delays of Dunning R3327-AT Tumors Affected by Various Combinations of PDT and Misonidazole

Treatment Group	No. of animals	Photo-sensitizer	Light dose (J)	MISO (mg/gm)	Time to regrow to 10x treatment vol.	Growth delay (days)
Control	10				8.3 ±0.6	0
Laser dose 1	9	Photofrin I	1224		11.4 ±0.9	3.1
Laser dose 2	9	Photofrin I	2376		16.4 ±1.7	8.1
Laser only (44-45°C)	5		2160		8.8 ±0.4	0.5
PDT (40-41°C)	10	Photofrin II	2160		17.1 ±5.4	8.8
PDT (44-45°C)	5	Photofrin II	2160		21.6 ±6.9	13.3
MISO + PDT (40-41°C)	10	Photofrin II	2160	0.5 before	23.5 ±7.5	15.2
MISO + PDT (44-45°C)	5	Photofrin II	2160	0.5 before	23.3 ±4.5	15.0
PDT + MISO (40-41°C)	10	Photofrin II	2160	0.5 after	24.6 ±8.9	16.3
MISO alone	10			0.5 before	8.5 ±0.8	0.2
MISO + laser (40-41°C)	10		2160	0.5 before	10.5 ±1.4	2.2
MISO + laser (44-45°C)	8		2160	0.5 before	12.7 ±2.1	4.4

TABLE II-2
Comparison of Response to PDT or PDT plus MISO of the Dunning R3327-AT and R3327-H Tumors

Tumor	PDT treatment	Partial response	Complete response	% Cure
R3327-AT	2160 J	10/18	4/18	0 (0/18)
R3327-AT	2160 J + MISO	10/35	24/35	48 (17/35)
R3327-H	2000 J	3/8	5/8	38 (3/8)
R3327-H	2000 J + MISO	1/12	11/12	67 (8/12)

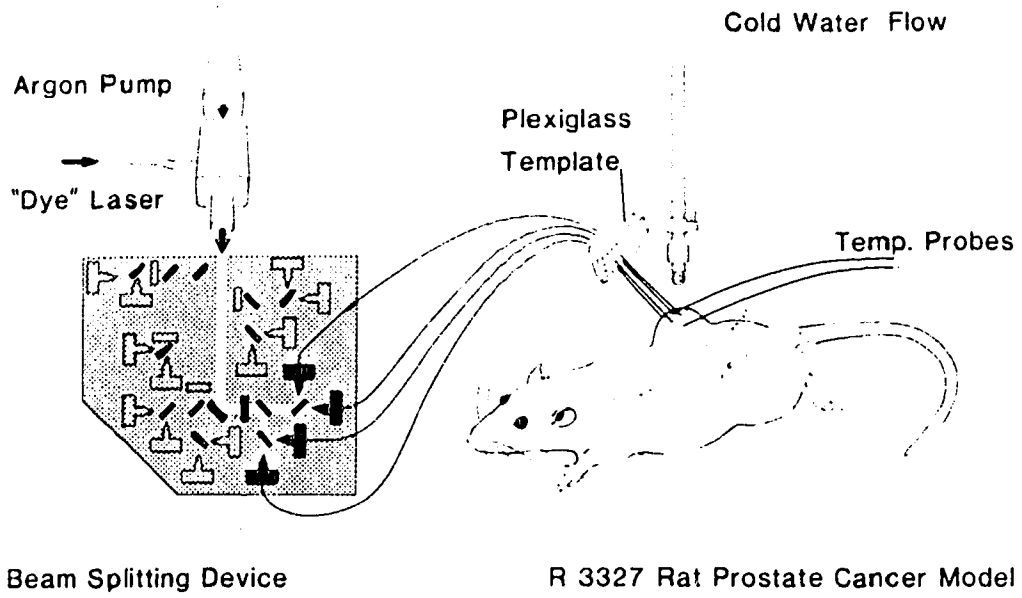

Fig.II-1 Experimental arrangement for intratumor irradiation of rat prostate tumors. Laser light is split and focussed onto the ends of the optical fibers, which are terminated in cylindrical diffusing tips and inserted into or around the tumor mass. Temp., temperature.

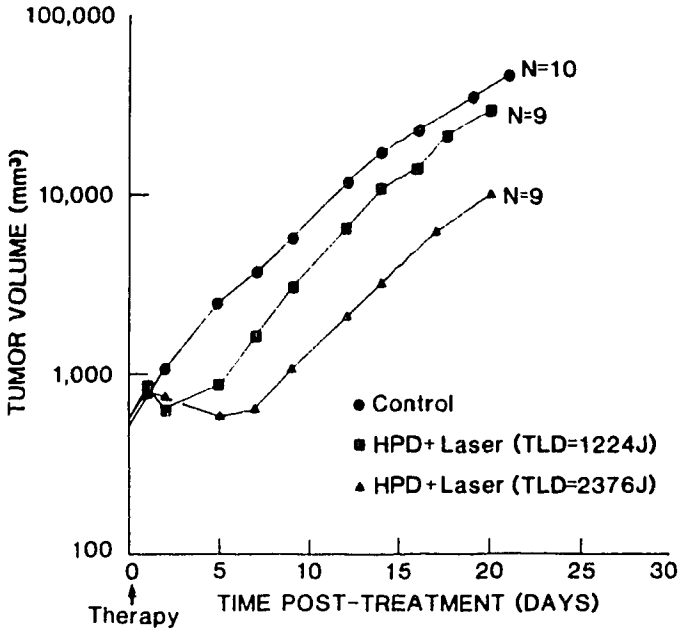

Fig.II-2 Effect of total light dose in PDT of the Dunning R3327-AT Tumor. Points, average tumor volumes in each treatment group. Groups include controls (N=10 animals) and PDT with Photofrin I and total light doses (TLD) of 1224 J (N=9) and 2376 J (N=9) of laser energy.

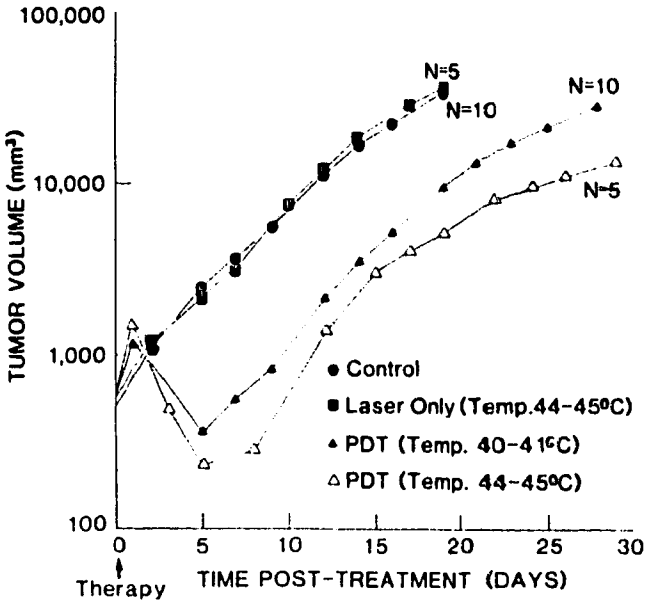

Fig.II-3 Effect of hyperthermia in PDT of the Dunning R3327-AT tumor. Average tumor volumes are shown following PDT with Photofrin II when the tumor core temperature was maintained in the ranges of 40-41°C (N=10 animals) and 44-45°C (N=5); also shown are controls and a group with laser therapy only.

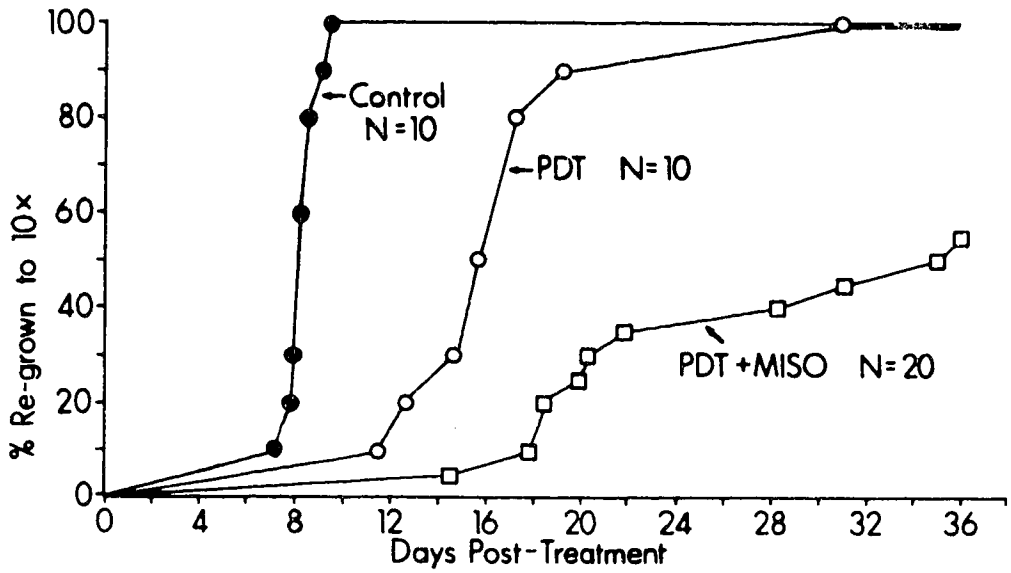

Fig.II-4 Effect of MISO in PDT of the Dunning R3327-AT tumor. Points, percentage of the respective group that has regrown to 10x treatment vol. Shown are controls, PDT with Photofrin II at 40-41°C and a combined group including MISO given either before or after PDT at 40-41°C.

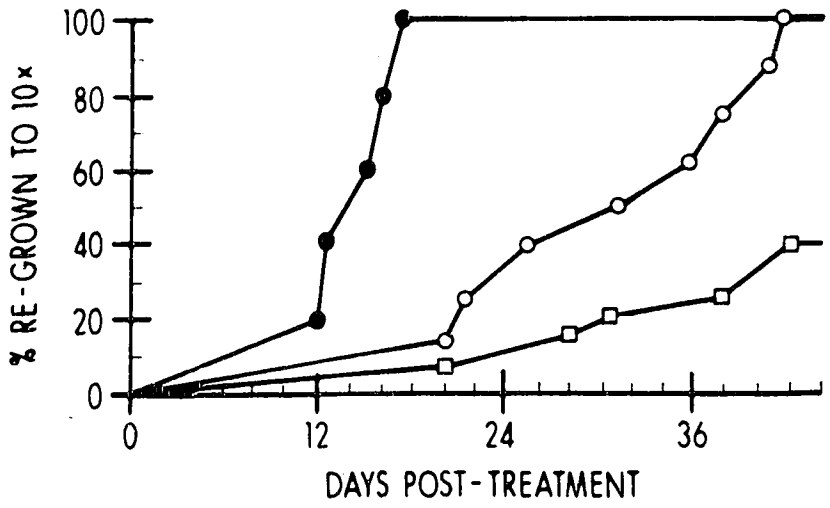

Fig.II-5 Effect of MISO in PDT of the Dunning R3327-AT tumor. Same experiment as in Fig.II-4, repeated 1 yr later. Shown are controls (5 tumors,solid circles), PDT only (8 tumors,open circles) and PDT plus MISO given before or after (15 tumors,open squares).

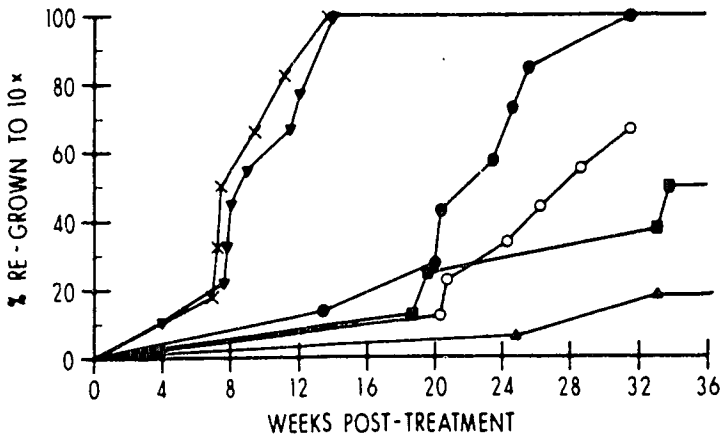

Fig.II-6 Effect of MISO in PDT of the Dunning R3327-H tumor. Points, percentage of the respective group that has regrown to 10x treatment vol. Control tumors shown as inverted solid triangles, tumors treated with 2000 J of light only shown as crosses, tumors treated with PDT at 1000 J (cooled by water flow) shown as solid circles, tumors treated with PDT at 1000 J (cooled by light chopping mechanism) shown as open circles, tumors treated with PDT at 2000 J (water cooled) shown as solid squares and tumors treated with PDT at 2000 J and MISO before or after (water cooled) shown as solid triangles. Maximum intratumor temp. was 41°C for all tumors receiving laser light.

LITERATURE CITED

1. A.A. Sandberg and R. Gaunt, "Model systems for studies of prostatic cancer," Sem. Oncol. 3:177-187, 1976.

2. J.T. Isaacs, W.D.W. Heston, R.M. Weissman and D.S. Coffey, "Animal models of the hormone-sensitive and insensitive prostatic adenocarcinomas, Dunning R3327-H, R3327-HI, and R3327-AT," Cancer Res. 38:4353-4359, 1978.

3. J.T. Issacs, G.W. Yu and D.S. Coffey, "The characterization of a newly identified, highly metastatic variety of Dunning R3327 rat prostatic adenocarcinoma system: the MAT LyLu tumor," Invest. Urol. 19:20-23,1981.

4. C. Thorndyke, B.E. Meeker, G.Thomas, W.H. Lakey, M.S. McPhee and J.D. Chapman," The radiation sensitivities of R3327-H and R3327-AT rat prostate adenocarcinomas," J. Urol. 134:191-198, 1985.

5. D. Mador, B. Ritchie, B. Meeker, R. Moore, F.G. Elliot, M.S. McPhee, J.D. Chapman and W.H. Lakey," Response of the Dunning R3327-H prostate adenocarcinoma to radiation and various chemotherapeutic drugs," Cancer Treat. Rep. 66:1837-1843, 1982.

6. M.R. Arnfield, S. Gonzalez, P. Lea, J.Tulip and M. McPhee, "Cylindrical irradiator fiber tip for photodynamic therapy," Lasers Surg. Med. 6: 150-154,1986.

7. J.H. Kinsey, D.A.Cortese and H.B. Neel, "Thermal considerations in murine tumor killing using hematoporphyrin derivative phototherapy," Cancer Res. 43: 1562-1567, 1983.

8. E.J. Hall, M. Astor, C. Geard, and J. Biaglow," Cytotoxicity of Ro-07-0582; enhancement by hyperthermia and protection by cysteamine," Br. J. Cancer 35:809-815,1977.

9. N.M. Bleehen, D.J. Honess and J.E. Morgan, "The combined effects of hyperthermia and hypoxic cell sensitizers," In: C. Streffer, D. Van Beuningen, G. Dietzel, et al. (eds.), Cancer Therapy by Hyperthermia and radiation. Baltimore: Urban and Schwarzenberg, Inc., 1978, pp.62-71.

10. S.M. Waldow, B.W. Henderson and T.J. Dougherty, "Potentiation of photodynamic therapy by heat: effect of sequence and time interval between treatments in vivo," Lasers Surg. Med. 5:83-94, 1985.

11. P. Vaupel, "Oxygen supply to malignant tumors," In: Tumor Blood Circulation: Angiogenesis, Vascular Morphology and Blood Flow of Experimental and Human Tumors." Hans-Inge Peterson (ed.), Boca Raton: CRC Press, Inc., 1979, pp.143-168.

12. J. Moan and S. Sommer, "Oxygen dependence of the photosensitizing effect of hematoporphyrin derivative in NHIK 3025 cells," Cancer Res. 45: 1608-1610, 1985.

13. R.M. Sutherland, "Selective chemotherapy of non-cycling cells in and in vitro tumor model," Cancer Res. 34:3501-3503, 1974.

14. G. Graschew and M Shopova, "Hypoxia, misonidazole and hyperthermia in photodynamic therapy of tumors, "Lasers Med. Sci. 1:181-186, 1986.

15. W.M. Star, H.P.A. Marijnissen, A.E. van den Berg-Blok, J.A.C. Versteeg, K.A.P. Franken and H.S. Reinhold, "Destruction of rat mammary tumor and normal tissue microcirculation by hematoporphyrin derivative photoradiation observed in vivo in sandwich observation chambers," Cancer Res. 46:2532-2540, 1986.

16.S.H. Selman, M.Kreimer-Birnbaum, J.E. Kaunig, P.J. Goldblatt, R.W. Keck, and S.L. Britton," Blood flow in transplantable bladder tumors treated with hematoporphyrin and light,"Cancer Res. 44:1924-1927,1984.

Chapter III: OPTICAL PROPAGATION IN TISSUE WITH ANISOTROPIC SCATTERING*

I. INTRODUCTION

Optical propagation in random or turbid media has been studied in a variety of contexts and applications including blood oximetry, the paint and paper industry, oceanic and atmospheric propagation, plant physiology and skin phototherapy. Some recent investigation in this area have focussed on dosimetry for photodynamic therapy, a new and promising modality of cancer treatment.[1,2]

Approximate solutions to the Boltzmann transport equation have frequently been used in radiative transfer studies. This approach, where the complexity of the wave interaction with inhomogeneities is replaced by an average scattering coefficient has been successfully employed for many years[3], although its relationship to the fundamental Maxwell's equations has not been fully delineated[4].

Diffusion theory is the simplest approximation to the Boltzmann equation and is easily applied in three-dimensional geometry, which has led to its use in studies of

* A version of this chapter has been published. M.R. Arnfield, J. Tulip and M.S. McPhee, "Optical propagation in tissue with anisotropic scattering," IEEE Transactions on Biomedical Engineering BME-35: 372-381, 1988.

light distribution in tissue. Numerous experiments have demonstrated that optical attenuation in tissue follows a simple exponential decay for broad beam illumination, or an exponential times 1/r for a point source in spherical geometry[5-8]. Since the diffusion length can be directly obtained from the form of the exponential, this important parameter governing the optical distribution has been the most commonly studied of tissue optical parameters. Other investigations have established the usefulness of a diffusion description of optical propagation in blood[9,10].

In the case of soft tissues, numerous and varied morphological features may influence light scattering including changes in refractive index at cell boundaries, the presence of intracellular organelles such as cell nuclei and mitochondria, as well as the extracellular matrix, etc. Sizes of these features vary in a wide range from micron to greater than millimeter dimensions, as for example in the case of vascular networks, where frequent and abrupt changes in color and optical density occur. These conditions present a considerable problem in modelling an average scattering interaction, since the specific form of the angular scattering phase function is strongly dependent on the size of scattering centers relative to the wavelength of incident light. However in general, scattering in tissue at optical wavelengths may be considered to arise due to refraction from objects of size comparable to or greater

than the wavelength of incident light. This type of scattering is approximately modelled by the Mie theory[11] which deals with scattering from spheres of arbitrary size. A general characteristic of this theory is the presence of a strong forward scattered component in the phase function, where the extent of forward scattering depends on the size of scattering centers relative to wavelength and the relative refractive indices of scatterers and substrate.

Experimental evidence supports the hypothesis that light scattering in tissue is anisotropic with significant forward scattering. Bruls and van der Leun[12] and Fine et al.[13] demonstrated forward-peaked scattering functions for human stratum corneum and epidermis at ultraviolet and visible wavelengths. Other results confirming forward scattering have been reported by Wilksch et al.[14] for pig muscle and Hemenger et al.[15] for blood. Although various mathematical techniques have been utilized in transport problems to account for the effects of anisotropic scattering[16], relatively little work has been done with specific reference to optical propagation in tissue. Diffey[17] has proposed a one-dimensional numerical model with anisotropic scattering for skin optics.

The purpose of the present work is to show that the transport approximation to the Boltzmann equation[18] provides a good description of three-dimensional light distributions

in high albedo tissue with forward scattering characteristics. The original motivation for this investigation was the need for accurate dosimetry in photodynamic therapy of solid tumors, especially its potential use in the treatment of human prostate cancers[19]. For this reason the experimental part of the work was restricted to a detailed study of the Dunning R3327-AT rat prostate tumor model which both in histology and visual appearance is similar to some types of human prostatic carcinoma[20]. Scattering and absorption coefficient and diffusion length measurements on R3327-AT tumor material were performed in order to verify the validity of the theoretical model which relates the small scale optical constants to the diffusion length in a straightforward manner.

II. THEORY

The transport of radiant energy in a medium containing uniformly distributed scattering and absorbing particles is governed by an integro-differential equation known as the equation of transfer, which is equivalent to the Boltzmann equation used in neutron transport theory and the kinetic theory of gases. For monochromatic light the equation of transfer is

$$\underline{\Omega}\cdot\nabla I(\underline{x},\underline{\Omega}) = -kI(\underline{x},\underline{\Omega}) + k_s \int_{4\pi} I(\underline{x},\underline{\Omega}') \cdot f(\underline{\Omega}'\rightarrow\underline{\Omega})d\Omega' + S(\underline{x},\underline{\Omega}) \qquad (1)$$

where

$I(\underline{x},\underline{\Omega})$ = angular energy flux density at position $\underline{x}$ and angle $\underline{\Omega}$ in $W \cdot m^{-2} \cdot sr^{-1}$

$f(\underline{\Omega}' \rightarrow \underline{\Omega})$ = angular distribution of light scattered from angle $\underline{\Omega}'$ into angle $\underline{\Omega}$

k_a = absorption coefficient in m^{-1}

k_s = scattering coefficient is m^{-1}

$k = k_a + k_s$ = extinction coefficient

$S(\underline{x},\underline{\Omega})$ = volume source intensity in $W \cdot m^{-3} \cdot sr^{-1}$.

The quantity $I(\underline{x},\underline{\Omega})$ is also known as the specific intensity or sometimes simply the radiance and specifies the angular dependence of the flow of optical power at position $\underline{x}$. Since the absorption of light in tissue is independent of the direction on optical propagation, the radiance $I(\underline{x},\underline{\Omega})$ is of less importance in dosimetry than its integral over 4π solid angle, which is known as the space irradiance $\Phi(\underline{x})$:

$$\Phi(\underline{x}) = \int_{4\pi} I(\underline{x},\underline{\Omega}) d\Omega \quad . \tag{2}$$

The angular distribution of light per scattering event $f(\underline{\Omega}' \rightarrow \underline{\Omega})$ is often called the phase function and is normalized to unity when integrated over 4π solid angle. When the phase function is independent of angle, the scattering is said to isotropic. For anisotropic scattering the phase function depends only on the angle between the incident and scattered radiation. A useful parameter is the

mean cosine of scattering, defined as

$$g = \int_{-1}^{1} \mu f(\mu)\, d\mu \qquad (3)$$

where μ is the cosine of the angle between incident and scattered light.

In some situations it is useful to model the phase function as being sharply peaked in the forward direction, superimposed on a lower isotropic background. This type of phase function is an approximation of experimental results in R3327-AT tumor tissue, as will be shown later (Fig.III-4) and may be represented by

$$f(\mu) = g \cdot \delta(\mu-1) + \frac{(1-g)}{4\pi} \qquad (4)$$

where δ is the Dirac delta function. The use of a phase function of the type in neutron transport theory is known as the transport approximation[18]. The first and second terms represent the forward and isotropic scattering components respectively; g ranges from zero for isotropic scattering to nearly unity for strongly forward scattering media.

In the equation of transfer (1), the term on the left hand side represents the change in the flux density due to photon transport. The first term on the right hand side represents losses due to absorption and scattering. The second term on the right represents the gain due to scattering of photons back into the original direction of motion and the last term is the contribution from sources. Exact solutions of (1)

are known only for some simplified geometries and isotropic scattering. We will be concerned with one of these, the solution for an isotropic point source of unit power located at the origin; a derivation can be found in Weinberg and Wigner[21]. For the case of an isotropic phase function the solution is given by

$$\Phi(r) \approx \frac{\gamma}{4\pi D}\frac{e^{-\alpha r}}{r} + \frac{1}{4\pi}\frac{e^{-\beta r}}{r^2} \tag{5}$$

where

$$\gamma = \frac{2k_a}{k_s} \cdot \frac{k^2 - \alpha^2}{\alpha^2 - k_a k} \tag{6}$$

$$\beta = \frac{5k}{4} \tag{7}$$

and

$$D = k_a/\alpha^2 \tag{8}$$

is the diffusion coefficient. The first term in (5) represents the asymptotic part of the optical distribution. The attenuation constant α is the inverse of the diffusion length (penetration depth) in the medium and is given by

$$\alpha \approx \sqrt{3k_a k}\,(1 - 2k_a/5k) \; . \tag{9}$$

The second term in (5) represents the optical flux in the rapidly changing or transient region close to the source.

Our next concern is how this point source solution to the transport equation might be modified in order to accommodate the effects of anisotropic scattering. It turns out that if the phase function given by (4) is used in place of isotropic scattering in the derivation from the Boltzmann equation, the same form for the space irradiance given by (5) results. However, since the effective scattering

coefficient is now reduced to account for the effects of anisotropic scattering, the total coefficient for scattering and absorption becomes

$$k = k_s(1 - g) + k_a \quad . \tag{10}$$

Equations (5), (7), (8) and (9) remain unchanged but (6) is modified to read

$$\gamma = \frac{2k_a}{(1-g)k_s} \cdot \frac{k^2 - \alpha^2}{\alpha^2 - k_a k} \quad . \tag{11}$$

The first term in equation (5) represents the asymptotic optical field from an isotropic point source in an infinite homogeneous medium. This expression is very similar to the solution from diffusion theory for the same problem, which is given next for comparison. The diffusion equation is derived from the transport equation under the assumption that the angular power $I(\underline{x},\underline{\Omega})$ is only weakly dependent on direction $\underline{\Omega}$. The steady state diffusion equation for the space irradiance is

$$\nabla^2\Phi - \frac{k_a}{D}\Phi = 0 \tag{12}$$

and the solution for a point source of unit power in spherical geometry is given by

$$\Phi(r) = \frac{1}{4\pi D} \frac{e^{-\alpha r}}{r} \tag{13}$$

Where α is given by $\alpha \approx \sqrt{3k_a k}$. The constant factor $1/4\pi D$ in the solution is obtained by considering a small sphere about the origin and requiring that the total power passing

through the sphere equal the source power (see for ex. Ref. 21 or 22).

The diffusion point source condition (13) is in fact an overestimate of the space irradiance at large distances. The first term in (5) is a better representation of the asymptotic distribution. The reason for this difference is that the diffusion solution underestimates the space irradiance at small distances, since it lacks the transient term in (5). Since the total optical power over all space from both solutions must be the same, the diffusion representation of the asymptotic field is higher to compensate.

The solution of the diffusion equation for a pencil beam of light has been solved by Johnson[9] for the case of isotropic scattering. This solution is an approximation for the field of a beam of light emerging from an optical fiber. We consider the inhomogeneous diffusion equation:

$$\nabla^2\Phi - \frac{k_a}{D}\Phi = \frac{-(1 - g)\cdot k_s\Gamma_o}{D} \qquad (14)$$

where Γ_o is the volume flux density of unscattered photons in $W\cdot m^{-2}$. This is the same as equation (9) in Johnson[9], except that the effective scattering coefficient $(1-g)k_s$ has been used in place of k_s. The right hand side of (14) represents sources produced by the initial scattering of light from the emerging beam. If we assume the phase function of equation (4), these photons are diffuse since

they are distributed isotropically by the first scattering event. The solution of (14) is straightforward by application of the Green's function technique, where the solution is constructed by integrating the solution for a point source over the volume density of photon sources. The correct asymptotic point source Green's function is given by the first term of (5), so that

$$\Phi(\underline{x}) = \frac{\gamma}{4\pi D} \int_V \frac{e^{-\alpha|x-x'|}}{|\underline{x}-\underline{x}'|} \cdot (1 - g)k_s \, \Gamma_o(\underline{x}') \, dV \qquad (15)$$

where $|\underline{x} - \underline{x}'|$ is the distance between the unscattered source photons and the field point $\underline{x}$.

In order to simplify the calculations from equation (15) the assumption is made that the diameter of the fiber optic tip is negligible. Also neglected are the beam divergence and refraction at the interface between tissue and fiber tip. In this approximation Γ_o is modelled as a line source that decreases exponentially at the rate $(1-g)k_s + k_a$, which is the rate of attenuation of the beam as it penetrates the tissue. We consider a spherical geometry with the optical source at the origin, emitting in the $\Theta=0$ direction. The optical distribution is independent of azimuthal angle so that equation (15) becomes

$$\Phi(r,\Theta) = \frac{\gamma}{4\pi D} \int_o^R \frac{e^{-\alpha|r-r'|}}{|\underline{r}-\underline{r}'|} \cdot (1 - g)k_s \, e^{-[(1-g)k_s+k_a]r'} \, dr' \qquad (16)$$

where $|\underline{r} - \underline{r}'| = (r^2 + r'^2 - 2rr'\cos\Theta)^{1/2}$.

Equation (16) can be approximated by the following expression:

$$\Phi(r,\Theta) \approx \Phi_o(\Theta) \frac{e^{-\alpha(\Theta)\cdot r}}{r} . \qquad (17)$$

This equation for the optical distribution was first tried ad hoc as a representation of experimental space irradiance data (see Results). However the same equation was found to be a good approximation to the results of calculations using equation (16). For fixed Θ, equation (16) was evaluated numerically at a representative series of values of r and equation (17) then fitted to these points with $\Phi_o(\Theta)$ and $\alpha(\Theta)$ as free parameters. Errors between equation (16) and (17) were typically less the 2% for values of radii r > 3 mm.

III. MATERIALS AND METHODS

A. Tumor Material

The tumor line used in these experiments was an anaplastic variant of the Dunning R3327 rat prostate adenocarcinoma which has been maintained at the Cross Cancer Institute since 1981 by serial implantation in the flanks of male Fisher X Copenhagen rats. The volumes of tumors used in light distribution experiments or as the source of samples for scattering and absorption coefficient measurements varied from 20 to 30 cm^3. Dissected tumors displayed poor vascularity and a fairly uniform beige/white color throughout most of the tumor, with the exception of the peripheral layer nearest the skin, which was moderately well

developed with blood vessels. The larger specimens had a somewhat darker necrotic core and occasional cysts. There appeared to be a general tendency to greater fluid content throughout the tissue as the tumor size increased. Tumors showing obvious cysts upon dissection were omitted from the study because of the effect of a semitransparent fluid region on optical propagation.

Samples used in the scattering and absorption coefficient studies were prepared from cubes of tissue with approximately 7 mm sides that were taken from intact tumors. Immediately after excision, the cubes were placed in a sample tube in a protective embedding medium (Tissue-Tek O.C.T. 4583, Miles Scientific, Il.) and quick-frozen in liquid nitrogen to minimize ice crystal formation and consequent cellular damage. Sections of 120 μm thickness were cut from the samples (either immediately or after frozen storage) using a cryostatic microtome and then placed between two 2.5 cm diameter circular glass plates. Three 3 mm square x 115 μm thick teflon spacers were placed between the plates near the edge and a thin strip of tape was attached around
the perimeter of the plates to prevent their relative movement. Tissue samples were always thawed completely prior to measurements being taken.

B. Goniometer

A goniometer was constructed as illustrated in Fig. III-1. The source of collimated light was a 1.0 mW linearly polarized helium-neon laser emitting at 632.8 nm. The laser was focussed by a 36 cm focal length lens to an approximately 1 mm diameter spot on the surface of the tumor sections. Circular apertures were placed immediately in front of and behind the lens to block stray light. Light intensity was measured using a radiometer on a 24 cm radius semicircular arc from 0° to 165° with respect to the direction of laser beam incidence. The regions between 70° to 110° and 165° to 180° were shadowed by the apparatus geometry. Measurements were taken at 0.5° intervals between 0° and 10°, at 12° and at 5° intervals from 15° to 70° and 110° to 165°. An aperture of 14 mm diameter was placed in front of the light detector active surface. At angles of less than 12°, a smaller (4 mm) diameter aperture corresponding to 1° of arc was used due to the higher scattered light intensity in this region, allowing more precise angular discrimination of the scattered light intensity.

The mean free path in each sample was calculated by applying Beer's law:

$$I = I_o e^{-d/\lambda} \qquad (18)$$

where

$\lambda = k^{-1}$ = mean free path

d = sample thickness

I = intensity of unscattered part of beam after traversing the sample

I_o = intensity of equivalent beam through a reference sample.

The angle subtended by the aperture when collecting the unscattered (primary) light I for mean free path measurements was 17 mRad. The reference samples were prepared in the same manner as the tissue samples except that the transparent O.C.T. embedding medium was used between the glass plates in place of a tissue section. Due to a close refractive index match to glass, the O.C.T. prevented spurious reflective losses in the reference sample by eliminating the internal air/glass interfaces. Specular reflection from the internal tissue/glass interfaces of the samples was estimated as less than 1% and hence neglected.

C. Absorbance Measurements

The absorbance of thin tissue sections was measured using the integrating sphere technique of Costa et al.[23] adapted to available equipment. Fig. III-2 shows a schematic of the integrating sphere arrangement; for clarity the upper hemisphere is not shown. The internal diameter of the integrating sphere was 12.7 cm. In its standard use, a sheet of 0.13 mm thick transparent plastic with a 2.1 x 3.2

cm oval barium sulfate reflectance coating at its center is held within the sphere as shown. The purpose of the coating is to produce a diffuse light distribution by reflecting a collimated beam striking the surface at 45° incidence. A known percentage of the diffuse light distribution is measured by a detector attached to the sampling port, providing an accurate (calibrated) measurement of the total power of the incident beam.

In this case the standard operation of the integrating sphere was modified for absorbance measurements by placing the sample to be measured near the center of the sphere, intercepting the path of the laser beam before it struck the reflectance coating. The same arrangement as in the goniometer experiment was used for focussing the laser beam onto the sample. Provision was made to move the integrating sphere along the vertical axis in order to obtain the average absorption from various locations in the sample. Depending on the width of the tissue section, between 8 and 12 separate measurements were taken. Identical series of measurements were done on a reference sample both before and after each tissue sample in order to account for small systematic fluctuations in laser beam intensity.

The absorption coefficient for each sample was obtained from

$$k_a = -(1\sqrt{2}C_r t)\ \ln\ (I/I_o) \qquad (19)$$

where

I = integrated intensity from the sample

I_o = integrated intensity from a reference sample

t = sample thickness

C_r= correction for refraction at the glass plate interfaces.

D. Space Irradiance Measurements

The source of optical distributions within R3327-AT tumors was an implanted optical fiber fed by an argon-ion pumped dye laser as the light source. The dye laser, tuned by a dichroic mirror, emitted at 630 nm with an approximately 0.05 nm full width at half maximum line width. The light intensity emitted from the source fiber was kept constant for each tumor and was monitored by sampling a small fraction of the input laser beam. Source intensities of 80-120 mW were used, low enough to prevent changes in tissue optical properties due to thermal effects

A second implanted optical fiber acted as a probe, collecting a portion of the light distribution at a given location. The length of the probe fiber from the tumor to

the radiometer was 1 m. Both source and probe fibers were held inside stainless steel needles to provide rigidity, minimizing lateral movement of the fiber during insertion which could result from density variations in the tumor and/or tissue compression at the needle and fiber tip. The end of each holding needle was filed flat and the edge was sharpened around the circumference of the needle tip to facilitate penetration into the tissue. The optical fibers were flat-cleaved and positioned so that the flat surface was aligned with the tip of the holding needle. A calibrated positioning stand was constructed which allowed for insertion of the probe fiber into excised tumors in 1 mm steps (with 0.1 mm accuracy) from four different directions, as indicated in Fig. III-3. Because of azimuthal symmetry, measurements were needed in only a single plane containing the source fiber.

Two series of light distribution measurements were performed using different sizes of fiber and needle assemblies. In experiment #1, a 0.6 mm diameter fused silica core optical fiber was used with 1.48 mm outer diameter stainless steel needle. In experiment #2, a 0.3 mm diameter fused silica core fiber was used with a 0.91 mm outer diameter stainless needle. Measurement series were taken from each of the four directions beginning 20 mm from the source fiber tip, moving towards the source and continuing past it and ending the same distance away, pointing away from the source tip. In

both experiments, it was not possible to obtain the full 40 mm ranges of data for all the tumors since the periphery of some tumors was less than 20 mm from the source fiber tip.

The optical powers in Watts registered by the radiometer attached to an implanted probe fiber for various locations and orientations are indicated by $p(r,\Theta;\varphi)$ in Fig.III-3. The argument Θ indicates one of the four (positive) axes, corresponding to 0, $\pi/2$, π or $3\pi/2$ radians and r is the radial distance from the source fiber tip. The actual positions of the probe fibers were displaced somewhat from the indicated axes because of interference by the source fiber. The argument φ indicates the direction of light propagation corresponding to the probe orientation, defined by the normal to the flat surface of the fiber tip. For isotropically distributed light, radiance is independent of the optical propagation vector $\underline{\Omega}$. In this case the space irradiance $\Phi(r,\Theta)$ is related to the measured optical power by

$$\Phi(r,\Theta) = \frac{4\pi}{\Omega_a} \cdot \frac{p(r,\Theta;\varphi)}{A_c}$$

A_c is the cross-sectional area of the probe fiber core and Ω_a is the acceptance solid angle of the probe fiber in tissue, which is given by

$$\Omega_a = 2\pi[1 - \cos(\sin^{-1}\frac{NA}{n})] \qquad (21)$$

where NA is the numerical aperture of the optical fiber and n is the refractive index of tissue. For non-isotropically distributed light the magnitude of $p(r,\Theta;\varphi)$ depends on the

probe orientation corresponding to to φ and equation (20) must be modified to represent an appropriate angular average. In the experiments described above, on each axis two measurement series of 40 mm length were taken by probe fibers inserted from opposite sides of the tumor. The space irradiance $\Phi(r,\Theta)$ was therefore estimated from the average of two distinct, oppositely oriented probe measurements $p(r,\Theta;\varphi)$ at each location.

IV. RESULTS AND ANALYSIS

A. Scattering and Absorption Measurements on Thin Tissue Sections

The results of scattering and absorption coefficient measurements are summarized in the first column of Table III-1. All bracketed numbers in the Tables and the text correspond to 95% confidence intervals.

A mean free path of 37 (±16) μm was the average of values obtained by application of Beer's Law to transmission data from the goniometer. Nine tissue sections taken from various locations in two different tumors were measured. The thickness of the tissue sections was 115 μm, corresponding to approximately 3 mean free paths. In view of this, it was necessary to consider the possible influence of multiple scattering on the mean free path results. Direct evidence of multiple scattering was a diffuse glow that could be seen in the tissue sample in the area adjacent

to the focal spot of the laser beam. One possible effect was that of light being scattered out of the narrow (17 mRad) acceptance angle of the detector and then scattered back into it. This would increase the apparent mean free path by increasing the value of I in equation (18). This specific effect has been investigated by Crilly[24], who measured apparent mean free path versus sample thickness in a variety of tissues including human blood, muscle, adipose and lactating gland and pig testis and brain. It was found that the apparent mean free path differed from its actual (extrapolated) value by less than 10% in all cases, providing the sample thickness was no greater than 3.2 to 6.9 times the mean free path. This particular effect of multiple scattering was therefore discounted in the current experiment.

The mean cosine of scattering was the other parameter derived from the goniometer experiment. Calculations based on equation (3) were performed on the angular scattering distribution of each of five tissue sections from two different tumors, yielding an average value of mean cosine of 0.86 (± 0.08). In the calculations, each set of data was corrected for angle-dependent refraction at the air-glass interface. Light that was registered twice due to overlapping measurements at angles less that 10° was taken into account. An additional correction was applied to the goniometer data to compensate for the cosΘ dependence of

light intensity from a surface, where Θ is the angle between the measurement location and the surface normal. The semi-log plot in Fig. III-4 is the average of five experimental distributions, showing a sharp peak centered at 0° and a much lower background. There is also a suggestion of a second peak, smaller than the forward peak, centered at 180°; however this could not be resolved due to the limitations of the experimental setup. Multiple scattering was expected to affect the calculated value of mean cosine by increasing the apparent angle of scattering. Unfortunately, it was not feasible in our experiment to use thinner slabs because of the low intensity and "noisy" appearance of the angular scattered light signal. The value of $g = 0.86$ must therefore be considered a lower limit on the actual value of the mean scattering cosine.

Absorption coefficients were calculated as discussed in the methods section, to yield an average of $k_a = 0.49\ cm^{-1}$ for five samples. These values do not take into account the increased effective path length in the samples due to multiple scattering, which would be expected to result in an overestimate of the absorbance.

B. Space Irradiance Measurements

Figure III-5 shows the average of space irradiance fall-off curves of six tumors in experiment #1 on the forward, side and back axes. The data was adjusted to 100 mW input power.

These curves display a significant difference in overall intensity among the three axes. The equivalent average fall-off curves from experiment #2 are not shown but gave a similar result. As was discussed previously, the space irradiance at each position was estimated by taking the average of measurements using two oppositely oriented probe fibers. In other words, the fiber tip was at the same location for each of the two measurements, the probes having been inserted from opposite sides of the tumor. For example, for a point on the $\Theta=0$ axis at distance r from the source fiber tip, the space irradiance was calculated from the average of the measured directional fluxes $p(r,0;0)$ and $p(r,0;\pi)$. Typical uncertainties for the space irradiance at a given position among the tumors in each experiment were 30-40%.

In order to verify that the space irradiance attenuation was consistent with the model given by equation (17), least squares fits to the average experimental data using equation (17) with $\Phi_o(\Theta)$ and $\alpha(\Theta)$ as free parameters are given in Fig.III-5 (dashed lines). No assumptions about the tissue optical constants (i.e. k_s,k_a,g) were necessary for this procedure since equation (16) was not used. Equation (17) was also fitted in the same way to the attenuation data of each of the four positive axes for each individual tumor. The resulting values of $\Phi_o(\Theta)$ and $\alpha(\Theta)$ from individual tumors were averaged for each experiment and are listed in

Table III-2 as experimental values. A total of six tumors were included in experiment #1 and eight tumors in experiment #2.

C. Transport Equation Solution

Theoretical fall-off curves for an "average" tumor in each of the two experiments were produced by using equation (16) to calculate the space irradiance at 1 mm intervals from the source fiber tip. Equation (17) was then fitted to these curves in the same way as it was fitted to the experimental fall-off data to generate the "best theoretical fit" values of $\Phi_o(\Theta)$ and $\alpha(\Theta)$ in Table III-2.

The choice of k_s, k_a, g and α used in equation (16) to produce these results was guided by two considerations. First, the values had to be consistent with the experimentally determined optical constants given in Table III-1 and second, the calculations from (16) had to reproduce reasonably well the space irradiance distributions in the tumors. A number of parameter sets were tried in equation (16) before arriving at the values given in Table III-1, which appeared to best fulfill the above requirements.

D. Comparison of Experimental and Theoretical Space Irradiance

In comparing the experimental and theoretical values of $\Phi_o(\Theta)$ and $\alpha(\Theta)$ in Table III-2, two main sources of error

need to be addressed. The first difficulty is that using equation (16) to calculate the space irradiance along the forward ($\Theta=0$) axis requires the integral upper bound to be truncated. In particular, upper bounds were chosen as the point at which the unscattered beam intensity was equal to 10% of its initial amplitude. This corresponded to distances from the source of 3.1 mm and 4.4 mm in experiments #1 and #2 respectively. The theoretical values of $\Phi_o(\Theta)$ resulting from using an integral upper bound of 2 cm in equation (16) were calculated for the $\Theta=\pi/2$ and the $\Theta=\pi$ and the $\Theta=\pi$ axes for comparison. For experiment #1 the resulting $\Phi_o(\Theta)$ were 4% and 2% greater than when using the 3.1 mm upper bound. For experiment #2 the difference was less than 1% for both axes. The errors on the $\Theta=0$ axis were necessarily greater since these points were closer to the neglected unscattered portion of the source beam. As an example of the far field error, the space irradiance (16) was calculated for $\Theta=0$, r=2 cm, using an upper bound of 1 cm. The corresponding calculations for experiment #1 and #2 using 3.1 mm and 4.4 mm were smaller than these results by 34% and 38% respectively.

Figures III-6 and III-7 present the space irradiance attenuation data along with the theoretical curves in a manner which illustrates the forward axis error in the near field. Square symbols on each figure represent the ratio of the measured space irradiance on the $\Theta=\pi/2$ and $\Theta=3\pi/2$ axes (averaged together) to the space irradiance on the $\Theta=0$ axis, averaged over the group of tumors in the experiment. Circular symbols represent the ratios of the measured $\Theta=\pi$ axis space irradiance to the $\Theta=0$ axis space irradiance. Typical uncertainties for individual points were 20-30%. The discrepancies between experimental and calculated ratios on the upper curves of each figure were concentrated in the region less that 6 mm from the source fiber tip. The discrepancies were magnified at points approaching the integral cutoff due to the singularity in the source integral, which causes an overestimate in the forward axis irradiance.

The other major source of error between theory and experiment was due to light scattering and absorption caused by the source as well as the probe fiber/needle assemblies. The blocking and absorption of optical flux would be expected to be greatest in the vicinity of the source fiber assembly which would tend to decrease the measured space irradiance along the $\Theta=\pi$ axis. This is borne out by comparing the theoretical $\Theta=\pi$ to $\Theta=0$ axis ratio curves with the experimental ratios in Figs. III-6 and III-7 (lower

curves and circles). As expected, in both cases the experimental space irradiance on the $\Theta=\pi$ axis was lower than predicted. This discrepancy was more pronounced in experiment #1, where the cross-sectional area of the holding needle was 2.6 times as large as in experiment #2.

Apart from the above problems, the theoretical values of the leading constants $\Phi_o(\Theta)$ in Table III-2 are in relatively good agreement with the experimental $\Phi_o(\Theta)$, which had uncertainties ranging between 30 and 70%. The attenuation constants $\alpha(\Theta)$ are also consistent with experimental values. Lastly, it should be noted that the predicted space irradiance was lower than that of diffusion theory by the factors $\gamma = 0.94$ and $\gamma = 0.91$ in experiments #1 and #2 respectively.

V. DISCUSSION

It appears that forward scattering is an essential characteristic of tissue which plays an important role in establishing overall optical distribution. The observed anisotropic distributions from a pencil beam source contrast with the symmetrical, circular optical distributions predicted by diffusion theory[9]. The relationship among optical parameters given by equation (9) also governs the penetration of broad beams used in photodermatology. As previously suggested by Diffey[17] as well as by the data presented here, the use of the standard Kubelka-Munk model[25]

may have to be reevaluated in this and other applications due to its neglect of forward scattering.

Another implication of scattering anisotropy is that the local microscopic angular distribution of light (i.e. the radiance) may not become isotropic until the beam penetrates relatively deeply into tissue. Images of tumors and blood vessels in breast tissue can be routinely resolved using diaphonography at red and near infrared wavelengths at a depth of 2 cm [26]. It is difficult to see how information from an implanted object at this depth could be transmitted if the angular distribution becomes nearly isotropic after a few mm only, as has been suggested on the basis of diffusion theory [7].

It is interesting to compare the experimental and theoretical results for the mean cosine of scattering in R3327-AT tumor tissue with other published reports. Recently Jacques and Prahl[27] compared a one-dimensional solution to the transport equation with reflectance and transmission data from albino mouse dermis at 488 nm. Values were derived for absorption coefficient k_a, scattering coefficient k_s and scattering anisotropy g of 2.8 cm^{-1}, 239 cm^{-1} and 0.74 respectively. By comparison with these results, R3327 tumor at 630 nm shows lower absorption, approximately the same scattering coefficient and a greater degree of forward scattering. The latter point is

consistent with the data of Bruls and van der Leun[12] who showed that forward scattering is generally greater at longer wavelengths. A more comprehensive series of experiments by Flock et al.[28] has confirmed and extended these observations of forward scattering in tissue. Measurements of mean scattering cosine for chicken and bovine muscle, pig brain and 1% human blood were all in the range 0.94 - 0.974. The mean cosine of VX-2 tumor was somewhat lower at 0.639. In all cases, the tissue sample thickness in these scattering experiments exceeded the mean free path in the sample, as in the measurements of R3327-AT tumor reported here. For this reason, the mean cosine of these tissues may also have been underestimated due to multiple scattering effects.

Although it was not employed in the present study, the approximate point source solution given by equation (13) can also be useful in estimating the tissue optical constants, including mean cosine of scattering. This may be illustrated by applying this solution to published data of Svaasand and Ellingsen[7], who measured optical distributions at various visible wavelengths from 200 μm diameter optical fibers implanted in human brain tissue. In this study, experimental data was given in terms of a factor denoted by k_s, which defines the absolute value of space irradiance and thus can be converted into the constant $1/4\pi D$ that precedes the exponential in (13). Data was also given for the

attenuation coefficient α (inverse diffusion length). If these results are combined, then k_a can be calculated via the formula $k_a = \alpha^2 D$. For example, a range of values of k_s of between 1.7 and 2.0 is given for 635 nm light in adult human brain and a typical value of diffusion length of 1.2 mm is suggested. These values yield a range for the absorption coefficient of between 1.53 and 1.8 cm^{-1}. The analysis can be carried a step further if the mean free path of the tissue is known. For example if the mean free path of 12 μm measured by Crilly[24] for porcine brain is used in equation (9), a range of mean cosine g is obtained of between 0.982 and 0.984 which is comparable to the range for g given in Table III-1.

VI. CONCLUSIONS

Attenuation measurements from implanted fiber optic sources in R3327-AT tumors show that light penetration is greatest in the direction of the beam itself and least in the backwards direction. This anisotropy of the spatial distribution of light persists to distances of at least 2 cm from the source and is a result of strong anisotropy in the scattering phase function.

Predictions of space irradiance utilizing the transport approximation show general agreement with experimental space irradiance results. Moreover, the specific optical constants used in the model are consistent with actual

measured values of scattering, absorption and attenuation coefficients. The theory can be applied to other optical sources, for example broad or implanted cylindrical irradiators[29] and should be useful in future studies of amorphous media with known forward scattering properties including blood[30], tissue and tissue-equivalent optical phantoms.

TABLE III-1
R3327-AT Tumor Optical Constants

	Measurements on thin tissue sections	Best theoretical fit to space irradiance data	
		Expt.1	Expt.2
Mean free path (μm)	37 ±16	40	40
Absorption coefficient (cm^{-1})	0.49 ±0.44	0.54	0.60
Mean cosine of scattering	>0.86	0.970	0.979

TABLE III-2
Comparison of experimental attenuation data with best theoretical fit using equations (16) and (17).

Experiment 1

	$\Phi_o(\Theta)$ (mW·cm^{-1})		$\alpha(\Theta)$ (cm^{-1})	
Axis (Θ)	Expt.	Theory	Expt.	Theory
0	220 ±75	296	3.67 ±0.46	3.62
$\pi/2$	93 ±65	143	3.41 ±0.38	3.47
π	34 ±9.5	99	3.52 ±0.35	3.45

Experiment 2

	$\Phi_o(\Theta)$ (mW·cm^{-1})		$\alpha(\Theta)$ (cm^{-1})	
Axis (Θ)	Expt.	Theory	Expt.	Theory
0	310 ±108	282	3.20 ±0.39	3.33
$\pi/2$	113 ±51	95	3.04 ±0.28	3.06
π	77 ±45	60	3.21 ±0.38	3.04

Note: All data is adjusted to 100 mW source strength

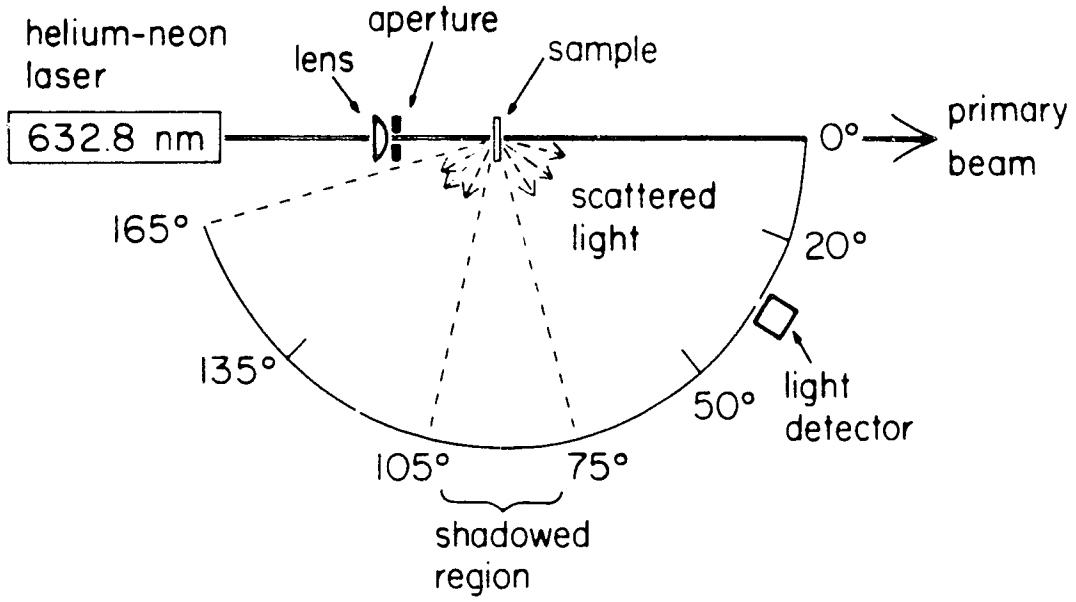

Fig.III-1 Goniometer schematic for measuring angular scattering distributions of tissue section.

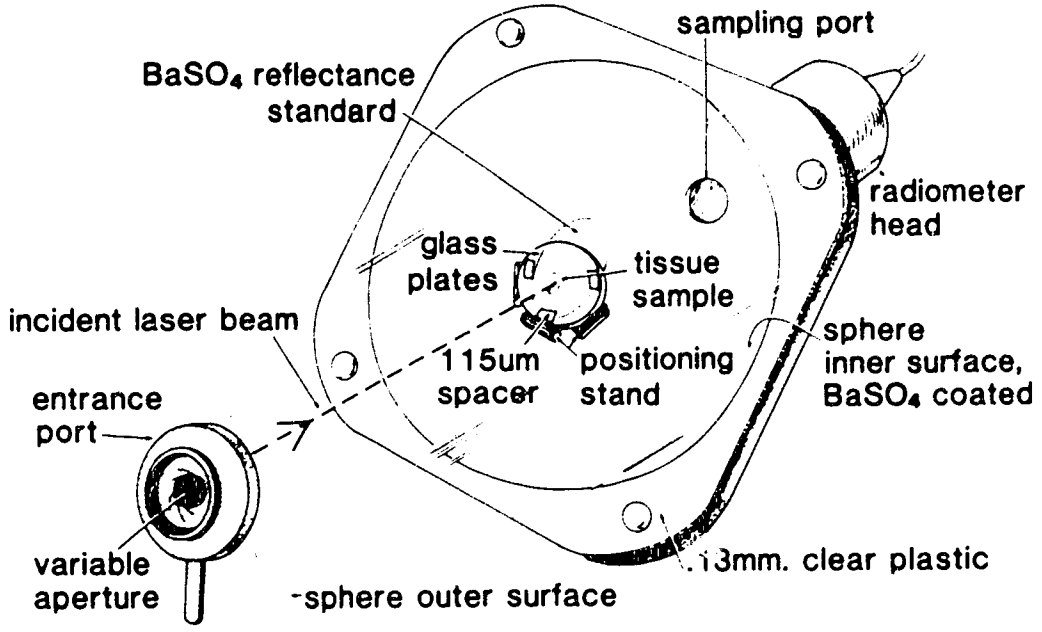

Fig.III-2 Cut-away view of integrating sphere for absorbance measurements of tissue sections.

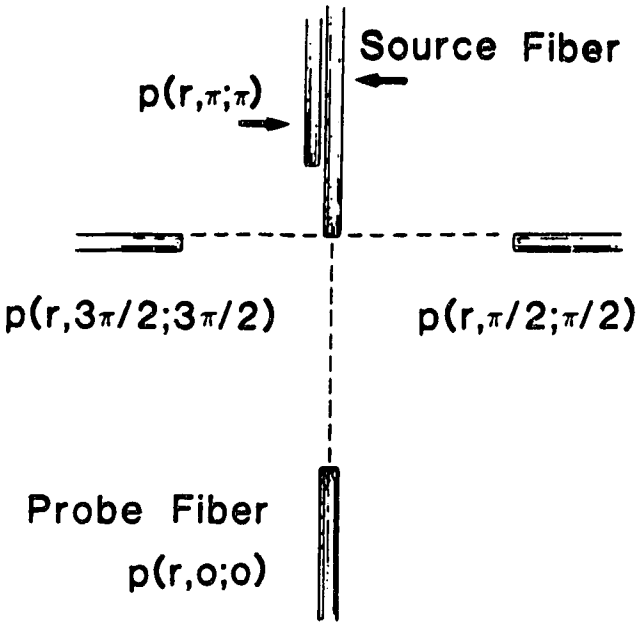

Fig.III-3 Schematic of space irradiance measurements with probe locations and orientations labeled according to rotation in the text.

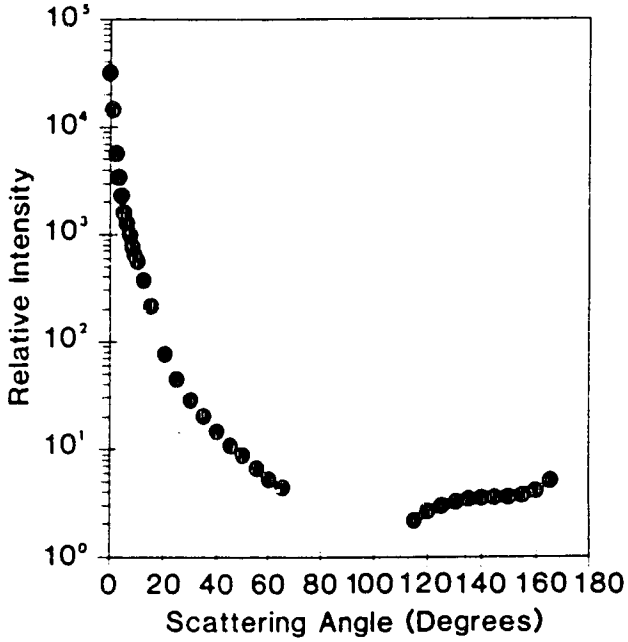

Fig.III-4 Mean angular scattering distribution of five 115 μm thick sections of R3327-AT tumor. Shown is the raw data before applying the correction described in the text.

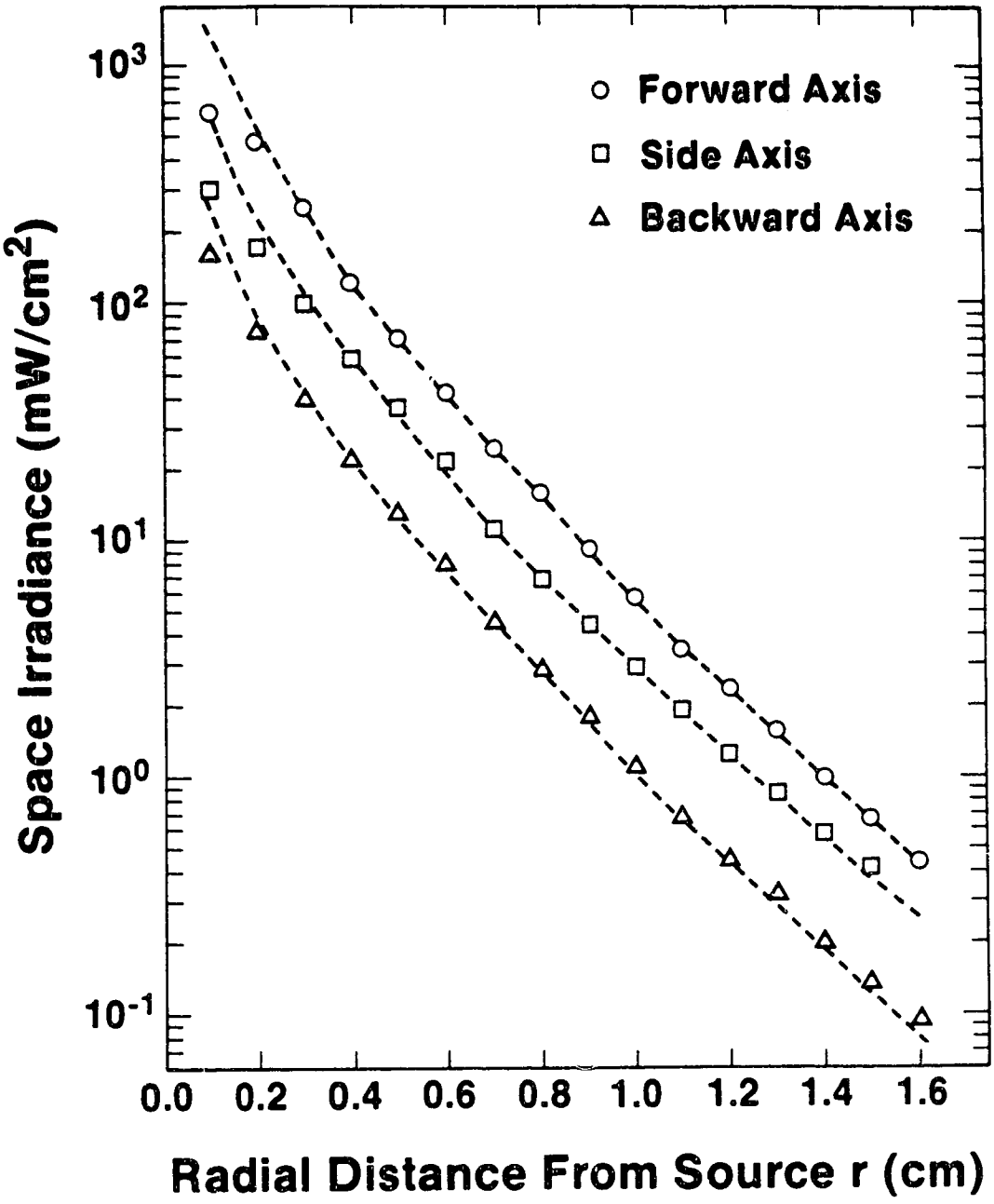

Fig.III-5 Space irradiance vs distance from source along forward, side and back axes. Shown is the average of the six tumors in experiment 1, together with curves fitted to the experimental data according to equation (17).

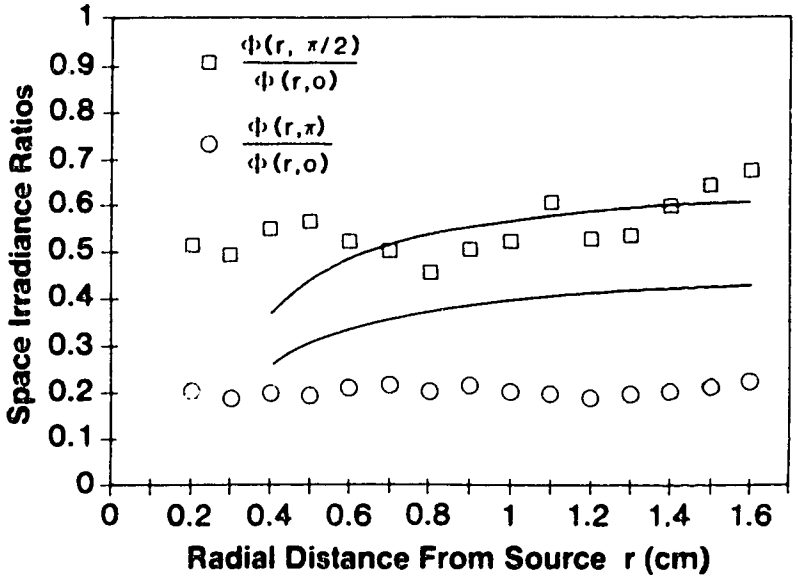

Fig.III-6 Space irradiance ratios from experiment 1 using 0.6 mm diameter core fiber optic source and probes. Square symbols and upper theoretical curve correspond to ration $\Phi(r,\pi/2)/\Phi(r,0)$. Circular symbols and lower theoretical curve correspond to ratio $\Phi(r,\pi)/\Phi(r,0)$.

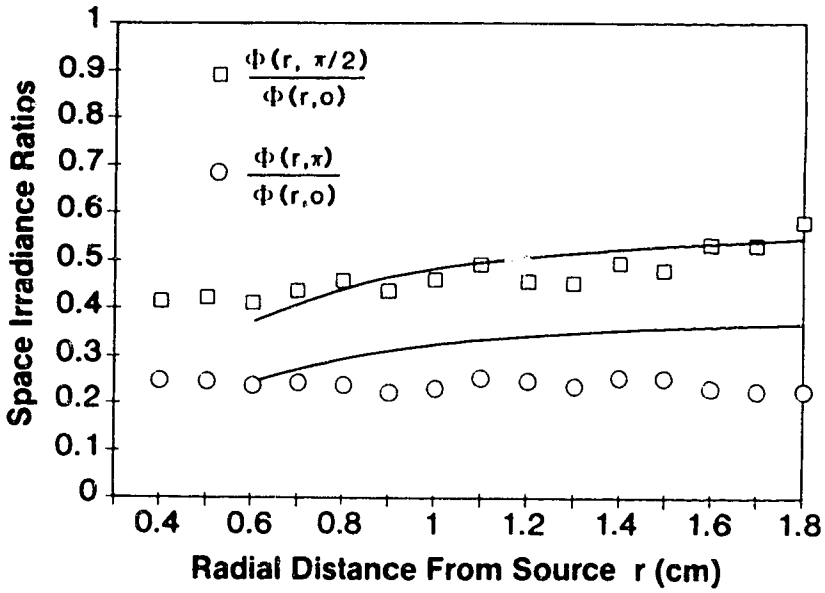

Fig.III-7 Space irradiance ratios from experiment 2 using 0.3 mm diameter core fiber optic source and probes. Square symbols and upper theoretical curve correspond to ratio $\Phi(r,\pi/2)/\Phi(r,0)$. Circular symbols and lower theoretical curve correspond to ratio $\Phi(r,\pi)/\Phi(r,0)$.

LITERATURE CITED

1. B.C. Wilson and M.S. Patterson,"The physics of photodynamic therapy," Phys. Med. Biol. 31:327-360, 1986.

2. B.C. Wilson and G.Adam." A Monte Carlo model for the absorption and flux distribution of light in tissue," Med. Phys. 10:824-830, 1983.

3. S. Chandrasekhar, Radiative Transfer. New York: Dover, 1960.

4. R.L. Fante," Relationship between radiative-transport theory and Maxwell's equation in dielectric median" J. Opt. Soc. Amer. 71:460-468, 1981.

5. B.C. Wilson, W.P. Jeeves, and D.M. Lowe, "In vivo and post mortem measurements of the atttenuation spectra of light in mammalian tissues, "Photochem. Photobiol. 42:153-162, 1985.

6. J. Eichler, J. Knof, and H. Lenz, "Measurements on the depth of penetration of light (0.35-1.0 μm) in tissue," Rad. Environ. Biophys. 14:239-242, 1977.

7. L.O. Svassand and R. Ellingsen, "Optical properties of human brain," Photochem. Photobiol. 38:293-299, 1983.

8. D.R. Doiron, L.O. Svaasand and A.E. Profio, "Light dosimetry in tissue: Application to photoradiation therapy, " In: Porphyrin Photosensitization, D. Kessel and T. J. Dougherty (eds.). New York: Plenum, 1981, pp.63-76.

9. C.C. Johnson, "Optical diffusion in blood," IEEE Trans. Biomed. Eng. BME-17:129-133, 1970.

10. L. Reynolds, C. Johnson and A. Ishimaru, "Diffuse reflectance from a finite blood medium: Applications to the modeling of fiber optic catheters," Appl. Opt. 15:2059-2067, 1976.

11. M. Kerker, The Scattering of Light. New York:Academic, 1969.

12. W.A.G. Bruls and J.C. van der Leun, "Forward scattering properties of human epidermal layers," Photochem. Photobiol. 40:231-242, 1984.

13. I. Fine, E. Loewinger, A. Weinreb and D. Weinberger, "Optical properties of the sclera," Phys. Med. Biol. 30:565-571, 1985.

14. P.A. Wilksch, F. Jacka and A.J. Blake, "Studies of light propagation through tissue," In: Porphyrin Localization and Treatment of Tumors, D.R. Gomer and C.J. Gomer (eds.). New York: Alan R. Liss, 1984, pp.149-161.

15. R.P. Hemenger, "Optical properties of turbid media with specularly reflecting boundaries: Applications to biological problems," Appl. Opt. 16:2007-2012, 1977.

16. K.D. Lathrop, "Anisotropic scattering approximations in the monoenergetic Boltzmann equation," Nucl. Sci. Eng. 21:498-508, 1965.

17. B.L. Diffey," A mathematical model for ultraviolet optics in skin," Phys. Med. Biol. 28:647-657, 1983.

18. B. Davison, Neutron Transport Theory. Oxford: Clarendon, 1957.

19. S. Gonzalez, M.R. Arnfield, B.E. Meeker, J. Tulip, W.H. Lakey, J.D. Chapman and M.S. McPhee, "Treatment of Dunning R3327-AT rat prostate tumors with photodynamic therapy in combination with misonidazole," Cancer Res. 46:2858-2862, 1986.

20. D.M. Lubaroff, L. Canfield and C.W. Reynolds, "The Dunning tumors," In: Models for Prostate Cancer. New York: Alan R. Liss, 1980, pp 243-263.

21. A.M. Weinberg and E.P. Wigner, The Physical Theory of Neutron Chain Reactors. Chicago, Il: Chicago Press, 1958.

22. S. Glasstone and A. Sesonske, Nuclear Reactor Engineering, 3rd ed. Princeton, NJ: Van Nostrand, 1982.

23. L.F. Costa, F. Grum, and T.E. Wightman, "Direct absorptance measurement of florescent and turbid samples in a 4π geometry," Color Res. Appl. 1:183-200, 1976.

24. R. Crilly, M.Sc. thesis, Univ. Alberta, Edmonton, Canada, 1987.

25. S.Wan, R.R. Anderson and J. A. Parrish, "Analytical modeling for the optical properties of the skin with in vitro and in vivo applications," Photochem. Photobiol. 34:493-499, 1981.

26. R.J. Bartrum, Jr. and H.C. Crow, "Transillumination lightscanning to diagnose breast cancer: A feasibility study," Amer. J. Roent. 142:409-414, 1984.

27. S.L. Jacques and S. A. Prahl, "Modeling optical and thermal distributions in tissue during laser irradiation," Lasers Surg. Med. 6:494-503, 1987.

28. S.T. Flock, B.C. Wilson and M.S. Patterson, "Total attenuation coefficients and scattering phase functions of tissues and phantom materials at 633 nm," Med. Phys. 14:835-841, 1987.

29. M. Arnfield, S. Gonzalez, P. Lea, J. Tulip and M McPhee, "Cylindrical irradiator fiber tip for photodynamic therapy," Lasers Surg.Med. 6:150-154, 1986.

30. G.D. Pederson, N.J. McCormick and L.O. Reynolds, "Transport calculations for light scattering in blood," Biophys. J. 16:199-297, 1976.

Chapter IV: OPTICAL DOSIMETRY FOR INTERSTITIAL PHOTODYNAMIC THERAPY*

I. INTRODUCTION

Photodynamic therapy has received increasing attention as a treatment method for various cancers. Most successful treatments to date have involved superficial tumors, including tumors of the lung, bladder, head and neck, and skin [1]. Significant problems however, may be associated with the effective treatment of large, invasive lesions. Since the presence of oxygen in tissue is necessary in order to initiate the photochemical reaction, regions of hypoxia in larger tumors may limit the therapeutic response [2-4]. Another problem is the limited penetration of light in tissue, which may prevent a sufficient light dose from being delivered to the tumor.

Limited light penetration has led various investigators to attempt the treatment of some solid tumors by the direct implantation of fiber optics, coupled to a dye laser [3-7]. Improvements in the uniformity of the optical distribution may be achieved by the addition of diffusing tips to the optical fibers[3,4,8,9] and by the introduction of multiple sources within a single tumor mass[3,4,7]. This interstitial

* A version of this chapter has been accepted for publication . M.R. Arnfield, M.P. Chetner, J. Tulip and M.S. McPhee, "Optical dosimetry for interstitial photodynamic therapy," Medical Physics, in press.

application of light has created the need for accurate light dosimetry. Bolin et al.[10] investigated theoretical factors which influence the optimum placement of multiple fiber optic sources in tumors. Isodose distributions in tissue have been mapped experimentally using a photographic method[11] and by measurements with fiber optic probes in a three dimensional grid [12].

Some of the theoretical models of light propagation in tissue that have been proposed include diffusion theory [13,14], the transport approximation[15] and a multiple flux model[16]. A number of experimental studies have provided information about optical properties of a variety of tissue types. These studies have demonstrated that the optical attenuation coefficient (i.e. the inverse penetration depth) is highly variable not only from one tissue to another, but also among samples of the same type of tissue [13,14,17,18]. This fact presents a difficulty in predicting dose distributions accurately within any particular tissue volume.

Cancer of the prostate is the second most common cancer among North American men. The Dunning R3327-AT rat prostate adenocarcinoma is an anaplastic tumor model with similarities to human prostate cancer[19]. This model has been used to test the efficacy of multiple fiber interstitial photodynamic therapy with the ultimate aim of

applying it to human prostate cancer [3,4]. We report here the results of a series of experiments using the R3327-AT tumor, which were carried out in order to evaluate a new technique with potential application to in vivo interstitial dosimetry.

II. THEORY

Recent studies have focussed on the details of light scattering interactions in soft tissue[15,20,21]. With the notable exception of dark colored organs (eg. spleen, liver), in most tissues the scattering coefficient for 630 nm light exceeds the absorption coefficient by approximately two orders of magnitude[17]. Another key characteristic of light scattering in tissue is it's anisotropy; a singly scattered photon is much more likely to be scattered from its original direction of motion by a small angle than by a large angle. As is well known from transport theory, the effects of forward scattering can be approximated by reducing the value of the scattering coefficient by an amount proportional to 1-g, where g is the mean cosine of scattering, defined as

$$g = \int_{-1}^{1} \mu \, f(\mu) \, d\mu \quad . \qquad (1)$$

In this expression μ is the cosine of the angle between the incident and scattered light and $f(\mu)$ is the angular scattering phase function. The reduced scattering coefficient may also called the transport coefficient, k_{tr},

by analogy with the transport cross-section of neutron transport theory [22]. It is given by

$$k_{tr} = (1-g)k_s \qquad (2)$$

where k_s is the scattering coefficient.

A simple model of light distribution in an absorbing and isotropically scattering medium has been described which is more accurate that diffusion theory[23]. This formula can be applied to the case of an anisotropically scattering medium, by replacing everywhere the isotropic scattering coefficient by the transport coefficient k_{tr}. In this approximation, the space irradiance at distance r from an isotropic point source of unit power is given by

$$\Phi(r) = \frac{\gamma}{4\pi Dr} e^{-\alpha r} + \frac{1}{4\pi r^2} e^{-(5/4)kr} \qquad (3)$$

where

$$D = k_a/\alpha^2 \qquad (4)$$

$$k = k_{tr} + k_a \qquad (5)$$

$$\gamma = \frac{2k_a}{k_{tr}} \cdot \frac{k^2 - \alpha^2}{\alpha^2 - k_a k} \qquad (6)$$

and

$$\alpha = \sqrt{3k_a k}\,(1 - (2k_a)/(5k)) \quad . \qquad (7)$$

D is the diffusion coefficient, k_a is the absorption coefficient, k is the total effective coefficient for scattering and absorption, γ is a parameter accounting for absorption in the region close to the source and α is the attenuation coefficient (inverse penetration depth).

For isotropic scattering, equation (3) agrees within 1% with the rigorous solution to the transport equation for a point source, providing the ratio of scattering coefficient to the sum of the scattering and absorption coefficients exceeds 0.9 [23]. The equivalent condition for anisotropic scattering is $k_{tr}/k > 0.9$. In this scattering dominant case, the first term in (3), which represents the asymptotic distribution, dominates the second term, which mainly represents photons coming directly from the source. In fact for typical R3327-AT tumor optical parameters, the second term represents less than 1% of the right hand side of (3) at distances greater than 3 mm from the source. For this reason it is neglected in the analysis that follows.

For interstitial phototherapy, a source emitting along a cylindrical length improves the uniformity of light distribution in tissue. A cylindrical source may be approximated as a sum of discrete point sources, each point source representing a different section along its length. We seek to represent the space irradiance $\Phi(\underline{x})$ arising from a cylindrical source of power p_o, with the end points of the emitting region located at positions $\underline{x}_1$ and $\underline{x}_2$. The source can be divided into N sections, each section being associated with a point source located at its center. These point sources are assigned weights w(i), which account for non-uniform emission along the length of the source. The

space irradiance is given by

$$\Phi(\underline{x}) = \frac{p_o \gamma}{4\pi D} \sum_{i=1}^{N} w(i) \frac{e^{-\alpha \cdot X(i)}}{X(i)} \qquad (8)$$

where

$$X(i) = \left| \underline{x} - \underline{x}_1 - \frac{(i-0.5)}{N} \cdot (\underline{x}_2 - \underline{x}_1) \right| \qquad (9)$$

and

$$\sum_{i=1}^{N} w(i) = 1 \quad . \qquad (10)$$

In real tissue the attenuation α is not constant, but varies with position depending on the local tissue density, fluid content, blood supply, and other factors. Thus, the value of α appearing in (8) is an approximation which represents an average attenuation coefficient in the tissue region between the field point and the cylindrical source.

III. MATERIALS AND METHODS

A. Tumors

All experiments were performed using R3327-AT tumors, grown in the flanks of male Fisher X Copenhagen f1 hybrid rats. Seven tumors with an average volume of 14 cm^3 were used. Tumors were excised prior to the experiments to facilitate access to the tumor.

Figure IV-1 illustrates the experimental setup. The tumor was placed behind a fixed template and a flat plate was then positioned behind the tumor to prevent movement during the experiment. One panel of the template had been prepared

with a series of holes in a grid pattern with the hole centers 2.35 mm apart. Four translucent 2 mm outer diameter plastic needles were inserted through the template into the tumor to form a square with 9.4 mm spacing. Steel inserts were used within the plastic needles during insertion to ensure that they were inserted parallel to one another. The presence of the four needles in the tissue largely prevented tissue sag during the measurements. There did not appear to be any significant blood drainage during the experiments, consistent with the poor vascularity of the R3327-AT tumor[19]. Dissection of tumors after the experiments showed minimal blood pooling at the needle locations.

B. Calibration of Sources

The four fiber optic sources that were used in the experiments were illuminated by an argon pumped dye laser, tuned to 630 nm. The laser beam was split equally four ways and focussed onto the proximal ends of four 600 μm core diameter fused silica optical fibers. A cylindrical irradiator fiber tip was attached to the distal end of each fiber, as previously described[9].

Measurements were performed on each cylindrical tip to determine the weighting parameters w(i). The measurements were done with the tip inside a plastic needle, to account for light scattering by the needle itself as well as possible fiber tip/needle interface effects. A 1 mm wide by

2 mm long slit in front of a radiometer was placed against the plastic needle containing the cylindrical source. The needle and source were then moved in 1 mm steps in the direction of the source axis with a light reading being taken at each step. Each reading corresponded to a 1 mm wide cross-sectional slice of the needle, giving a direct measure of w(i). Azimuthal variation of the source output was checked by rotating the tip 180° and repeating the above procedure. The azimuthal variation for individual tips was approximately 5%.

C. Fiber Optic Probes

Two types of miniature light detectors were constructed from optical fibers. The first type consisted of a 300 μm core diameter optical fiber that was inserted into a 1.08 mm outer diameter stainless steel needle. The tip of the optical fiber was cleaved and aligned with the tip of the needle, which was sharpened around its circumference to facilitate penetration when inserted into tissue. A radiometer was placed at the distal end of the optical fiber to detect light transmitted down the fiber. The amount of light collected by the flat tip probe fiber, φ, was related to the space irradiance in tissue, Φ, by the expression

$$\Phi = \frac{4\pi\varphi}{\Omega_a A} \qquad (11)$$

where A was the cross-sectional area of the fiber core and

Ω_a the acceptance solid angle of the fiber, given by

$$\Omega_a = 2\pi \left[1-\cos\left(\sin^{-1}\frac{NA}{n}\right)\right] . \qquad (12)$$

Here n = 1.4 is the assumed refractive index of R3327-AT tumor and NA is the numerical aperture of the fiber. This value of refractive index is consistent with reported values in other tissues at 630 nm [24].

D. Miniature Isoprobe Detectors

A second type of detector was produced by modifying the tips of 300 μm core diameter fibers. The purpose of these fiber tips was to sample the space irradiance at a specific location in tissue, by collecting light with equal efficiency from all incident angles, i.e. isotropically. For this reason they will be referred to as "isoprobes" (see Fig.IV-1). These fiber tips were similar to an isotropic detector described previously, which consisted of a resin sphere mounted on a cleaved optical fiber[25].

It was necessary to calibrate the readings given by the isoprobes with respect to the actual space irradiance in tissue. The isoprobes were not designed for direct insertion in tissue, but instead were used within interstitially implanted plastic needles. The isoprobe response was related to the space irradiance by cross calibrating it against readings taken by the flat tip probe at the same tumor locations. These measurements were taken under the same conditions as the actual dosimetry

experiments, i.e. at evenly spaced positions along the transverse central axis of Fig.IV-2, using four cylindrical irradiators as light sources. For one of the isoprobes, the average and standard deviation of the ratio of isoprobe to flat probe response for a total of twenty-six points in three different tumors was 0.44 (0.12).

E. Isoprobe Light Measurements in Tumors

Experiments in rat tumors were designed in order to compare theoretical dose predictions with actual measurements in tissue. Each experiment was performed in two stages. In the first stage, a series of sample measurements were obtained using an isoprobe and the resulting data was employed in interpolating dose distributions. For these measurements, one of the cylindrical sources was removed from its plastic needle and the isoprobe inserted into the needle, so that the isoprobe tip was placed at the former location of the center of the cylindrical source. Each of the three remaining cylindrical sources was then illuminated one at a time by the dye laser, generating three separate light measurements from the isoprobe. The isoprobe was then removed from the needle and the original cylindrical source replaced. The process was then repeated with the isoprobe in each of the remaining three needle locations, generating a series of twelve sample measurements in total.

Measurement errors due to fluctuations in the dye laser power were accounted for by monitoring the laser power at the times of the isoprobe measurements. All data was then adjusted to a source intensity of 100 mW. Another possible source of error was anisotropy in the probe response. Since light was received through the sides of the holding needle, very little was collected into the top end of the isoprobe. For this reason, measurements only along a single axis of rotation were considered to be adequate. The isoprobe was tested by rotating it within the plastic needle and taking measurements at different orientations. The standard deviation of measurements taken at random orientations (without moving the plastic needle) was between 4 and 5%. Variations in isoprobe readings due to repositioning error or rotation of cylindrical sources within their holding needles was similarly found to be in the 2 - 5% range.

For each isoprobe measurement, equation (8) was solved numerically for an attenuation coefficient $\alpha(i,j)$, where i and j refer to the source and probe locations respectively. Details of this procedure are given below. The resulting array of twelve attenuation coefficients was then employed to calculate the space irradiance in the tumor at any desired locations, as discussed in the Results section.

F. Validation: Flat Probe Light Measurements in Tumors

The second stage of the tumor experiments consisted of a series of direct measurements of space irradiance. A flat tip fiber optic probe was inserted into the tumor and readings were taken at a series of locations 1 mm apart as the needle was gradually moved into the tumor. These measurements were taken along two lines designated as the transverse and sagittal central axes, as shown in Fig.IV-1.

The values of space irradiance were derived from flat probe measurements using equation (11). However, it should be noted that at least two factors can be identified which may limit the accuracy of this relation. First, (11) is based on the assumption that the angular distribution of light at the probe tip is isotropic, which may not be true in all cases. Second, the presence of the fiber and holding needle assembly itself affects the local distribution of light. As previously shown, if the fiber tip is pointing away from the light source the amount of light detected will be reduced due to "shadowing" by the fiber and needle assembly[15].

IV. RESULTS AND ANALYSIS

A. Attenuation Coefficients

Experimental data together with corresponding theoretical curves were obtained from seven separate rat tumors. In each experiment the theoretical calculations for the individual tumor were based on twelve sample isoprobe

measurements. Results of these measurements in one tumor are given in Table IV-1 as an example. Each entry in the table is an attenuation coefficient that was derived from a single isoprobe measurement. The column headings indicate the numbered needle locations of the isoprobe; the row numbers indicate the location of the 100 mW cylindrical sources.

The attenuation coefficients $\alpha(i,j)$ in Table IV-1 were calculated from the corresponding isoprobe measurements using equation (8). The magnitude of the isoprobe reading determined the space irradiance and hence the left hand side of (8). The right side of (8) was partly determined by known quantities which included the source power p_o, source increment weights $w(i)$ and field point to source increment distances $X(i)$. The remaining factors D, γ and α were uniquely determined by equations (4), (6) and (7) respectively through a suitable choice of absorption and transport coefficients k_a and k_{tr}. The solution to (8) for a given isoprobe reading thus consisted of finding the best choice of these latter two parameters.

Equation (8) presents a single relation for the two unknowns k_a and k_{tr}. In the Dunning R3327-AT tumor, values of the various optical parameters have previously been determined[15]. The average scattering coefficient k_s was estimated to be 250 cm^{-1} and a range for the mean cosine of

scattering g was estimated to be 0.97 - 0.98. Since it is the product of k_s and (1-g) that is of interest rather than their individual values, it is convenient to fix k_s = 250 cm^{-1} and select an initial value for mean cosine g in the previously determined range 0.97 -.098. Although this procedure provides a useful starting point, the best choice of g can in fact be determined more precisely in retrospect, by comparing theoretical with experimental space irradiance results, as will be discussed below.

Once k_s and g were estimated in the above manner, (8) was then solved numerically for the absorption coefficient k_a. Considering the variability of tissue characteristics, it may seem somewhat artificial to assume fixed values for the tumor scattering parameters. However the R3327-AT adenocarcinoma is histologically quite homogeneous, consisting of sheets of anaplastic cells with no acini[19]. Hence, it seems unlikely that there would be large variations in the scattering parameters on a scale much greater than cellular dimensions. However the degree of absorption represented by k_a may be considered a variable, since it depends on the local distribution of hemoglobin and other chromophores.

The above procedure was used to generate the attenuation coefficients in Table IV-1. As is readily apparent from (8), the optical transparency is primarily dependent on α,

which defines the rate of exponential attenuation of light in tissue. The variation between pairs of isoprobe readings for the cases where source and probe locations were exchanged (eg. $\alpha(1,2)$ vs. $\alpha(2,1)$) were in general quite small, as would be expected. The average difference between attenuation coefficients for this case was found to be about 3%. There were somewhat larger differences among the derived attenuation coefficients when all pairs of needles within the same tumor were considered (standard deviation: 8%). This is reflected by significant variations in attenuation coefficients in Table IV-1.

B. Space Irradiance: Theory

The overall light distribution in a tumor was calculated from the array of attenuation coefficients $\alpha(i,j)$. Two distinct mathematical approaches were taken for these calculations. In the first approach, a local average attenuation coefficient was assigned to the tissue region around each cylindrical irradiator by the formula

$$\alpha(i) = \frac{1}{3} \sum_{\substack{j=1 \\ j \neq i}}^{4} \alpha(i,j) \qquad (13)$$

where i = source, j = probe.

The space irradiance at any point in the tumor was then

calculated by summing over the four sources:

$$\Phi(\underline{x}) = \sum_{i=1}^{4} \frac{p_o(i)\,\gamma(i)}{4\pi\, D(i)} \sum_{k=1}^{N} w(i,k)\, \frac{e^{-\alpha(i)\cdot X(i,k)}}{X(i,k)} \,. \qquad (14)$$

In (14), all symbols are the same as previously defined for (8), with i referring to one of the four sources.

The second approach was based on interpolation of the twelve attenuation coefficients. For example, we consider the problem of calculating the space irradiance at position P_2 in Fig.IV-2. This diagram shows a transverse slice through a tumor, at the same vertical level as the isoprobes. The four plastic needles are shown in cross-section. Direct measurements of space irradiance were taken in seven tumors at 1 mm intervals along the central axis indicated by the dashed line. In three of these tumors, irradiance measurements were also taken along the axis which passes through point P_1, running parallel to the plastic needles. The attenuation coefficients associated with the region around source #1 are illustrated on the diagram. The contribution from source #1 to the irradiance at P_2 was calculated using the interpolated attenuation coefficient

$$\alpha = \alpha(1,3) + \frac{\Theta}{\pi/4} [\alpha(1,4,) - \alpha(1,3)] \qquad (15)$$

where Θ is the angle shown in the figure. Similarly, point P_4 was calculated by linear interpolation between coefficients $\alpha(1,2)$ and $\alpha(1,3)$. Interpolation was not possible for points such as P_3, which were assigned a

coefficient corresponding to the nearest pair of needles ($\alpha(1,4)$ in this case). The contributions to the space irradiance at each point from the other three sources were calculated in the same manner.

C. Comparison Between Theory and Experiment

Figure IV-3 shows the result of intratumor irradiance measurements along the transverse central axis in a tumor, together with theoretical curves. The dashed and solid curves represent results of the attenuation coefficient averaging and interpolation methods respectively. There are only minor differences between these two curves, as was the case for most of the tumors. Figure IV-4 shows experiment versus theory in one tumor along the sagittal central axis through point P_1. Since this axis did not lie within plane of Fig.IV-2, only the averaging method was applicable to this case.

A factor which may have affected the accuracy of the theoretical results was the neglect of the tumor boundary conditions in the space irradiance calculations. This would apply to locations near the tumor surfaces, corresponding to points at either end of Figs.IV-3,IV-4 and IV-5.

As mentioned earlier, the optimum selection of the mean scattering cosine g was determined by comparison of theory versus experiment. Figure IV-5 shows two interpolated

curves together with data from the transverse central axis of a tumor. For both curves the assumed value of scattering coefficient k_s was 250 cm^{-1}. The assumed values of g were 0.964 and 0.974 for the solid and dashed curves respectively. This illustrates the main effect of varying g, which was to scale the overall magnitude of the theoretical curves. For example, the average difference between predicted space irradiance values was approximately 13% for these two values of g. An assumed value of g of 0.964, corresponding to a transport coefficient of 9.0 cm^{-1} gave the best overall agreement between theory and the entire series of experiments. The average values of absorption and attenuation coefficients calculated from individual isoprobe measurements were 0.469 (0.129) cm^{-1} and 3.55 (0.48) cm^{-1} respectively.

Lastly, Plates IV-1 and IV-2 show sample isodose calculations for transverse and sagittal slices respectively through a tumor. Dose is given in units of J/cm^2, resulting from four cylindrical irradiators illuminated for 55 minutes at a power of 175 mW per fiber. The transverse distribution represents the tumor section shown in Fig.IV-2; the sagittal distribution corresponds to the plane containing the sagittal central axis and perpendicular to the transverse central axis. An inhomogeneous optical distribution resulting from variable attenuation is apparent in both figures.

V. DISCUSSION

Attenuation characteristics of tissue are highly variable, depending not only on the specific tissue type and the particular sample, but also on the time and conditions of measurements. It has been shown that measurements on the same samples may give significant differences in attenuation if performed *in vivo* or *postmortem* [26]. Although direct measurements both *in vitro* and *in vivo* frequently display a well defined and constant rate of attenuation, irregular attenuation may also exist within individual samples. Particularly large variations have been found in volumes containing mixed tumor and normal tissue[18]. All of these sources of variability make the tasks of prediction and control of light distribution in tissue potentially more difficult. Additional problems can be expected for *in vivo* dosimetry arising from changes in blood flow and oxygenation status.

The accuracy of the present technique is necessarily constrained by the restricted number of isoprobe measurement locations. The agreement between theory and experiment in Figs.IV-3,IV-4 and IV-5 appears to be less than optimum. In Fig.IV-5 the data points reveal a higher average optical attenuation in the region represented on the right side versus the left side of the graph. This difference is less on the theoretical curve. Discrepancies between theory and

experiment may also arise from factors other than the limited number of isoprobe measurements. The experimental points themselves are not necessarily accurate representations of the space irradiance. These points are derived from equation (11), which gives the space irradiance in terms of the amount of light collected by a fiber optic probe. The accuracy of this representation of space irradiance presupposes that the amount of light collected is independent of the orientation of the probe fiber. This is in general not the case, due to perturbations in the optical distribution caused by the presence of the probe fiber and its holding needle. Additional experimental error may be introduced by inaccurate positioning of the probe needle.

Further inaccuracies are to be expected due to the approximations in the theory as well as those inherent to the experimental technique. For example the probe needle may pass through a region of hyperemia, resulting in increased light absorption. If the surrounding tissue volume is by contrast relatively transparent, the isoprobe readings from nearby plastic needles will also be relatively high. Thus the calculated average attenuation in the vicinity of the probe needle will predict a higher space irradiance than is actually present at that location. Another factor which could influence the results is tissue distortion due to insertion of the plastic needles.

As illustrated by Fig.IV-5, the accuracy of this interstitial technique depends to some degree on an accurate knowledge of average tissue scattering characteristics. Only recently have direct measurements on the relevant parameters of total scattering coefficient and mean cosine of scattering been performed in some tissue[15,21]. Flock et al.[21] measured both of these quantities for a variety of tissues, including bovine and chicken muscle, pig brain, pig adipose and VX2 tumor. In the first three tissues the mean cosine of scattering was in the range of 0.940-0.965; it was somewhat lower in pig adipose and VX2 tumor at 0.771 and 0.639 respectively. Measurements of mean cosine taken with a similar apparatus yielded a value of 0.86 for Dunning R3327-AT tumor in Chapter III, whereas theoretical considerations from both that and the present study imply the true value is in the range 0.96-0.98. This discrepancy was attributed to multiple scattering effects, since the sample thickness in the goniometer experiment exceeded the tissue mean free path by a factor of 3.2.

VI. CONCLUSION

A technique for interstitial light dosimetry has been described. Estimated light distributions have been mapped by interpolating sample measurements of space irradiance which were taken at various locations in excised solid tumors. Significant variations in the light attenuation rate were detected within individual tumors. This result

implies the need for measurements of tissue optical properties on an individual basis.

Direct measurements of space irradiance *in vitro* in seven R3327-AT tumors suggest the general validity of the theoretical approach. A knowledge of scattering parameters for the particular tissue has been identified as a key factor that defines the correct scaling of the theoretical curves. However, discrepancies between theory and experiment of 40% or more at some locations indicate the limitations of this method and raise rather than answer the question of what constitutes "reasonable accuracy" in PDT dosimetry. Improved accuracy will probably require a greater number of sample measurements to account for random inhomogeneities in the tissue. Further studies are planned to explore the potential of this new technique.

TABLE IV-1

Attenuation coefficient array $\alpha(i,j)$ in cm^{-1}, from a single rat tumor. Each $\alpha(i,j)$ was calculated using equation (8) from a separate isoprobe reading in the tumor.

		ISOPROBE			
	j / i	1	2	3	4
SOURCE	1	--	3.37	3.28	3.60
	2	3.32	--	2.80	3.09
	3	3.32	2.91	--	3.19
	4	3.69	3.15	3.42	--

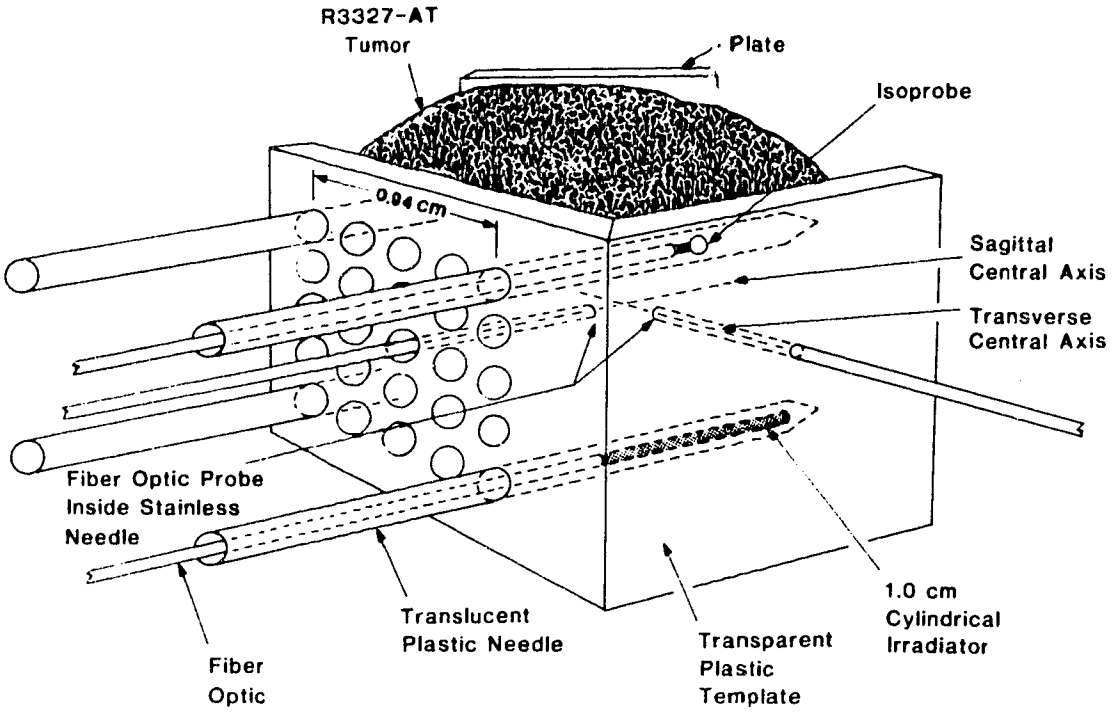

Fig.IV-1 Experimental set-up, with four translucent plastic needles in a 0.94 x 0.94 cm grid. One needle is shown containing a cylindrical irradiator and another a miniature isoprobe light detector. Optical fibers within two stainless steel needles directly probe the tumor space irradiance along orthogonal axes through the center of the tumor.

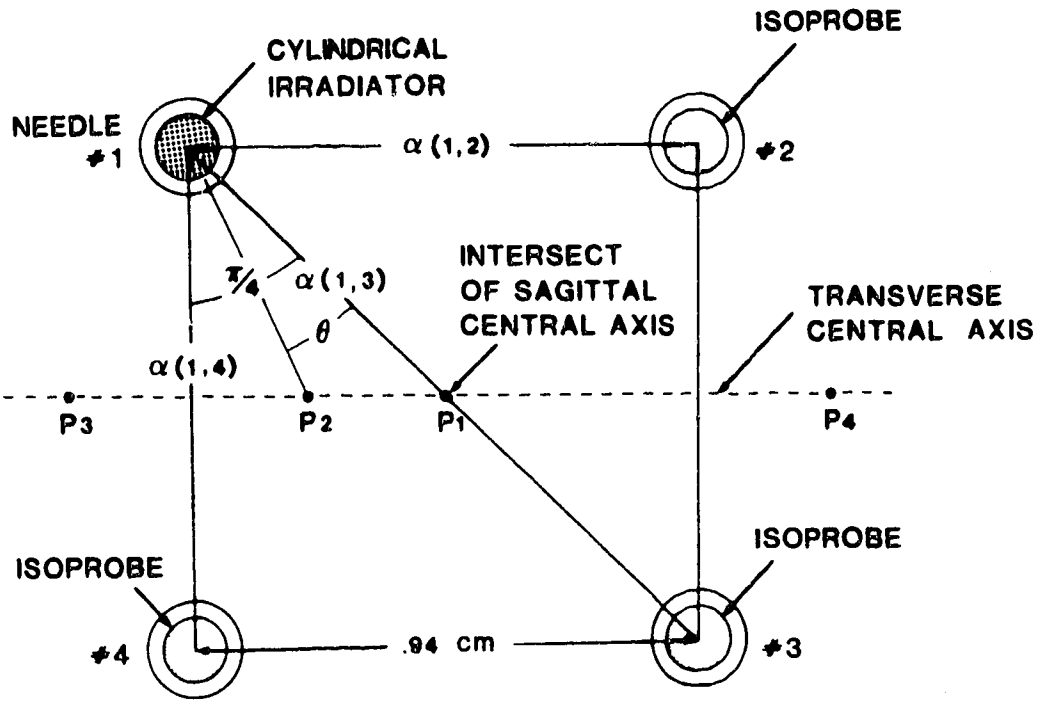

Fig.IV-2 Schematic of a tumor transverse section, illustrating the method of calculating space irradiance by interpolation of attenuation coefficients.

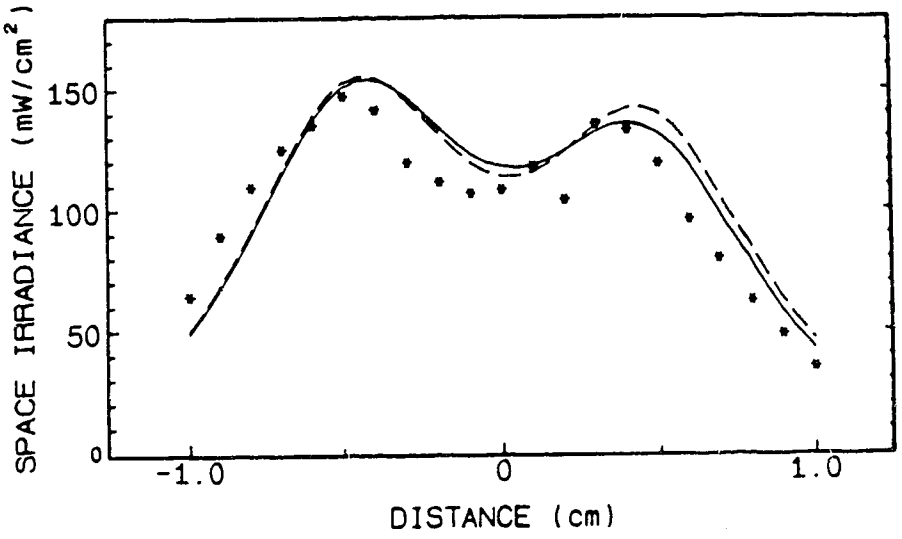

Fig.IV-3. Space irradiance data on the transverse central axis from four 100 mW cylindrical sources. The solid curve was calculated from the attenuation coefficient array by the interpolation method; the dashed curve was calculated by the averaging method.

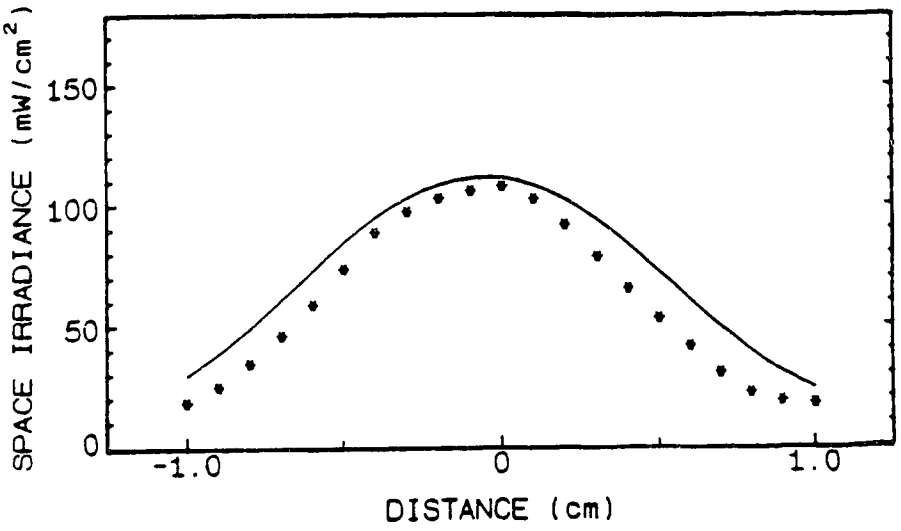

Fig.IV-4. Space irradiance data on the sagittal central axis from four 100 mW cylindrical sources. The theoretical curve was calculated from the attenuation coefficient array by the averaging method.

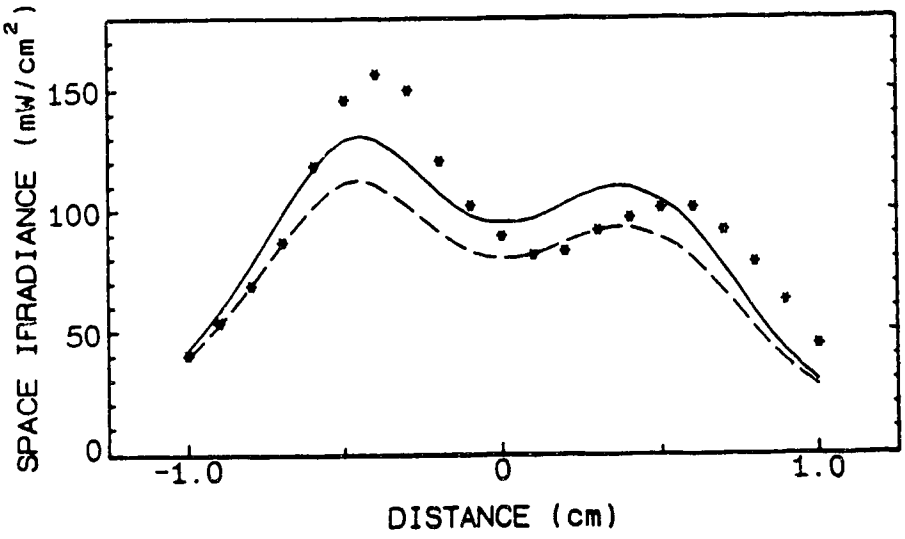

Fig.IV-5. Space irradiance data on the transverse central axis from four 100 mW cylindrical sources. The solid curve was calculated using g = 0.964; the dashed curve was calculated using g = 0.974.

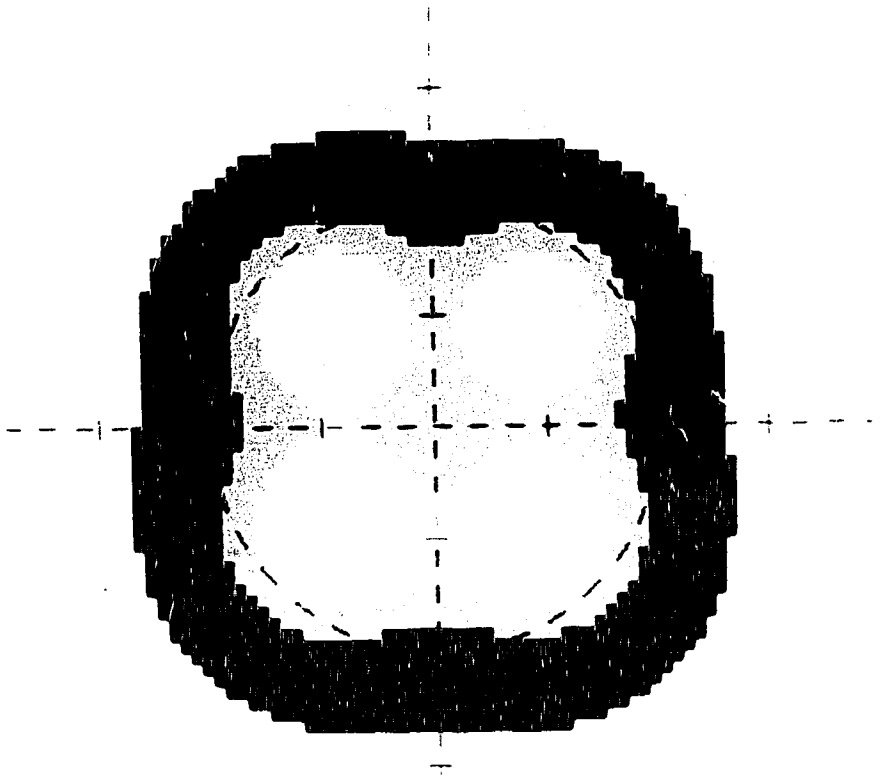

Plate IV-1. Transverse section isodose distribution from a 55 min. treatment of a rat tumor by four 175 mW cylindrical sources. This figure represents the same tumor section illustrated by Fig.IV-2. The square containing the dose information represents a 4x4 cm area. The white, light grey, dark grey and black regions represent minimum doses of 500, 250, 120 and 50 J/cm^2 respectively.

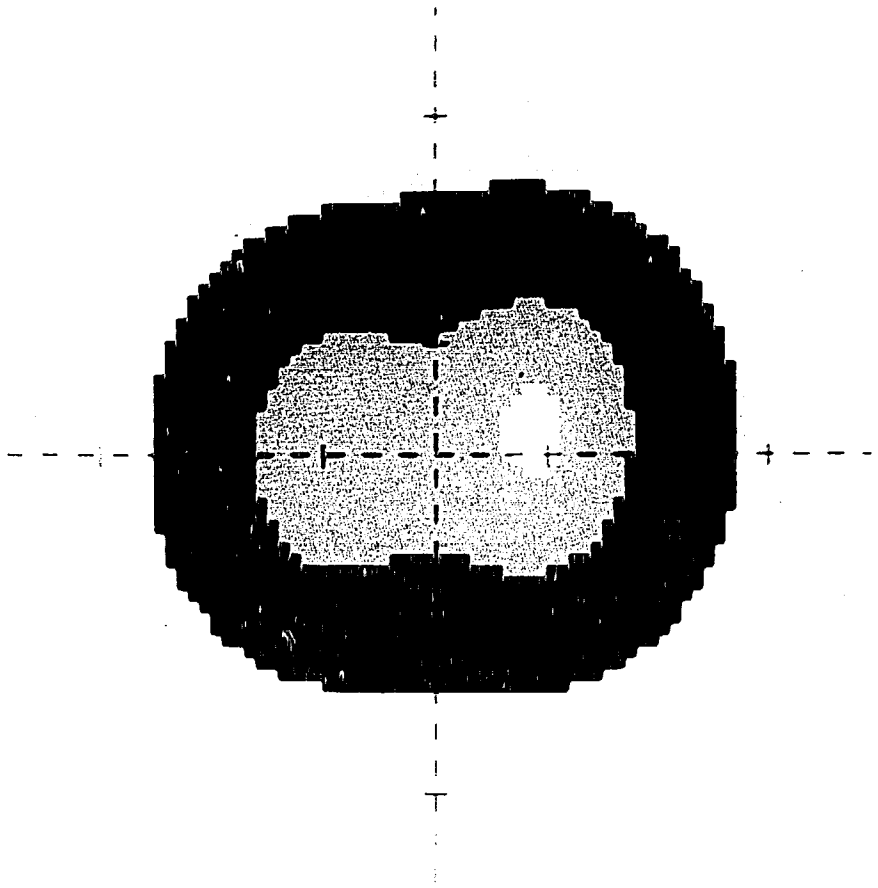

Plate IV-2. Sagittal section isodose distribution from a 55 min. treatment of a rat tumor by four 175 mW cylindrical sources. This tumor section corresponds to the plane that contains the sagittal central axis and is perpendicular to the transverse central axis. Scale and dose representation as in Plate IV-1.

LITERATURE CITED

1. T.J. Dougherty, "Photosensitization of malignant tumors," Sem. Surg. Oncol. 2, 24 (1986).

2. G. Graschew and M Shopova, "Hypoxia, misonidazole and hyperthermia in photodynamic therapy of tumors," Lasers Med. Sci. 1, 181 (1986).

3. B.D.Hirsch, N.C. Walz, B.E. Meeker, M.R. Arnfield, J. Tulip, M.S. McPhee, and J.D. Chapman, "Photodynamic therapy-induced hypoxia in rat tumors and normal tissues," Photochem. Photobiol. 46, 847 (1987).

4. S. Gonzales, M.R. Arnfield, B.E. Meeker, J. Tulip, W. H. Lakey, J.D. Chapman, and M.S. McPhee, "Treatment of Dunning R3327-AT rat prostate tumors with photodynamic therapy in combination with misonidazole," Cancer Res. 46, 2858 (1986).

5. T.J. Dougherty, R.E. Thoma, D.G. Boyle, and K.R. Weishaupt, "Interstitial photoradiation therapy for primary solid tumors in pet cats and dogs", Cancer Res. 41, 401 (1981).

6. J.H. Kinsey, D.A. Cortese, and H.B. Neel, "Thermal considerations in murine tumor killing using hematoporphyrin derivative phototherapy", Cancer Res. 43, 1562 (1983).

7. M.S. McPhee, C.W. Thorndyke, G. Thomas, J.Tulip, D. Chapman, and W.H. Lakey, "Interstitial applications of laser irradiation in hematoporphyrin derivative-photosensitized Dunning R3327 prostate cancers," Lasers Surg. Med. 4, 93 (1984).

8. O.J. Balchum, D.R. Doiron, and G.C. Huth, "Photoradiation therapy of endobronchial lung cancers employing the photodynamic action of hematoporphyrin derivative", Lasers Surg. Med. 4, 13 (1984).

9. M.R. Arnfield, S. Gonzales, P.Lea, J.Tulip, and M.S. McPhee,"Cylindrical irradiator fiber tip for photodynamic therapy," Lasers Surg. Med. 6, 150 (1986).

10. F.P. Bolin, L.E. Preuss, and R.C. Taylor, "Optimization of photodynamic therapy light dose distribution and treatment volume by multi-fiber insertions," Photochem. Photobiol. 46, 609 (1987).

11. A.L. McKenzie and P.O. Byrne, "Can photography be used to measure isodose distributions of space irradiance for laser photodynamic therapy?," Phys. Med. Biol. 33, 113 (1988).

12. F.P. Bolin, L.E. Preuss, R. C. Taylor, and T. S. Sandhu, "A Study of the three-dimensional distribution of light (632.8 nm) in tissue," IEEE J. Quant. Electr. QE-23, 1734 (1987).

13. D.R. Doiron, L.O. Svaasand, and A.E. Profio, "Light dosimetry in tissue: Application to photoradiation therapy," in Porphyrin Photosensitization, edited by D. Kessel and T. J. Dougherty (Plenum, New York, 1981), p.63.

14. L.O. Svaasand and R. Ellingsen, "Optical properties of human brain," Photochem. Photobiol. 38, 293 (1983).

15. M.R. Arnfield, J. Tulip, and M.S. McPhee, "Optical propagation in tissue with anisotropic scattering," IEEE Trans. Biomed. Eng. BME-35, 372 (1988); Errata to reference (15), to be published.

16. W.M. Star, J.P.A. Marijnissen, and M.J.C. van Gemert, "Light Dosimetry in optical phantoms and in tissues: I. Multiple flux and transport theory," Phys. Med. Biol. 33, 437 (1988).

17. B.C. Wilson and M.S. Patterson, "The physics of photodynamic therapy," Phys. Med. Biol. 31, 327 (1986).

18. T.J. Muller and B.C. Wilson, "An update on the penetration depth of 630 nm light in normal and malignant human brain tissue in vivo," Phys. Med. Biol. 31, 1295 (1986).

19. J.T. Isaacs, W.D.W. Heston, R.M. Weissman, and D.S. Coffey, "Animal models of the hormone sensitive and insensitive prostatic adenocarcinomas, Dunning R3327-H, R3327-HI and R3327-AT," Cancer Res. 38, 4353 (1978).

20. W.A.G. Bruls and J.C. van der Leun, "Forward scattering properties of human epidermal layers," Photochem. Photobiol. 40, 231 (1984).

21. S.T. Flock, B.C. Wilson, and M.S. Patterson, "Total attenuation coefficients and scattering phase functions of tissues and phantom materials at 633 nm," Med. Phys. 14, 835 (1987).

22. B. Davison, Neutron Transport Theory (Clarendon Press, Oxford, 1957).

23. A.M. Weinberg and E.P. Wigner, The Physical Theory of Neutron Chain Reactors (Chicago Press, Chicago, IL 1958).

24. F.P. Bolin, R. C. Taylor, L.E. Preuss, and R.J. Ference,"The refractive index of mammalian tissue," Photochem. Photobiol. 47, 11s (1988) (abstract).

25. J.P.A. Marynissen and W.M. Star, "Phantom measurements for light dosimetry using isotropic and small aperture detectors," in Porphyrin Localization and Treatment of Tumors, edited by D.R. Doiron and C.J. Gomer (Liss, New York, 1984), p.133.

26. B.C. Wilson, W.P. Jeeves, and D.M. Lowe, "In vivo and postmortem measurements of the attenuation spectra of light in mammalian tissues," Photochem. Photobiol. 42, 153 (1985).

Chapter V : PHOTODYNAMIC THERAPY DOSIMETRY IN POSTMORTEM AND IN VIVO RAT TUMORS AND A TISSUE - EQUIVALENT PHANTOM*

I. INTRODUCTION

Photodynamic therapy (PDT) is coming into increasing use as a treatment for cancer. Among cancers that have been successfully treated are lung, bladder and esophageal tumors[1]. Best results have been obtained with superficial lesions, and although significant palliation of bulky tumors has been achieved[2,3], cures may be difficult to obtain when the tumor size exceeds about 1.5 cm [4,5].

Various strategies have been proposed as means of modifying and enhancing the photodynamic effect in tumors. Fingar et al.[6] studied the effects of changing the oxygenation status of tumors. Others have observed improved cure rates in animal tumors by combining PDT with a radiosensitizer[7], chemotherapeutic agents[8], or with external hyperthermia[9]. Another route involves optimizing the light dose to tumors by implanting fiber optic light guides directly within the tumor mass. In Chapter IV, results were given of dosimetry tests in excised R3327-AT tumors, using four interstitial cylindrical sources in a square array. In the present

* A version of this chapter has been submitted for publication. M.R.Arnfield, J.Tulip and M.S.McPhee, "Photodynamic therapy dosimetry in postmortem and in vivo rat tumors and a tissue-equivalent phantom."

chapter, the needle arrangement has been expanded to 10 needles and the dosimetry procedure modified somewhat. Results are presented of experiments with postmortem and in vivo tumors, as well as a tissue-equivalent phantom.

II. THEORY

Tissue can be regarded (ideally) as a turbid medium with uniform distribution of scatterers and absorbers, which in transport theory is characterized by a scattering coefficient k_s and an absorption coefficient k_a. In many analyses the scattering is assumed to be isotropic, since this is the easiest case to deal with mathematically. However, it has been demonstrated that rather than being isotropic, scattering is in fact strongly forward directed in various tissues which include chicken and bovine muscle[10], pig brain[10], pig adipose[10] and human epidermis[11], as well as in blood[10,12]. The net effect of forward scattering can be approximated by the simple device of replacing the isotropic scattering coefficient k_s by what may be termed the transport coefficient k_{tr}, given by

$$k_{tr} = k_s(1-g) \qquad (1)$$

where g is the average cosine of the scattering phase function.

In the literature on PDT dosimetry, the term space irradiance is often used to denote the angle integrated

light flux at position $\underline{x}$. It has units of $W \cdot m^{-2}$ and is given by

$$\Phi(\underline{x}) = \int_{4\pi} I(\underline{x},\underline{\Omega})\, d\Omega \qquad (2)$$

where $I(\underline{x},\underline{\Omega})$ is the specific (angular) intensity in $W \cdot m^{-2} \cdot sr^{-1}$. A simple model of light propagation in tissue described in Chapter III was based on an approximation originally used in neutron transport theory. In this model, the space irradiance at radial distance r from an isotropic point source is given by

$$\Phi(r) \approx \frac{1}{4\pi r^2} \left(\frac{r\gamma}{D} \cdot e^{-\alpha r} + e^{-(5/4)kr}\right) \qquad (3)$$

where

$$\alpha \approx \sqrt{3k_a k}\,(1 - 2k_a/5k) \qquad (4)$$

$$D = k_a/\alpha^2 \qquad (5)$$

$$k = k_{tr} + k_a \qquad (6)$$

and

$$\gamma = \frac{2k_a}{k_{tr}} \cdot \frac{k^2 - \alpha^2}{\alpha^2 - k_a k} \cdot \qquad (7)$$

The attenuation coefficient α is the inverse of the familiar penetration depth, D is the diffusion coefficient, k is the total effective coefficient for scattering and absorption, and γ is a factor accounting for absorption in the region close to the source. Equation (3) is a good approximation for the space irradiance from a point source in cases where scattering dominates absorption. In this case, the second term in (3) is small compared to the first term, except close to the source.

A source emitting along a cylinder can be approximated by a sum of point sources. If the two ends of a source of total power p_o reside at $\underline{x}_1$ and $\underline{x}_2$, the space irradiance at $\underline{x}$ is given by

$$\Phi(\underline{x}) \approx \frac{p_o}{4\pi} \sum_{i=1}^{N} w(i)\{ \frac{\gamma}{D} \frac{e^{-\alpha X(i)}}{X(i)} + \frac{e^{-(5/4)kX(i)}}{X(i)^2} \} \quad (8)$$

where

$$X(i) = \left| \underline{x} - \underline{x}_1 - \frac{(i-0.5)}{N} \cdot (\underline{x}_2 - \underline{x}_1) \right| \quad (9)$$

and $$\sum_{i=1}^{N} w(i) = 1 \quad . \quad (10)$$

The w(i) are weighting factors to account for non uniform emission along the source length.

III. MATERIALS AND METHODS

A. Dosimetry Enclosure

All dosimetry experiments were performed using a rectangular chamber constructed of 3/8 inch thick plexiglass panels, as shown in Fig.V-1. The front and back panels of the chamber has identical arrangements of 2 mm diameter holes, consisting of two concentric patterns plus one hole at the center. The diameters of the inner and outer circles were 2.0 and 4.0 cm. The holes of the front and back panels were aligned so that up to a maximum of 19 needles could be held in a parallel arrangement. One of the side panels of the enclosure had three adjacent holes through which a 1.08 mm diameter needle could be inserted into the chamber interior, as pictured.

B. Tumors and Phantom

Three different substrates were used for dosimetry tests: postmortem and in vivo R3327-AT rat prostate tumors and a liquid phantom material consisting of a lipid emulsion in combination with a light absorbing dye. The R3327-AT adenocarcinoma is a poorly vascularized, anaplastic variant of a neoplasm discovered by Dunning which arose spontaneously in the prostate of a Copenhagen rat in 1961[14]. Two experiments were performed with rats lying atop the dosimetry enclosure. The rats were induced under light halothane anesthesia and maintained with ketamine hydrochloride and xylazine. Volumes of these tumors were 15 and 8 cm^3. A third experiment was done with an excised 11 cm^3 tumor.

A tissue equivalent phantom was produced by mixing 160 ml of a lipid emulsion (Soyacal 20%, Alpha Therapeutics Corp.,Toronto) with 240 ml of a 4.4×10^{-4} molar solution of Nile blue perchlorate (Eastman Kodak Co.,Rochester, N.Y.). The average particle size of the lipid emulsion was 0.3 μ (personal communication, Alpha Therapeutics Corp.) and its refractive index was 1.45. Nile blue is an organic dye with an absorptivity of 7.7×10^4 $cm^{-1}/(mole \cdot l)$ at 635 nm (Kodak data sheet #JJ-169). The lipid and dye mixture was sonicated for 5 min with an ultrasonic probe just prior to, and for 1 min periods at regular intervals during dosimetry

tests. This procedure was found to improve the stability of the optical characteristics of the liquid.

C. Light Sources

Interstitial light sources consisted 1.0 cm long cylindrical diffusing tips attached to ten 600 μm diameter fused silica core optical fibers[15] (see Appendix I). A beam splitting arrangement divided the 630 nm beam from a dye laser approximately equally into the ten fibers. The variation of output power along the length of each tip was measured as described in Chapter IV. The ten tips used in experiments were selected for minimal variation in output power with respect to rotation of the tip (SD<5% for all tips).

D. Fiber Optic Light Probes

Two types of fiber optic light probes were constructed. The first type consisted of a cleaved 300 μm core diameter optical fiber inserted into a 1.08 mm diameter steel needle. The fiber tip was aligned with the end of the needle and the other end of the fiber was attached to a radiometer. The space irradiance at the probe tip, Φ, was derived from the following expression:

$$\Phi = \frac{4\pi\varphi}{\Omega_a A} \qquad (11)$$

where φ was the optical power collected by the fiber, A was the cross-sectional area of the fiber core and Ω_a was the

acceptance solid angle of the fiber. The acceptance angle is given by

$$\Omega_a = 2\pi \left[1 - \cos\left(\sin^{-1}\frac{NA}{n}\right)\right] \qquad (12)$$

where n = 1.4 and n = 1.45 were the assumed refractive indices of tumor and phantom mixture respectively and NA was the optical fiber numerical aperture.

A second type of fiber optic detector was produced by modifying the tips of 300 μm core diameter fibers. The purpose of these "isoprobes" was to sample the space irradiance at a specific location in tissue by collecting light approximately isotropically. To prepare an isoprobe, the coating and cladding of a fiber was stripped a distance of 1 cm from the fiber tip. By simultaneously rotating the fiber and heating the fiber core with a miniature acetylene torch, a sphere with an approximate diameter of 1 mm was formed. This sphere was then sprayed with three coats of white paint. The exposed length of fused silica between the sphere and the remaining optical fiber was painted black in order to prevent the entrance of light in this region. The entire tip was then sprayed with transparent enamel.

The isoprobe response was calibrated with respect to the space irradiance in tumor or phantom. This was accomplished indirectly, by comparing the amount of light collected by the isoprobe to the light collected by the flat probe, when

placed at the same location. Since the accuracy of relation (11) depends on the local angular distribution of light, which is affected by the geometric arrangement of sources and probe, these calibration experiments were carried out using multiple cylindrical sources in a geometry similar to that used in the actual experiments. In the case of R3327-AT tumor, isoprobe calibrations were done with four sources in a square array, as described in the previous chapter. For the lipid phantom, the array consisted of six sources in a hexagonal arrangement. A total of 26 independent comparisons of the isoprobe to flat probe response were taken in R3327-AT tumors, whereas two independent comparisons were taken in different phantom mixtures. The results of these tests for the ratio of isoprobe to flat probe responses (and standard deviations) were 0.44 ±0.12 and 0.80 ±0.02 for tumor and phantom respectively.

E. Isoprobe Light Measurements in Tumors and Phantoms

A total of six cylindrical sources, corresponding to needles #1 through #6, where used in tumor experiments. This was the maximum number, owing to the limited size of the tumors. In the lipid phantom, an additional four sources were used in holes #7 through #10. Isoprobe measurements were taken by removing one of the sources and replacing it with the isoprobe fiber, so that the isoprobe tip was placed at the previous position of the center of the 1.0 cm source. Isoprobe measurements were also taken in needle #11,

although no source was placed at this location. After replacing one of the sources with the isoprobe, one of the other surrounding sources was briefly illuminated by the dye laser. The amount of light subsequently collected by the isoprobe, depended on the power emitted by the cylindrical source, as well as the attenuation characteristics of the intervening tumor or phantom material. The light received by the isoprobe was related to the space irradiance using equation (11), after adjusting for the difference in response of the isoprobe with respect to the flat probe. Equation (8) shows that the value of space irradiance is mainly determined by the average attenuation coefficient α, which was calculated from the isoprobe readings as will be described in the Results section. In tumors, measurements were taken for every combination of sources #1 through #6 and probe location #1 through #6 plus #11, to generate an array of isoprobe readings. Additional readings were taken at locations #7 through #10 in the phantom.

The power emitted by each source fiber tip was measured prior to each experiment and the dye laser output was monitored throughout the experiments, to account for fluctuations in laser output. The variation in isoprobe response under rotation or repositioning of the isoprobe was less that 5%. The equivalent variation for repositioning of the sources was also under 5%.

F. Validation: Flat Probe Light Measurements in Tumors and Phantoms

It was described in the previous section how various measurements were taken in order to determine average attenuation coefficients. This information was later used to interpolate the space irradiance at intermediate points, between the isoprobe measurement locations. These interpolated values were compared to space irradiance measurements, which were taken at 1 mm intervals within tumors by means of a flat tip probe (see section III-D for description). Figure V-1 indicates the three axes along which these flat probe measurements were taken, perpendicular to the plastic needles. The stainless steel needle containing the probe fiber, was inserted through one of the three holes in the side panel of the dosimetry enclosure and then gradually inserted into the tumor in 1.0 mm increments. A light reading was taken at each increment. Plastic needle #11 was not in place during these measurements, since it would have interfered with the passage of the flat probe needle through the center of the enclosure. In tumors, flat probe measurements were taken only on the 0-axis in Fig.V-1. All three axes were used in the lipid phantom.

IV. RESULTS AND ANALYSIS

A. Scattering, Absorption and Attenuation Coefficients

The space irradiance arising from a cylindrical source was given approximately by the first term on the right side of equation (8), where the attenuation coefficient α and other parameters D and γ appearing in this relation were uniquely specified by the absorption and transport coefficients, k_a and k_{tr} through equations (4), (5),and (7) respectively. By taking measurements with a source in one plastic needle and an isoprobe in another, the left hand side of (8) is specified, after converting the isoprobe reading at location $\underline{x}$ into a corresponding space irradiance. However, since the equation involves two unknowns, it is necessary to assume a value for either k_{tr} or k_a in order to solve the equation based on a single isoprobe reading. In Chapter IV one approach to this dilemma was described, which was to assume an average or typical value for the transport coefficient k_{tr} (i.e. the effective scattering coefficient) for R3327-AT tissue. In this way, the problem of calculating values of absorption and attenuation (and ultimately space irradiance) from isolated isoprobe readings became tractable. The average value of k_{tr} = 9.0 cm^{-1} was determined as a "best fit" value, by comparing calculated space irradiance values with direct measurements taken with a fiber optic probe.

One of the goals of the experiments in the present chapter was to see if average values of k_{tr} could be estimated strictly from isoprobe measurements. One way to accomplish this is to take two independent isoprobe measurements at different distances from the same source, which can then be used to set up two relations as described above. In these calculations, the second term in (8) was neglected, since it was small relative to the first term except near sources. In the phantom material, the second term represented approximately 10% of the total light flux at a 1 cm distance from a source, whereas it represented less than 1% for tumor at the same distance. Hence this approximation was more accurate for tumor tissue than for the phantom. This difference was due to the different ratios of absorption to total scattering in the two cases.

Two equations, arising from a pair of distinct isoprobe readings at different distances from the same source can, in theory, be solved uniquely for the two unknowns k_{tr} and k_a. The arrangement shown in Fig.V-1, consisting of six needles at the vertices of the inner hexagon and one in the center, was suitable for acquiring various pairs of isoprobe readings. For example, using source #1, measurements of space irradiance were taken with the isoprobe in needles #4 and #11. For the reading in needle #4, needle #11 was not present within the medium, in order not to interfere with light propagation between the source in #1 and the probe in

#4. These measurements defined two simultaneous relations for k_a and k_{tr}. Another example using source #1, of a pair of readings which could be solved for k_{tr} and k_a, is the isoprobe placed in needles #5 and #6. In this way, for each source location, a number of pairs of simultaneous equations for k_{tr} and k_a could be set up and solved. After this was done, these derived values of k_{tr} were averaged together, to obtain an average for the particular tumor or phantom.

A practical difficulty with the above method for determining k_a and k_{tr}, is that for there to be a solution to the two equations requires that the optical coefficients be reasonably constant in the region containing the needles. However, variations in absorption were sometimes large in the three tumors that were studied. The R3327-AT tumor is a fast growing tumor which quickly outgrows its blood supply, resulting in a necrotic tumor core. Dissection of the tumors after dosimetry tests showed a dark grey-brown area at the core which gradually (but irregularly) became lighter towards the tumor periphery, which was a light beige color.

A consequence of these color variations due to tumor physiology was that in some cases, the two isoprobe measurements from a single source were not consistent with the same transport and absorption coefficients. In other words, no pair of k_{tr} and k_a were able to simultaneously satisfy the equations arising from the pair of isoprobe

readings. However, in most cases a solution was possible. The results of these calculations are given as the average values of transport coefficient k_{tr}, in the first row of Table V-1. The values of k_{tr} in three tumors ranged between 9.42 and 15.2 cm^{-1}, in reasonable agreement with the result of 9.0 cm^{-1} deduced in the previous chapter.

In the lipid phantom material, the situation was quite favorable for calculating k_{tr} due to the optical uniformity of the medium, and yielded a value for transport coefficient of 1.86 $\pm$0.08 cm^{-1}.

After the average transport coefficient had been determined in each phantom or tumor, these results were used to calculate absorption and attenuation coefficients for each individual isoprobe reading, to generate arrays $k_a(i,j)$ and $\alpha(i,j)$ where i and j refer to the source and isoprobe locations respectively. The average values of absorption and attenuation coefficients from these arrays are given in Table V-1.

Before leaving the description of the isoprobe measurements, it should be noted that some difficulty was experienced in inserting the plastic needles into the tumors in a parallel fashion. This was especially true of the <u>in vivo</u> tumors due to overlying skin and the curvature of the tumor surface. After penetrating through to the far side of the tumor,

needle positions were adjusted when necessary in order to line up with the corresponding hole in the back wall of the chamber. This caused some distortion of the tissue. In both in vivo experiments, two of the needles penetrated both the tumor and the well-vascularized area between the tumor and the rat's flank. Isoprobe readings in these needles were smaller than equivalent values from other needles, presumably due to accumulation of blood in the vicinity of the needles.

B. Comparison Between Theoretical and Experimental Space Irradiance

Experimental space irradiance values were obtained at 1.0 mm intervals within tumors along the 0-axis and phantoms along the axes designated -0.5 cm, 0 and +0.5 cm in Fig.V-1. For these measurements, sources #1 through #6 were simultaneously illuminated in the tumors, or sources #1 through #10 in the phantom . These data were compared to theoretical values that were calculated in the following manner. First, the average transport coefficient k_{tr} together with arrays $k_a(i,j)$ and $\alpha(i,j)$ were obtained as discussed above. This information was then employed in calculating the space irradiance, which was estimated by summing the individual contributions of the six (or ten) sources. At this point the question arose as to the best value or values of attenuation coefficient α to use in the calculations of space irradiance. In Chapter IV two

alternative methods were employed, in determining the attenuation coefficients to be used in calculating the contribution to the space irradiance from a specific source. These methods were based on either averaging or interpolating the $\alpha(i,j)$. Since the variation among the $\alpha(i,j)$ was small in the lipid phantom, the calculated space irradiance results were essentially the same regardless of the method used for determining α. However, this was not true for the tumors because of large variations in the $\alpha(i,j)$. The averages and standard deviations of the attenuation coefficients $\alpha(i,j)$ and associated absorption coefficients $k_a(i,j)$ in postmortem and in vivo tumors and the phantom are given in Table V-1.

Because of this variability in tumors, it was important that the value of α that was used, reflect as closely as possible the actual attenuation in the tumor region near the position being calculated. Two different methods were adopted and the resulting theoretical curves compared. In the first method, the space irradiance at point $\underline{x}$ in a tumor was

calculated according to the formula

$$\Phi(\underline{x}) = \sum_{i=1}^{M} \frac{p_o(i)\,\gamma(i)}{4\pi\, D(i)} \sum_{k=1}^{N} w(i,k)\, \frac{e^{-\alpha(i)\cdot X(i,k)}}{X(i,k)}$$

$$+ \sum_{i=1}^{M} \frac{p_o(i)}{4\pi} \sum_{k=1}^{N} w(i,k)\, \frac{e^{-(5/4)k(i)\cdot X(i,k)}}{X(i,k)^2} \qquad (13)$$

where $\alpha(1)=\alpha(1,11)$, $\alpha(2)=\alpha(2,3)$, $\alpha(3)=\alpha(3,2)$, $\alpha(4)=\alpha(4,11)$, $\alpha(5)=\alpha(5,6)$, $\alpha(6)=\alpha(6,5)$, $\alpha(7)=\alpha(7,8)$, $\alpha(8)=\alpha(8,7)$, $\alpha(9)=\alpha(9,10)$ and $\alpha(10)=\alpha(10,9)$. In (13), the total number of sources M, was equal to six or ten for tumor or phantom respectively. The value of the total effective coefficient for scattering and absorption k(i), was derived from the absorption coefficient associated with $\alpha(i)$ in combination with the transport coefficient. Other symbols are defined as in equation (14), Chapter IV. The rationale behind this approach can be seen by referring to Fig.V-2. For each needle i, $\alpha(i)$ was equated with the $\alpha(i,j)$ corresponding to the region closest to the portion of the 0-axis closest to the needle. For example, $\alpha(2)$ was set equal to $\alpha(2,3)$ since the portion of the 0-axis closest to needle #2 was between needles #2 and #3.

Figure V-1 also illustrates the second method, which was based on interpolation of the $\alpha(i,j)$. For example, when calculating the contribution of source #1 to the field at

P_1, the attenuation coefficient used in (8) was

$$\alpha = \alpha(1,6) + \frac{\omega}{\pi/3} [\alpha(1,11) - \alpha(1,6)] . \qquad (14)$$

The contribution from source #2 at point P_2 was similarly calculated by interpolating between $\alpha(2,11)$ and $\alpha(2,3)$.

Figure V-3 gives a comparison in one of the <u>in vivo</u> tumors, of space irradiance measurements versus calculations. The squares correspond to axial measurements obtained with the flat probe, that were begun immediately after the insertion of plastic needles #1 through #6 and their corresponding sources. This sequence of measurements required 6 min to complete. After a lapse of 2 min, a series of isoprobe measurements was then undertaken in needles #1 through #6, which took 24 min to complete. Another lapse of 7 min was followed by a second set of flat probe measurements, indicated by crosses on Fig.V-3. Lastly, 48 min after the initial measurements, needle #11 was inserted into the tumor and isoprobe readings for each of sources #1 - #6 were obtained within this needle.

The upper curve in Fig.V-3 was calculated from the isoprobe measurements according to equation (13); the lower curve was calculated by the interpolation method, using readings taken in the central needle (#11). The curve obtained using (13) matches fairly well the second set of axial measurements, which were taken shortly after the isoprobe readings. Both

the isoprobe readings and this second set of flat probe readings indicate a substantial decrease in space irradiance with respect to the first set of measurements. The influence of the final isoprobe readings taken at the tumor core in needle #11 can be seen by the behavior of the lower curve at points intermediate between -0.9 and +0.9 cm. This interpolated curve is lower than the other curve, because the lower values of the isoprobe measurements at this dark region of the tumor affect the calculations pertaining to all six sources, rather than just sources #1 and #4.

Results from the second in vivo tumor are shown in Fig.V-4. The squares represent a first set of axial measurements; the crosses, a second set taken immediately afterwards. In this case, the second set was taken while withdrawing the flat probe from the tumor, whereas all other axial measurements were taken while pushing the probe into the tumor. A similar drop in magnitude of the second set of measurements was observed as with the other in vivo tumor. The two curves represent calculations based on two separate sets of isoprobe measurements. The upper curve represents isoprobe measurements that were taken before the axial measurements; the lower curve represents measurements taken afterwards. The lower curve shows the effects of a reduction in the amount of light received by the isoprobe in all of needles #1 - #6. However, this drop was not as pronounced as that seen between the two flat probe

measurement series. The upper isoprobe curve (corresponding to the earlier measurements) was calculated without using data from needle #11. This resulted in the large difference between the two curves in the region between -0.9 and +0.9.

Figure V-5 shows results from a single postmortem tumor which include a first (squares) and second (crosses) flat probe measurement series and calculated curves from two isoprobe series. In this case, the flat probe measurement series are similar in magnitude, although they are laterally displaced. The two curves are derived from distinct isoprobe series. The difference between them in the region between -1.0 and 1.0 cm is solely due to the fact that the second series included measurements in the central needle, whereas the first did not. Differences between corresponding isoprobe readings in needles #1 through #6 between the two series were small.

Experiments in the phantom yielded results displayed in Figs.V-6 and V-7. The squares and upper theoretical curve in Fig.V-6 correspond to the central axis and the crosses and lower curve correspond to the axis designated as -0.5 on Fig.V-1. Figure V-7 shows results for the +0.5 axis of Fig.V-1. Theory and experiment are in reasonable to good agreement for all three axes.

V. DISCUSSION

An important goal in PDT dosimetry is to predict the space irradiance at depth in tissue. Since tissue properties vary widely, it is necessary to obtain at least some limited measurements on a particular sample in order to do this with any degree of confidence. Such measurements can then be interpolated to other locations using a suitable theory. The results in the liquid phantom show that reasonable accuracy is possible in a homogeneous medium with such a technique. Similar lipid emulsions have been used as light diffusing media in PDT treatments of bladder cancer[16,17] and in other dosimetry studies[10,18]. Unpublished results in our laboratory indicate that the optical properties of these liquids can change with time, suggesting that these materials should be employed with care. The use of an ultrasonic probe immersed in the liquid appeared to lessen this problem.

On all axes in both the phantom and tumor experiments, there is an apparent lateral displacement between the theoretical curves and the experimental points (Figs.V-3 through V-7). Although this displacement varies in magnitude on the graphs, it appears to correspond, on average, to a physical displacement of approximately 1 mm. Due to the symmetry about the origin of the arrangement of light sources, the actual placement of the minima and maxima with respect to the origin should also be symmetrical. This gives good

reason to believe that the observed displacement is an experimental artifact. Such an effect can be explained, at least in part, by the directional nature of the flat tip fiber optic probes, which appear to be sampling the space irradiance at a location approximately 1 mm in front of the fiber tip. This distance is comparable in magnitude to the 1.08 mm diameter of the steel needle, which holds the optical fiber. A similar shadowing effect by the fiber/needle assembly was noted in Chapter III. We conclude, that this displacement between the apparent measurement location and the actual tip of the fiber optic probe, should be taken into account when comparing theory with measurements of light in tissue, taken with fiber optic probes of this type. A number of such experiments have been reported in the literature[19-23].

In contrast to the good agreement of theory with experiment in the phantom, the results in postmortem tumors from Chapter IV sometimes show significant discrepancies between theory and experiment. Results from the excised tumor in the current study are given in Fig.V-5. There are two theoretical curves shown; the difference between them is that the lower curve takes into account isoprobe readings taken at a single location at the tumor core,whereas the upper curve does not. The substantial difference in accuracy between these two curves clearly demonstrates the

importance of taking sample light readings at various locations throughout a tissue volume.

A source of experimental inaccuracies in tumor experiments was due to sideways drift of the flat probe holding needle, as it was inserted into the tumors. For example, for typical tumor optical parameters, a sideways drift of 1 mm would result in a change in the measured space irradiance of between 20% and 30%.

The results in in vivo tumors are very different from the postmortem results and raise some interesting questions. Marijnissen and Star[18] had reported that light readings taken with an isoprobe in a transparent catheter in tissue, decreased by up to 90% of their initial values, during the course of an hour during PDT treatments. The results in Figs.V-3 and V-4 also show large decreases in observed light intensities over approximately the same period of time, the extent of the decrease varying with location. These decreases are not due to thermal effects, since the average source power was only about 35 mW. Also, since no significant decrease in light transmittance was observed in the excised tumor, this suggests that the most obvious cause was vascular injury from the inserted needles, resulting in a continuous extravasation of blood. What is not clear, is how much of this decrease may have been due to localized pooling of blood around the plastic needles

containing the sources and isoprobe and/or the flat probe detector needle. The answer to this question has bearing on whether the observed decreases in light intensity are real or at least partly an artifact of the measurement process. Figure V-4 presents two sequences of direct space irradiance measurements in an in vivo tumor together with results of two sets of isoprobe measurements. The first set of isoprobe measurements was taken before the direct measurements, whereas the other set was taken after them. The difference between the isoprobe-derived curves is considerably less than the difference between the two sequences of direct measurements, although the latter were taken within only a few minutes of each other. This suggests that the large decrease in intensity observed in the second sequence of direct measurements was probably a localized phenomena, perhaps due to a collection of blood and other fluid in the path of the flat probe holding needle. On the other hand, the results for the other in vivo tumor suggest a different story. In Fig.V-3, the isoprobe measurements corresponding to the upper curve were taken between two sequences of direct irradiance measurements and in this case they are consistent with the drop in space irradiance that was observed, suggesting a more generalized decrease in space irradiance throughout the tumor and perhaps especially in the vicinity of the plastic needles. Dissection of this tumor after the experiment did

show some pooling of blood where the needles had been inserted.

In summary, interpolations of isoprobe measurements using a simple model of light distribution, are in agreement with direct measurements in a tissue-equivalent phantom. It appears that the average effective scattering coefficient in tissue can be estimated, based on a series of isoprobe measurements in interstitial needles. Such measurements could, in principle, be performed in a clinical setting prior to PDT. The dosimetry technique was reasonably accurate in predicting light intensities at measured points, in one postmortem tumor. Large variations in local absorption and attenuation coefficients were consistently found in tumors, as illustrated by the large standard deviations in optical parameters reported in Table I. Although calculations of space irradiance in in vivo tumors appeared to be reasonably consistent with measured values, such comparisons were difficult to make, due to rapid decreases in the apparent transparency of tumor tissue during the course of the experiments. The cause of these temporal changes in absorption in vivo, was tentatively attributed to leakage of blood from damaged vasculature. Further in vivo studies are needed, to examine these changes in optical properties and the significance of this phenomenon in photodynamic therapy dosimetry.

TABLE V-1
Average Optical Coefficients in R3327-AT Tumors and a Lipid Phantom

	Phantom	In vivo tumor #1	In vivo tumor #2	Postmortem tumor	7 Postmortem tumors (Chap.IV)
Tumor volume (cm^3)		15	8	11	8 - 19
Transport coefficient k_{tr} (cm^{-1})	1.86 ±0.08*	15.2 ±12.8*	9.4 ±4.6*	11.4 ±7.8*	9.0
Absorption coefficient k_a (cm^{-1})	1.13 ±0.04	0.77 ±0.33	0.81 ±0.37	0.56 ±0.14	0.47 ±0.13
Attenuation coefficient α (cm^{-1})	2.66 ±0.06	5.86 ±1.08	4.72 ±0.97	4.35 ±0.57	3.55 ±0.48
Penetration depth ($1/\alpha$) (mm)	3.76	1.71	2.12	2.30	2.82

All values of k_a and α were obtained by averaging the $k_a(i,j)$ and $\alpha(i,j)$ arrays.

* Average ± S.D. of values calculated from pairs of isoprobe readings (see text)

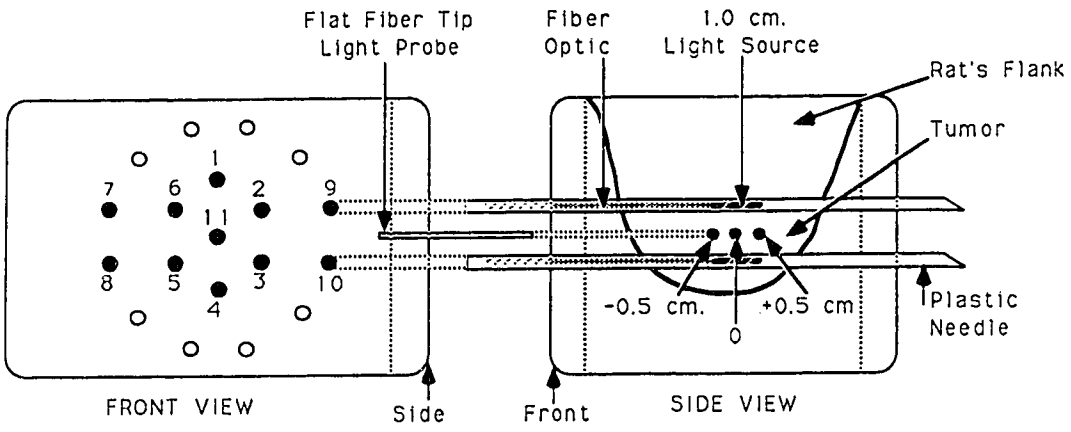

Fig.V-1 Front and side views of the dosimetry enclosure. Needle holes were evenly spaced on two concentric circles of 2.0 cm and 4.0 cm diameter, with one central hole (#11). Cylindrical 1 cm long light sources attached to fiber optics, were placed within 2 mm diameter plastic needles in holes #1 through #6 for tumors or holes #1 through #10 in the phantom. The flat tip light probe was inserted perpendicular to the plastic needles, into holes designated as -0.5 cm, 0 and +0.5 cm in the side wall of the chamber.

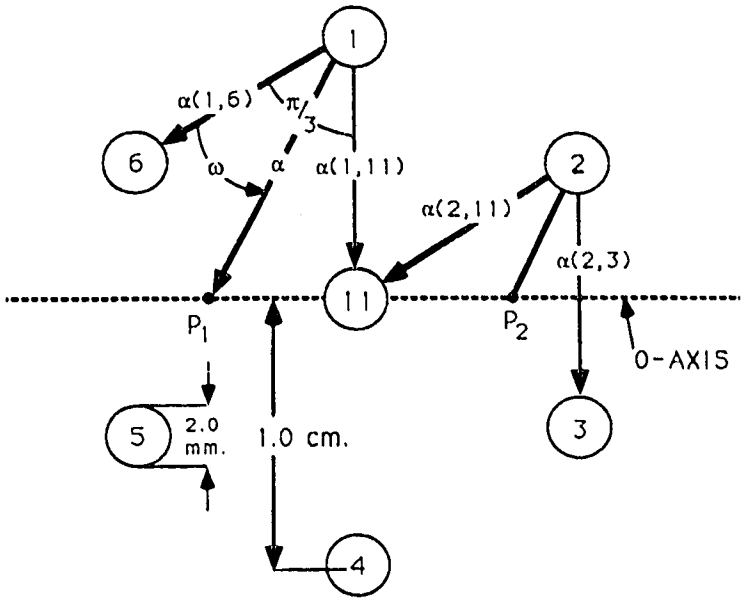

Fig.V-2 Diagram illustrating interpolation of attenuation coefficients for calculating space irradiance on the 0-axis. For example, the attenuation coefficient for source #1 and point P_1 is given by $\alpha = \alpha(1,6) + \frac{}{\pi/3}[\alpha(1,11) - \alpha(1,6)]$.

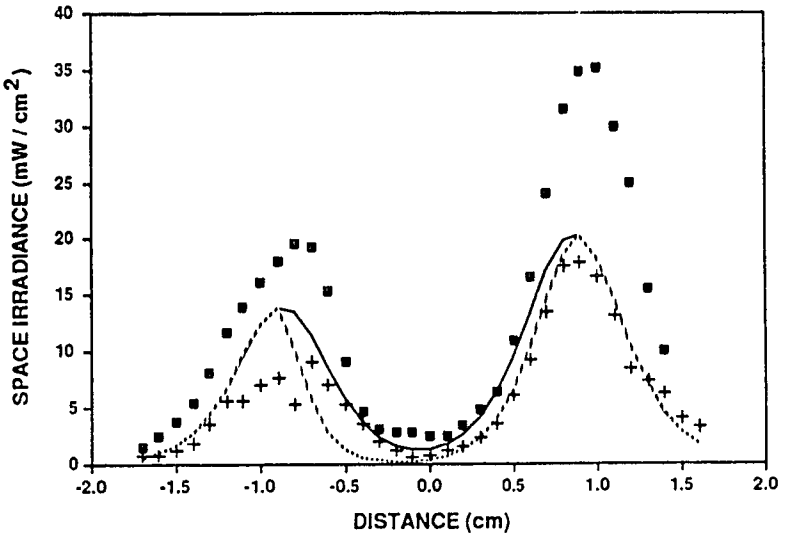

Fig.V-3 Space irradiance data on the 0-axis in <u>in vivo</u> tumor #1 vs theory, using six cylindrical light sources (avg. 35 mW). Squares and crosses, first and second flat probe measurement series respectively. Solid curve, theory based on isoprobe readings in needles #1 through #6. Dashed curve, theory based on the same readings in needles #1 through #6, plus additional readings in needle #11.

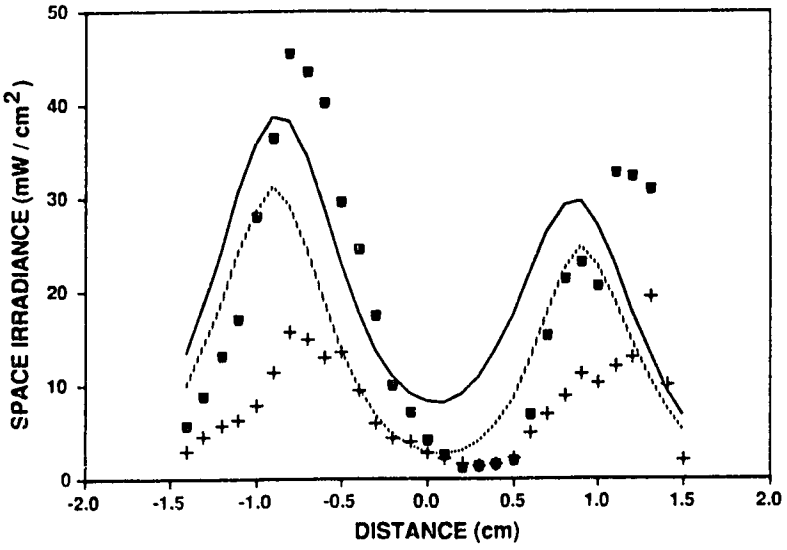

Fig.V-4 Space irradiance data on the 0-axis in in vivo tumor #2 vs theory, using six cylindrical light sources. Squares and crosses, first and second flat probe measurement series respectively. Solid curve, theory based on a first set of isoprobe readings in needles #1 through #6. Dashed curve, theory based on a second set of isoprobe readings in needles #1 through #6, plus #11.

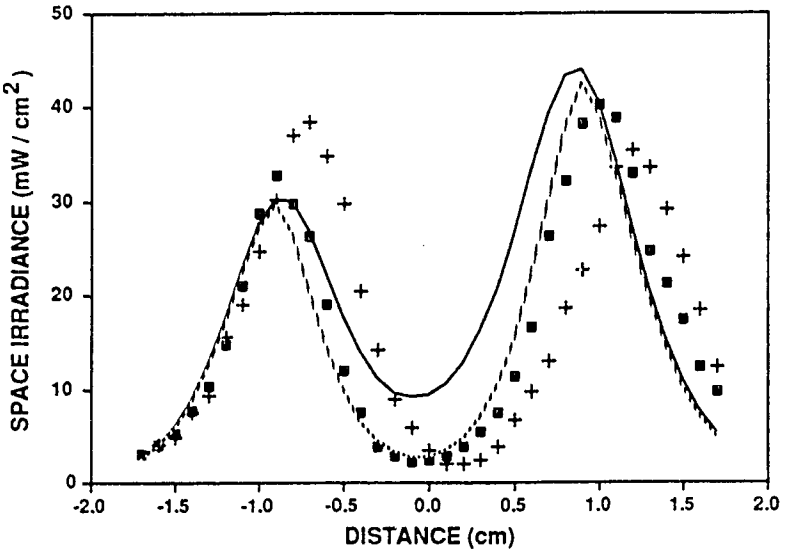

Fig.V-5 Space irradiance data on the 0-axis in a postmortem tumor vs theory, using six cylindrical sources. Squares and crosses, first and second flat probe measurement series respectfully. Solid curve, theory based on a first set of isoprobe readings in needles #1 through #6. Dashed curve, theory based on a second set of isoprobe readings, in needles #1 through #6 plus #11.

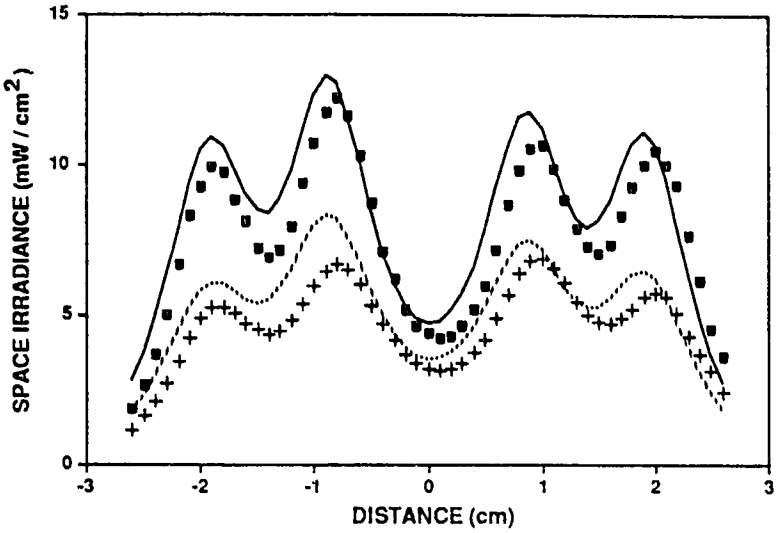

Fig.V-6 Space irradiance data on the 0 and -0.5 cm axes in a lipid phantom vs theory, using ten cylindrical sources. Squares and upper curve, 0-axis. Crosses and lower curve, -0.5 cm axis.

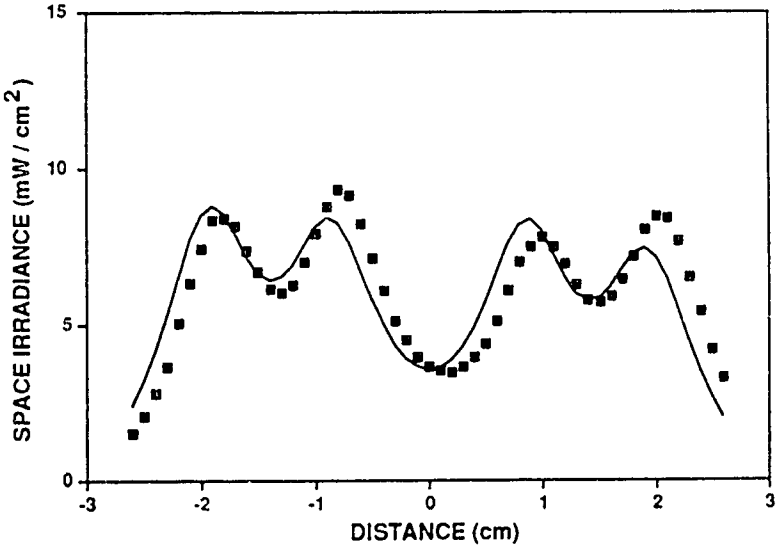

Fig.V-7 Space irradiance data on the +0.5 cm axis in a lipid phantom vs theory, using ten cylindrical sources.

LITERATURE CITED

1. T.J. Dougherty, "Photosensitization of malignant tumors," Sem. Surg. Oncol. 2:24-37, 1986.

2. O. Balchum, D.R. Doiron and G. Huth, "Photoradiation therapy of endobronchial lung cancer using the photodynamic action of hematoporphyrin derivative," Lasers Surg. Med. 4:13, 1984.

3. J.S. McCaughan, W. Hicks, L. Laufman, et al., "Palliation of esophageal malignancy with photoradiation therapy," Cancer 54:2905, 1984.

4. M.W. Berns and A.G. Wile, "Hematoporphyrin phototherapy of cancer," Radioth. Oncol. 7:233-240, 1986.

5. G.R. Prout, Jr., C.-W. Lin, R. Benson, Jr., et al., "Photodynamic therapy with hematoporphyrin derivative in the treatment of superficial transitional-cell carcinoma of the bladder," New Engl. J. Med. 317: 1251-1255, 1987.

6. V.H. Fingar, T.S. Mang and B.W. Henderson, "Modification of photodynamic therapy-induced hypoxia by Fluosol-DA (20%) and carbogen breathing in mice," Cancer Res. 48:3350-3354, 1988.

7. B.D.Hirsch, N.C.Walz, B.E.Meeker, M.R.Arnfield, J.Tulip, M.S.McPhee and J.D.Chapman, "Photodynamic therapy-induced hypoxia in rat tumors and normal tissues," Photochem. Photobiol. 46:847-852, 1987.

8. M.Y. Nahabedian, R.A. Cohen, M.F. Contino, T.M.Terem, W.H.Wright, M.W.Berns and A.G.Wile, " Combination cytotoxic chemotherapy with cisplatin or doxorubicin and photodynamic therapy in murine tumors," J. Natl. Cancer Inst. 80:739-743, 1988.

9. S. M. Waldow, B.W. Henderson and T.J. Dougherty," Potentiation of photodynamic therapy by heat: effect of sequence and time interval between treatments in vivo," Lasers Surg. Med. 5:83-94, 1985.

10. S.T. Flock, B.C. Wilson and M.S.Patterson, "Total attenuation coefficients and scattering phase functions of tissues and phantom materials at 633 nm," Med. Phys. 14:835-841, 1987.

11. W.A.G. Bruls and J.C. van der Leun, "Forward scattering properties of human epidermal layers," Photochem. Photobiol. 40:231-242, 1984.

12. J.M. Steinke and A.P. Shepherd, "Comparison of Mie theory and the light scattering of red blood cells," Appl. Opt. 27:4027-4033, 1988.

13 A. M. Weinberg and E.P. Wigner, The Physical Theory of Neutron Chain Reactors (Chicago Press, Chicago Il, 1958).

14. J.T.Isaacs, R.M.Weissman, D.S.Coffey and W.W.Scott, "Concepts in prostatic cancer biology: Dunning R3327-H, HI and AT Tumors," Prog. Clin. Biol. Res. 37:311-323, 1980.

15. M Arnfield, S. Gonzalez, P. Lea, J. Tulip and M.McPhee, "Cylindrical irradiator fiber tip for photodynamic therapy," Lasers Surg. Med. 6:150-154, 1986.

16. D. Jocham, G. Staehler, Ch. Chaussy, E. Unsold, C. Hammer, U. Lohrs and W. Gorisch, "Integral dye-laser irradiation of photosensitized bladder tumors with the aid of a light scattering medium," In: Porphyrin Localization and Treatment of Tumors, D.R.Doiron and C.J.Gomer, Eds. New York: Alan R.Liss, 1984, pp.249-256.

17. R. Baghdassarian, M.W. Wright, S.A. Vaugn, M.W. Berns, D.C. Martin and A.G. Wile, "The use of lipid emulsion as an intravesical medium to disperse light in the potential treatment of bladder tumors," J. Urol. 133:126-130, 1985.

18. J.P.A. Marijnissen and W.M. Star,"Quantitative light dosimetry in vitro and in vivo," Lasers Med. Sci. 2:235-241, 1987.

19. D.R.Doiron, L.O.Svaasand and A.E.Profio, "Light dosimetry in tissue: Application to photoradiation therapy," In: Porphyrin Photosensitization, D.Kessel and T.J.Dougherty, Eds. New York: Plenum, 1981, pp.63-76.

20. L.O.Svaasand and R.Ellingsen, "Optical penetration in human intracranial tumors," Photochem. Photobiol. 41:73-76, 1985.

21. B.C.Wilson, W.P.Jeeves and D.M.Lowe, "In vivo and post mortem measurements of the attenuation spectra of light in mammalian tissues," Photochem. Photobiol. 42:153-162, 1985.

22. F.P.Bolin, L.E.Preuss, R.C.Taylor and T.S.Sandhu, "A study of the three-dimensional distribution of light (632.8 nm) in tissue," IEEE J. Quant. Electr. QE-23:1734-1738, 1987.

23. M.R.Arnfield, J.Tulip and M.S.McPhee, "Optical propagation in tissue with anisotropic scattering," IEEE Trans. Biomed. Eng. 35:372-381, 1988.

Chapter VI : GENERAL DISCUSSION

Experimental and theoretical studies on tissue optical and thermal properties have burgeoned in recent years, mainly as a result of the advent of laser surgery in general and photodynamic therapy in particular[1,2]. Experimental studies of tissue optical properties have included postmortem and in vivo tissues and tissue-equivalent phantoms[3,4,5]. The requirements of PDT dosimetry have resulted in the development of a variety of special devices for interstitial, intraluminal and intracavitary illumination[6], for direct measurement of light in tissue[7] and for detection and analysis of HpD fluorescence as a diagnostic aid[8].

The challenge of future work in the area of tissue optics will be to bring this knowledge out of the laboratory and into the operating room and clinic. The present state of PDT dosimetry in clinical practice is empirical and essentially consists of prescribing a surface, intracavitary or interstitial dose based on past experience with the particular tissue type. For example, the total dose and dose rate for a cylindrical source implanted in a bronchial tumor have been specified at 200 J/cm and 400 mW/cm respectively[9]. As more sophisticated techniques for applying PDT clinically come into more frequent use, such as multiple and CT guided interstitial implantations, more sophisticated dosimetry will be required to keep pace.

However, dosimetry in the sense of ionizing radiation dosimetry, i.e. being able to predict dose at depth with reasonable accuracy, has not been possible as of yet in clinical PDT. The main difficulty in introducing dosimetry that takes into account the properties of the specific tissue undergoing PDT, is that the clinical situation does not usually allow the kind of physical intervention that would be needed. It will probably never be possible to calculate accurately depth-dose relationships simply by referring to pre-established tables of tissue properties, since penetration depths among samples of ostensibly similar tissues have been shown to vary widely[1,3]. This variability stems from the strong dependence of scattering and absorbing interactions of visible light on random inhomogeneities in tissue structure, density and coloration.

The use of the R3327-AT tumor tissue as a model for light propagation and dosimetry, has provided for the detailed scrutiny under various conditions of a large experimental solid tumor, which is histologically reproducible. The penetration depths at 630 nm that have been measured in R3327-AT tumors (eg. 1.7 to 2.8 mm) fall within the range of typical values for soft tissue[1]. In vivo penetration depths were found to be somewhat smaller than postmortem values. Wilson et al.[3] studied postmortem changes in penetration depth at visible wavelengths in rabbit muscle and liver and in pig brain. Light penetration was found to increase

postmortem in rabbit muscle at all wavelengths. In pig brain, penetration increased postmortem at 425 nm; however no significant increase was observed at wavelengths above 600 nm. No systematic changes in penetration were observed in liver samples. The changes in light penetration that were observed postmortem were attributed in part to blood drainage, and it appears likely that this also was a major contributor to postmortem differences in R3327-AT tumors.

Data presented in Chapter IV suggest that increased attenuation in vivo may be expected after the insertion of needles, due to leakage of blood from easily damaged tumor vessels and capillaries. This effect was observed in the absence of any photodynamic or thermal action. Decreases in light intensities of up to 90% over a period of one hour, have been observed with an interstitial light probe within tumors during photodynamic therapy[5]. Blood leakage secondary to vascular trauma might be greater during PDT than in its absence, as a result of increased blood flow in tissue. Using laser Doppler velocimetry, blood flow has been shown to increase during PDT by a factor of 3-10 in tissue involved with tumors[10].

The above considerations show that the use of optical phantoms and excised tissues although useful, is of strictly limited value as a model for in vivo dosimetry. A similar situation is faced by those studying mechanisms of

photodynamic tumor destruction and photosensitizer localization in tumors. In vitro studies on direct PDT cytotoxicity to cells do not appear to be relevant models of the processes leading to tumor destruction in vivo. Evidence from different studies shows that cell death in PDT treated tumors only occurs if the cells remain in the tumor environment following PDT. Cells that are removed from the tumor immediately after PDT and explanted to other animals in general remain viable[11]. By contrast, cell death is expressed in vitro as a consequence of direct photodynamic damage to the specific cell[12].

The question of the mechanism of tumor destruction in PDT has relevance to the optimal delivery of light dose. In ionizing radiation dosimetry, cell kill results from direct damage to cells, especially nuclear DNA. In PDT, the main target may be the vascular endothelium, which in the hours following PDT undergoes changes which eventually lead to vascular stasis and extravasation of erythrocytes[13]. It has been suggested that in some cases tumor regrowth has occurred because of preserved vascular structures near the base of tumors with surrounding islands of viable tumor, despite the application of high light and drug doses to the entire tumor[14]. Fingar and Henderson[15] found that long term control of two mouse tumor models was achieved only if a margin of normal tissue underlying the tumors was damaged. It these results turn out to be applicable to human tumors,

more attention may need to be focussed on the application of light to margins of normal tissue surrounding tumors.

Histological studies of experimental tumors have demonstrated that areas of PDT-induced necrosis are clearly and abruptly demarcated from remaining viable tissue. This fact has made it possible to examine geometric aspects of tumor necrosis as a function of different drug and light doses. Fingar et al.[14] studied the effects of PDT on RIF tumors in mice using different combinations of drug and light doses. These experiments showed that within certain ranges, the action of drug and light doses were reciprocal, that is, the percentage of remaining clonogenic cells at 24 h post-PDT depended on the product of drug times light, not their individual values. This was true only within limits defined by minimum or threshold dose levels of 1.2 mg/kg and 15 J/cm^2. At a fixed drug dose of 10 mg/kg, there was a linear increase in the depth of necrosis from the surface of the tumor, with a logarithmic increase in the dose of light. This relationship was due to the exponential decrease in light flux from the tissue surface, and suggests that a threshold dose for lethal damage was essentially constant throughout the tumor.

If the existence of a relatively constant threshold light dose is confirmed in other experimental tumor models as well as human tumors, this may be of key importance in future

treatment planning in PDT. However, much work remains to be done in determining to what extent the threshold light dose may vary with tumor location and physiological factors pertaining to uptake and distribution of the photosensitizer. Another critical problem is the best strategy for dealing with surrounding normal tissue and vasculature, which may contribute to eventual tumor regrowth by providing nutrients to remaining viable tumor cells.

An important consideration is the role of hypoxia in PDT of solid tumors. Photodynamic damage occurs mainly through the cytotoxic effects of singlet oxygen, which is formed by energy transfer from excited triplet state porphyrins to ground state oxygen molecules. It has been shown in vitro that oxygen levels of at least 1 % are necessary for a therapeutic effect[16]. Complete cessation of blood flow has been observed in tumors during the period from a few hours to one day after PDT[17]. As was mentioned earlier, cell death following PDT only occurs if the cells remain in this hypoxic environment, which may be the primary factor responsible for tumor necrosis. However, a pre-existing hypoxic fraction containing viable cells may represent regions of PDT-resistance in some solid tumors, the R3327-AT tumors being a prime example. The addition of the hypoxic cell cytotoxic agent MISO to PDT of these tumors was instrumental in improving the cure rate. A future direction in combined PDT-chemotherapy may involve other drugs of this

type, such as SR 2508 (etanidazole), which is currently undergoing clinical trials as a sensitizer in radiotherapy[18]. The chemotherapeutic agent adriamycin has also been shown to enhance the therapeutic effect in PDT of experimental tumors, although increased skin photosensitization may be a contraindication for some clinical uses[18].

A vigorous area of current research in PDT is the search for efficient photosensitizers at wavelengths of 650 nm and above, where tissue is most transparent to light. Two of the promising classes of compounds under investigation are chlorins[20] and phthalocyanines[21]. A new class of porphyrins have shown less skin photosensitization than Photofrin II and better efficiency at inducing necrosis in tumors[22].

Advances in dosimetry will be needed to take full advantage of these new photosensitizers. Progress towards this goal will require more data on in vivo tissue optical properties together with the development of techniques for measuring them in a manner acceptable in a clinical setting. It has been undertaken in this thesis to develop some of the principles of such a method, with the expectation that in situ light measurements will eventually be employed in clinical practice to calculate realistic light distributions in photodynamic therapy.

LITERATURE CITED

1. B.C. Wilson and M.S. Patterson, "The physics of photodynamic therapy," Phys. Med. Biol. 31:327-360, 1986.

2. A.J. Welch, "The thermal response of laser irradiated tissue," IEEE J. Quant. Electr. QE-20:1471-1481, 1984.

3. B.C. Wilson, W.P. Jeeves and D.M. Lowe, "In vivo and post mortem measurements of the attenuation spectra of light in mammalian tissues," Photochem. Photobiol. 42: 153-162, 1985.

4. L.W. Mason, A.J. Welch and M.J.C.van Gemert, "Photodynamic assay of light distributions in tissue phantoms," Lasers Surg. Med. 8:521-526, 1988.

5. J.P.A. Marijnissen and W.M. Star, "Quantitative light dosimetry in vitro and in vivo," Lasers Med. Sci. 2:235-241, 1987.

6. M.Arnfield, S. Gonzales, P.Lea, J. Tulip and M.McPhee, "Cylindrical irradiator fiber tip for photodynamic therapy," Lasers Surg. Med. 6:150-154, 1986.

7. J.P.A. Marynissen and W.M. Star, "Phantom measurements for light dosimetry using isotropic and small aperture detectors," In: Porphyrin Localization and Treatment of Tumors, D.R.Doiron and C.J. Gomer (eds.). New York: Alan R. Liss, 1984, pp. 133-148.

8. A.E. Profio and J. Sarnaik, "Fluorescence of HpD for tumor detection and dosimetry in photoradiation therapy," IBID, pp. 163-175.

9. O.J. Balchum, D.R. Doiron and G.C. Huth, "Photoradiation therapy of endobronchial lung cancers employing the photodynamic action of hematoporphyrin derivative," Lasers Surg. Med. 4:13-30, 1984.

10. T.DeLaney, R.Bonner, P.Smith, H. Pass and W. Travis, "Photodynamic therapy for surface malignancies: clinical results and correlation with blood flow effects secondary to photoirradiation," Rad. Onc. Biol. Phys. 13:186-187, 1987 (suppl).

11. B.W. Henderson, S.M. Waldow, T.S. Mang, W.R. Potter, P.B. Malone and T.J. Dougherty, "Tumor destruction and kinetics of tumor cell death in two experimental mouse tumors following photodynamic therapy, " Cancer Res. 45: 572-576, 1985.

12. M.W. Berns, A. Dahlman, F.M. Johnson, et al., "In vitro cellular effects of hematoporphyrin derivative," Cancer Res. 42:2325-2329, 1982.

13. J.S. Nelson, L.-H. Liaw, A. Orenstein, W.G. Roberts and M.W. Berns, "Mechanism of tumor destruction following photodynamic therapy with hematoporphyrin derivative, chlorin and pthalocyanine," J. Natl. Cancer Inst. 80: 1599-1605, 1988.

14. V.H.Fingar, W.R.Potter and B.W.Henderson, "Drug and light dose dependence of photodynamic therapy: a study of tumor cell clonogenicity and histologic changes," Photochem. Photobiol. 45: 643-650, 1987.

15. V.H.Fingar and B.W.Henderson, "Drug and light dose dependence of photodynamic therapy: A study of tumor and normal tissue response," Photochem. Photobiol. 46:837-841, 1987.

16. J.Moan and S.Sommer, "Oxygen dependence of the photosensitizing effect of hematoporphyrin derivative," Cancer Res. 45:1608-1610, 1985.

17. W.M.Star, H.P.A.Marijnissen, A.E.van den Berg-Blok, et al., "Destruction of rat mammary tumor and normal tissue microcirculation by hematoporphyrin derivative photoradiation observed in vivo in sandwich observation chambers," Cancer Res. 46:2532-2540, 1986.

18. J.M. Brown, "Sensitizers in radiotherapy," In: Innovations in Radiation Oncology, H.R Withers and L.J. Peters (eds.). New York: Springer-Verlag, 1988, pp.247-264.

19. E. S. Edell and D.A. Cortese, "Combined effects of hematoporphyrin derivative phototherapy and adriamycin in a murine tumor model," Lasers Surg. Med. 8:413-417, 1988.

20. J.S. Nelson, W.G. Roberts and M.W. Berns, "In vivo studies on the utilization of mono-l-aspartyl chlorin (NPe6) for photodynamic therapy," Cancer Res. 47:4681-4685, 1987.

21. W.-S. Chan, J.F. Marshall, G.Y.F. Lam and I.R. Hart, "Tissue uptake, distribution and potency of the photoactivatable dye chloroaluminum sulfonated pthalocyanine in mice bearing transplantable tumors," Cancer Res. 48:3040-3044, 1988.

22. M.C. Berenbaum, S.L. Akande, R. Bonnet, H. Kaur, S. Ioannou, R.D. White and U.-J. Winfield, "Meso-Tetra(hydroxyphenyl)porphyrins, a new class of potent tumor photosensitizers with favorable selectivity," Br. J. Cancer 54:717-725, 1986.

Appendix 1: CYLINDRICAL IRRADIATOR FIBER TIP FOR PHOTODYNAMIC THERAPY

A cylindrical, diffusing fiber tip was developed for application to interstitial photodynamic therapy. Details concerning the construction of the fiber tip will not be given here, since this information has been documented elsewhere (see footnote). However, a brief description of the tip, together with pertinent data regarding emission characteristics, is given below.

Cylindrical tips were 1 cm in length and consisted of a hollow dome of glass (pyrex), which was coated on its inner surface with a white epoxy (56C-white, Dexter Corp., Industry, CA). The glass dome was glued to the stripped and cleaved end of a 600 μm core diameter optical fiber, as illustrated in Fig.A1-1.

Tests were conducted to ascertain the cylindrical irradiator output characteristics using a 1 mW helium-neon laser, which was focussed onto the input end of the optical fiber. Measurements were taken of both the near and far field light distributions, of a total of six individual tips. Figure

* A version of this appendix has been published. M.R.Arnfield, S.Gonzalez, P.Lea, J.Tulip and M.S.McPhee, "Cylindrical irradiator fiber tip for photodynamic therapy," Lasers Surg. Med. 6:150-154, 1986.

A1-2 gives the average near field distribution of the six tips, as measured by a radiometer. The near field was measured by holding the radiometer detecting surface behind a narrow (0.5 mm wide) slit, which was 3 mm distant from the cylindrical tip. This assembly was scanned along the length of the tip, to produce a distribution as shown in Fig.A1-2. Error bars correspond to two standard deviations of the results from six tips, with each tip emitting 100 mW total power.

The far field distribution was obtained by moving the detector on a 31 cm radius circular arc, with the tip at the center of the circle. The resulting intensity measurements vs polar angle are given in Fig.A1-3. At each angle, the relative intensity is given by the radial distance from the origin to the plotted line. The error bars on Fig.A1-3 correspond to the typical variation of output power, under rotation of the tips about the optical fiber axis.

Lastly, the light transmission efficiency of the tips was measured. The average transmission of the tips was 91.6 ±2.6%, considered with respect to the power emitted by the bare fiber. Since a typical output efficiency for the bare optical fiber vs the laser input power was 85%, the combined efficiency of a treatment fiber was typically 0.85 x 0.92 x 100% = 78% .

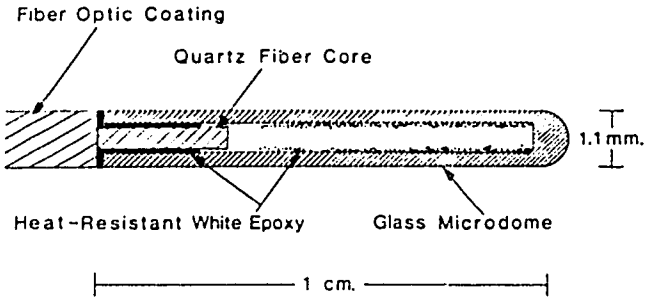

Fig.A1-1 Schematic diagram of a cylindrical irradiator.

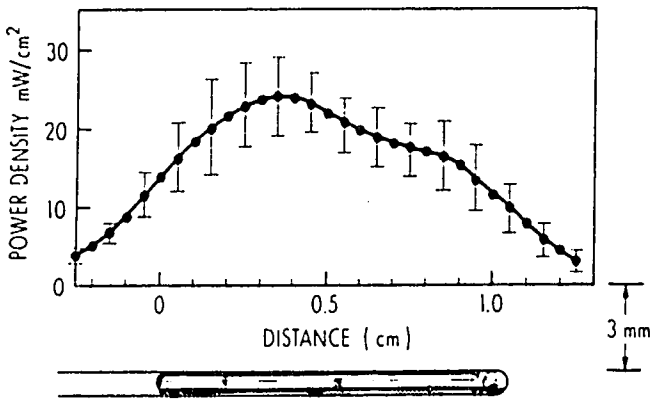

Fig.A1-2 Near field distribution of a cylindrical tip, emitting 100 mW total power.

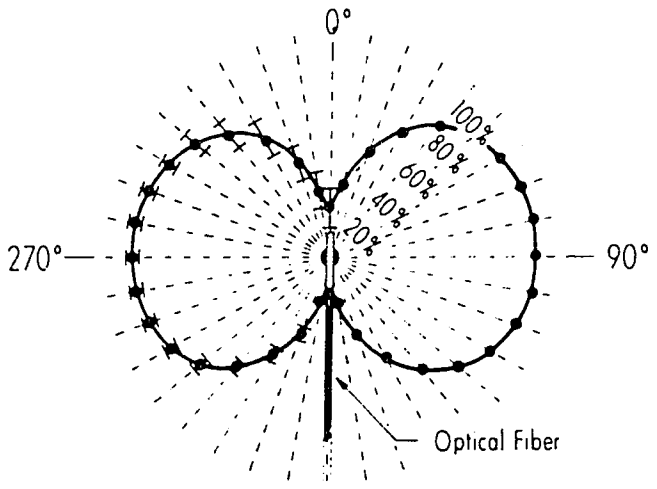

Fig.A1-3 Far field distribution, showing the relative light intensity on a circular arc around a cylindrical irradiator.